Hot-wiring azurin on gold surfaces
Stan, R.

Hot-wiring azurin onto gold surfaces

Proefschrift

ter verkrijging van

de graad van Doctor aan de Universiteit Leiden,

op gezag van Rector Magnificus prof.mr. P. F. van der Heijden,

volgens besluit van het College voor Promoties

te verdedigen op woensdag 27 Januari 2010

klokke 13.45 uur

door

Razvan Stan

geboren te Curtea de Arges, Romania, in 1979

Promotiecommisie:

Promotor: Prof. dr. T.J. Aartsma

Overige Leden: Prof. dr. G.W. Canters
                 Dr. J.J. Davis (Oxford University)
                 Dr. T. Oosterkamp
                 Dr. A. Kros
                 Prof. dr. J.M. van Ruitenbeek

To Solomon Marcus

Contents

Chapter 1

Introduction

Summary: *The growing field of molecular electronics is briefly surveyed with respect to the application of various surface science techniques, and the implementation of small organic molecules and proteins in the design and exploration of future electronic circuitries and biomaterials. The challenges facing the stability and retention of biological activity of such molecular adsorbates are contextualized, and means of circumventing some inherent hurdles to electron transfer are suggested, with reference to the chapters of this thesis.*

1.1 Protein adsorption on solid interfaces

Understanding the adsorption of proteins onto (synthetic) surfaces is of great significance in the field of biomaterials, because of its governing role in determining cellular responses in application such as tissue engineering and regenerative medicine, or in other research fields e.g. in nanotechnology or chromatography. The effects of adsorption on the bioactive state of proteins are also of critical importance in other applications, as in the development and optimization of surfaces for biosensors, bioactive nanoparticles, biocatalysis, bioanalytical systems for diagnostics or detection and in bioseparations. Because the number of degrees of freedom involved in surface engineering and design is large (e.g. types of functional groups present on the surface/proteins, their spatial distribution, surface topology etc), the chance of finding optimal conditions to control protein adsorption behavior by a trial-and-error approach for a given application is greatly reduced. Control of the protein adsorption can be achieved by creating appropriate protein mutants whose altered structure does not impede on the biological activity, while at the same time ensuring a defined attachment onto appropriate surfaces (e.g. engineering the surface residues of proteins so as to incorporate cysteines that are able to attach to silver or gold surfaces). Furthermore, the surface itself can be engineered through adsorption of molecular films (self-assembling monolayers). In so doing, some important advantages can be derived: 1) proteins can couple very specifically to functional groups off the surface, 2) optical and electrical properties of the proteins can be fine-tuned by changing the length/chemical structure of the self-assembling monolayers, 3) the functionalized surface itself will shield the proteins from the adverse effect of attachment onto bare surfaces, and 4) a type of chemical selectivity and molecular recognition can be achieved, if the self-assembling monolayers consist of different molecular phases that will preferentially attach to certain types of adsorbates from a mixture.

1.2 Scope of this thesis

This thesis aims at merging, through its focus on the study of adsorption of small organic molecules and proteins onto (mainly) gold electrodes, both the biosensor and the molecular electronics research fields. For the moletronics aspect, chapters 2-3 are concerned with the investigation of two OPV (oligo-phenylenevinylenes) molecular wires embedded in a matrix of alkanethiol self-assembling monolayers. Within this context, main research objectives are the: 1) unraveling of the details of assembly onto the gold surface lattice; 2) understanding of

2

the stochastic conductance switching; 3) uncovering of the electron transfer mechanism through the OPV located in the tunneling junction. Their surface assembly and electron transfer properties will mainly be studied with STM and conductive-AFM (C-AFM). Chapters 4-5 are a natural progression of chapters 2-3 into biosensors area, as the above-mentioned molecular wires can also attach to engineered proteins (azurins), such that: 1) a precise conformation of the protein with respect to a surface can be achieved; 2) a conductive path is established between the protein and the underlying electrode; 3) the denaturation of proteins is negated, through shielding from the bare surface. The electrical properties of the assembled complexes will be investigated in great part with C-AFM and electrochemical techniques which are briefly introduced in the next sections. This thesis can serve as a proof of concept for the design of future engineered enzymes (in a biosensor configuration), covalently attached to appropriate electrodes via appropriate OPVs, such that retention of biological activity and enhanced signal detection can be routinely achieved.

1.3 Biosensors and molecular electronics

A biosensor can broadly be defined as a compact analytical device incorporating a biological (or biologically derived) sensing unit integrated with a physicochemical transducer. The usual aim of such a device (1) is to produce either a discrete or continuous digital electronic signal that is proportional to the detection of a *single* analyte or a related group of analytes, as shown in Figure 1.

The biosensors have certain advantages over the conventional electrochemical and optical methods, particularly with respect to their ease of manufacturing, reduced cost, portability, capability for multi-target analyses, automation and exquisite sensitivity and specificity (2, 3). Consequently, an increasing span of protein-based sensors have been used for a multitude of applications, ranging from detecting environmental pollutants and food contaminants (4), to sensing of infectious diseases in the context of bioterrorism (5) and onto clinical applications i.e. cancer clinical testing (6) or blood glucose-level monitoring (7). The

Analyte $\longrightarrow$ Ligand (Signal detection) $\longrightarrow$ Transducer $\longrightarrow$ Signal recording

Enzymes	Amperometric
Chemoreceptors	Potentiometric
Antibodies etc.	Optical etc.

Figure 1. Operating principles of a biosensor.

optimistic perspective as to the practical possibilities that can be envisioned for these devices is matched by the research output, dating back as far as 1962 (8) and evidenced by more than 6000 publications in the 1996-2006 period alone (5), along with some 1100 awarded/pending patents (9). However, the commercialization of biosensors has lagged far behind this research outburst, due to a host of reasons, chief amongst which are: 1) their general lack of stability over extended periods of time; 2) time-delays in performing analyses, ranging from 15 minutes to hours; 3) sensor fouling due to the adventitious adsorption of components from the assays.

Mirroring the theoretical advances in biosensors research are the headways obtained in molecular electronics (*moletronics*) by using small organic molecules (often synthesized) not as sensing devices, but as building blocks for the fabrication of electronic components, in the form of switches, transducers and actuators (10). The main research objectives are challenging the Moore's law by increasing miniaturization on printed circuit boards (up to 10^{12} molecular switches per cm^2), obtaining low-power dissipation devices and decreasing production costs (11). One key advantage in the practical implementation of such organic constructs is the increased stability of operation, especially when compared to the macromolecules used for biosensors (the most stable of the biosensor devices, based on glucose oxidase, exhibits a progressive degradation, such that within weeks, enzymatic activity is greatly affected (12).

1.4 Nanotechnology and single molecule techniques

The growing field of nanotechnology has been greatly supported by the advent of scanning probe microscopy (SPM) techniques, most notably the Scanning tunneling microscope (STM) in 1981 and Atomic force microscope (AFM) in 1986. These and the many instrumental variations upon their design that followed (incorporating for instance electrochemical control of the surface potential), have a common feature, i.e. the measurement of an interaction (magnetic, frictional etc) between a sharp probe and a surface. The main advantage that these techniques possess is that single molecule(s) can be addressed repeatedly on a surface and various properties (mechanical, electrical etc) can be assessed. In contrast to the averaging values that other techniques yield over a great many molecules (e.g. electrochemistry and ellipsometry, as used in this thesis), each SPM measurement is generally reflective of very localized properties, and is unique in its dependence on both the details of surface assembly (when adsorbates are being probed) and the properties of the contact geometry between the SPM probes and the substrates. This latter property can be evidenced by the structural
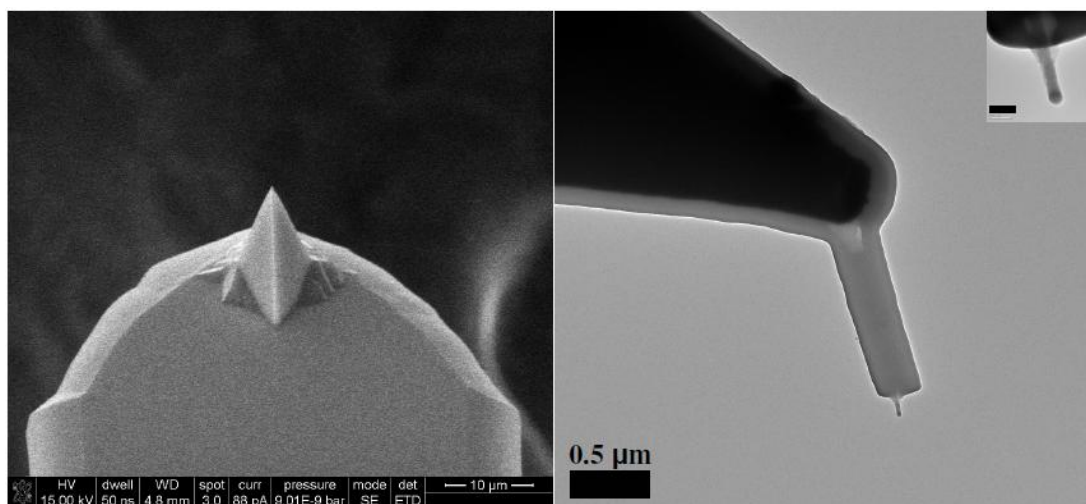
Figure 2. Left: Scanning electron micrograph (SEM) of an AFM cantilever with a bare Si_3N_4 tip, with a typical quoted radius between 10-30 nm (Olympus). Right: SEM of an AFM cantilever functionalized with a single walled, parylene coated, carbon nanotube; the inset presents a higher magnification image, scale bar is 50 nm. The actual contact area of the nanotube is ~ 2nm. Image credit Dr. Amol Patil.

changes of the SPM probes (in terms of size, contamination, wear etc) during and after measurements. Two examples of bare and functionalized AFM cantilevers shed light on the differences in size and flexibility of some AFM probes, as presented in figure 2:

As shown in Figure 2, the properties of the tip are essential in determining the resolution of the images and in obtaining valid spectroscopic results. Stiff cantilevers (Fig. 2, left) may perturb the assembly of molecular adsorbates, while flexible, functionalized cantilevers (i.e. with nanotubes that can buckle under compression – Fig. 2, right) present a decrease of tip contact area and high resistance to wear. For our purposes, we have made use of bare AFM tips, coated with conductive layers (Au, Pt, etc.), as the nanotube-functionalized tips have been very difficult to produce in sufficient amounts.

As this thesis is concerned with the study of electrical properties of various adsorbates at the molecular level, mainly by use of STM and (conductive)-AFM, we briefly present the operational principles of these instruments (Figure 3). STM (Fig. 3a.) is a non-invasive, contactless technique that relies only on conductive (or thin, non-conductive) samples to detect a (small) current resulting from the application of a voltage bias on the surface. Because the tunneling current is exponentially dependent with distance d between the STM tip and surface, small variations in *d* result in large changes in the detected current (one order of magnitude per Å). Furthermore, if the feedback current needed to keep the required current setpoint constant can be nullified or made very small, the piezo element will keep the STM

5
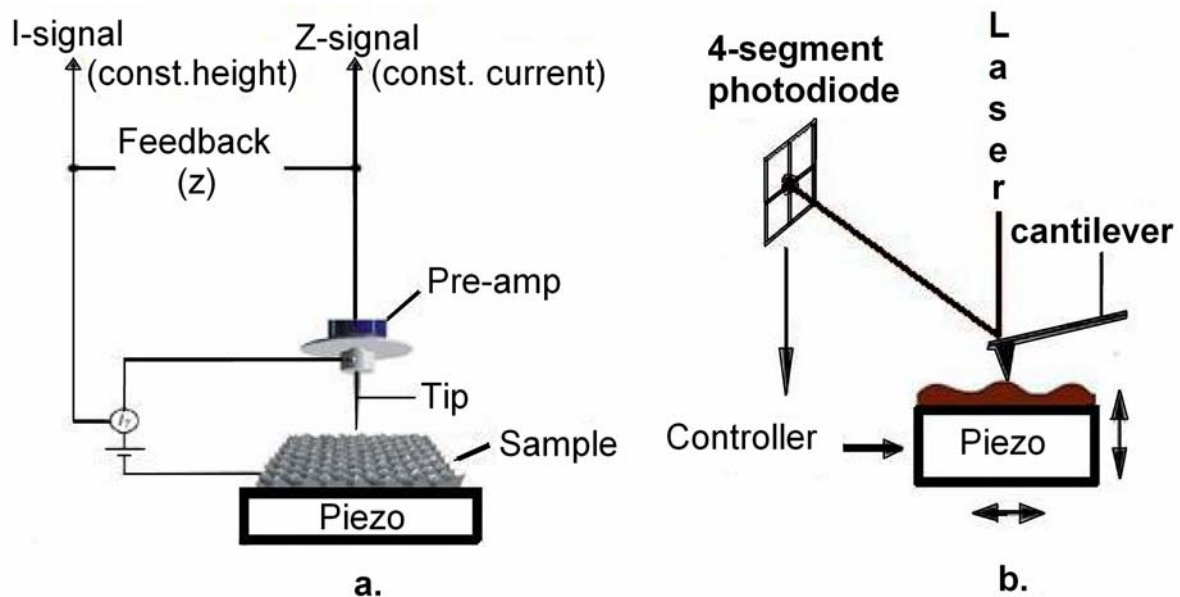
Figure 3. Architecture of the scanning tunneling microscope (a) and of an atomic force microscope (b)

probe in plane and STM will operate in constant height mode, regardless of the presence of adsorbates of different conductivities or of the sample corrugation. Alternatively, the Z-travel signal off the piezo element can be used to continuously adjust the height of the STM probe atop the surface, such that a constant current will be measured, reflecting the heterogeneity in surface conductivity/corrugation (constant current mode).

AFM (Fig. 3b.) operates by presenting a surface to a small stylus, mounted on a cantilever such that small deflections of the cantilever are produced at the proximity of the AFM tip with the sample, due to mechanical (contact) forces, van der Waals and electrostatic forces, capillary and solvation forces etc. These vertical deflections are being monitored by a laser signal reflecting off the (coated) back of the cantilever that further hits a 4-quadrant photodiode, thus ensuring a sensitive means by which the movements of the cantilevers can be tracked. The photodiode signal is further used to control a servo system that is responsible for the XYZ translations of the piezocrystal onto which the surface (Veeco microscopes) or the AFM stylus (Agilent microscopes) is mounted, and to control indirectly the force imparted by the tip on the substrate (usually it can be kept constant within a few tens of pN). Furthermore, if a bias voltage is imposed on the substrate, simultaneously with the force-controlled scanning, a tunneling current can be monitored, This methods is referred to as conductive-AFM, or C-AFM for short. This approach circumvents one of the main disadvantages of the STM (i.e. its reliance on the detected current to keep the feedback mechanism in place, potentially at the expense of the adsorbate's integrity). Ultimately, it is a

6

combination of these two techniques that ensures the electrical properties of individual molecules will be reliably assessed: the exquisite resolution of the STM provides detailed topographical information, while the use of C-AFM provides force feedback and Z-travel control when current-voltage spectroscopy is performed.

1.5 Protein film voltammetry

In our studies, we have made use of the cyclic voltammetry (CV) technique, whereby the potential of an electrode is cycled and the resulting current is measured. Such potential is controlled against a reference (non-polarizable) electrode. The excitation signal for CV is a linear potential scan between two values (switching potentials), with a triangular waveform (14). The method allows for the determination of reduction potentials of the adsorbed molecular species, of the active surface coverage (through integration of the total charge being measured) and of the electron transfer rates to and from electrodes. As the measured currents represent the contribution of a great many adsorbed molecules, CV is useful in complementing and extending the results single-molecule experimental approaches yield, i.e. the local probe techniques used in this thesis such as the STM and the AFM.

In contrast to the conventional voltammetry of free proteins in solution, the adsorption of molecules onto the surfaces and the application of a potential difference on the protein films (protein film voltammetry – PFV) has several key advantages (13), such as: 1) control and fine-tuning of the redox state of the entire sample; 2) screening for different reactivities (when the same working electrode i.e. the functionalized surface can be subjected to different electrolyte solutions or changes in pH etc); 3) the low-quantities of proteins are needed to create a protein monolayer (down to 10^{-12} M); 4) the increased sensitivity (due to the high concentration of the adsorbed proteins per electrode area); 5) determination of fast reactions, as PFV is less limited by the sluggish protein diffusion and by the kinetics of adsorption on the electrodes. As such, PFV is a powerful tool to investigate how electron transfer occurs at the protein's active sites and to determine the stability over time of the adsorbed molecular films.

References

1. A.P. Turner, I. Karube and G.S. Wilson (1987) *Biosensors: Fundamentals and Applications*. Oxford University Press.

2. B. Strehlitz, N. Nikolaus and R. Stoltenburg (2008) *Protein Detection with Aptamer Biosensors*. Sensors, 8, 4296-4307.

3. J. Castillo, S. Gáspár, S. Leth, M. Niculescu, A. Mortari, I. Bontidean, V. Soukharev, S.A. Dorneanu, A.D. Ryabov and E. Csoregi (2004) *Biosensors for life quality*. Sensor Actuator, 102, 179-194.

4. A.J. Baeumner (2003) *Biosensors for environmental pollutants and food contaminants. Anal. Bioanal. Chem.*, 377, 434-445.

5. B. Pejcic, R. De Marco and G. Parkinson (2006) *The role of biosensors in the detection of emerging infectious diseases.* Analyst, 131, 1079-1090.

6. A. Rasooly and J. Jacobson (2006) *Development of biosensors for cancer clinical testing.* Biosens. Bioelectron., 21, 1851-1858.

7. D.G. Buerck (1993) *Biosensors, theory and applications*. Technomic.

8. J.D. Newman and S.J. Setford (2006) *Enzymatic biosensors*. Mol. Biotechnol, 32, 249-268.

9. J.H.T. Luong, K. B. Male and J.D. Glennon. (2008) *Biosensor technology: Technology push versus market pull*. Biotechnolog. Adv., 26, 492-500.

10. D.M. Adams, L. Brus, C.E.D. Chidsey, S. Creager, C. Creutz, C.R. Kagan, P. V. Kamat, X. Lieberman, S. Lindsay, R. A. Marcus, R. M. Metzger, M. E. Michel-Beyerle, J. R. Miller, M. D. Newton, D. R. Rolison, O. Sankey, K. S. Schanze, J. Yardley and X. Zhu (2003) *Charge Transfer on the Nanoscale: Current Status*. J Phys. Chem. B, 107, 6668-6697.

11. J.C. Ellenbogen and K.S. Kwok (2002) *Moletronics: Future Electronics*. Mater Today, 5, 28-37.

12. T.I. Valdes and F. Moussy (2000) *In vitro and in vivo degradation of glucose oxidase enzyme used for an implantable glucose biosensor*. Diabetes Technol. Ther., 2, 367-376.

13. F. A. Armstrong (2002) *Protein Film Voltammetry: Revealing the mechanisms of Biological Oxidation and Reduction.* Russ. J Electrochem., 38, 58-73.

14. P. T. Kissinger and W. R. Heineman (1983) *Cyclic voltammetry.* J Chem Educ., 60, 702-706.

Chapter 2:

Conductance switching and organization of two cognate molecular wires on Au (1,1,1)

Razvan C. Stan[1], Nusrat J.M. Sanghamitra[1], Wang Xi[2], Jason J. Davis[2], Jeroen Appel[3], Alexander Kros[3], Gerard W. Canters[3], Thijs J. Aartsma[1]

[1] Department of Biophysics, Huygens Laboratory, Leiden University, 2300 RA, Leiden, The Netherlands
[2] Department of Chemistry, Oxford University, OX1 3TA, Oxford, United Kingdom
[3] Department of Chemistry, Gorlaeus Laboratory, Leiden University, 2333 CC, Leiden, The Netherlands

Abstract: *The dynamical distribution on Au(1,1,1) of two structurally related molecular wires has been investigated with ex-situ scanning tunneling microscopy (STM). The results point to a differential adsorption on gold with either incommensurate unit cells driven into assembly by strong lateral interactions, or to a dynamic, commensurate distribution along with the formation of distinct 2D phases. Scanning tunneling spectroscopy reveals a different response for each molecule, as can be expected from their different structures. We also observed diffusion-based conductance switching for only one of the molecular wires, possibly as a consequence of its weaker lateral interactions and of Au-S adatom formation.*

2.1 Introduction

Since the seminal publication of Aviram and Ratner (1) there has been great interest in the past decades to understand the details of assembly of organic molecules onto metal surfaces. In the quest to greater miniaturization of electronic circuitries, such simple adsorbates appear well-suited to complement and in the future replace the silicon-based components of current electronic devices, due to their ease and low cost of preparation, their self-assembling and molecular recognition properties and the modulation of electron transfer onto supporting electrodes (switching behavior) (2-5). Among the molecular systems used, the alkanethiol-based self-assembling monolayers (SAM) have been main subject of research due in part to the highly ordered, dense monolayers they form on metals (Au, Cu, Ag etc) and to their use in the industry for e.g. electrode coating with thin insulating layers and corrosion inhibition (6). However, such films have a restricted use in potential *moletronics* (portmanteau for molecular electronics) applications, since they are electrically insulating (7, 8). In consequence, in recent years the research focus has shifted towards using aromatic, self-assembling thin films such as OPV (oligo-phenylenevinylenes), since they can also form tightly packed, stable monolayers on appropriate surfaces, but with the advantage of increased electrical conductivity due to π-electron conjugation paths along the molecular frame.

Unlike the alkanethiol based SAM, the large, bulky OPV aromatic rings will induce a misfit between the underlying crystalline lattice atoms of the metal electrode and the head-groups of the molecular wires with the resulting stress producing domain boundaries and dislocation faults (11, 12). To improve on the quality of the aromatic SAM and try to resolve the issue of in-commensuration to the metal substrate, it has been noted that the introduction of a methylene ($-CH_2-$) spacer between the end-thiol and the aromatic moieties leads to better films in terms of structural integrity and also to pronounced *odd-even* effects. Such effect in the case of the *odd*-numbered aromatic SAM (where the number of the $-CH_2$ groups is 1, 3 etc) have been explained by the greater flexibility around the C$-$S bond, which translates into greater conformational freedom and lesser stress imposed onto the metal lattice (12-15). For the optimal design and fine-tuning of an OPV-based molecular device, precise knowledge of the details of the attachment to metal electrodes and of the intermolecular forces that govern their self-assembly is therefore essential. Within this context, the present study consists of two parts: 1) a structural description of the dissimilar topography adopted by two cognate, *odd*-numbered, aromatic molecular wires on Au (1,1,1) embedded within an alkanethiol SAM and

2) a presentation of the diffusion-based conductance changes that these molecules exhibit. The novel aspect being introduced here is the close similarity in the structure of the molecules that nonetheless translates into different assembly properties and behavior on the gold surface. As with other OPVs, these types of molecules have the potential to serve as electrical switches and transducers (9, 10). Furthermore, these molecular wires also have the capability of acting as molecular tethers, by linking appropriate redox proteins to electrodes, and thus providing a highly conductive path for interfacial electron transfer (Chapters 4 and 5 of this thesis).

2.2 Experimental section

Molecular wires:

The two molecules used in this study are shown below in Figure 1. For their synthesis, Heck reaction (16-20) and Mitsunobu chemistry (21) as performed by Lipshutz and coworkers (22) were used, as presented in Figure 2 which shows the synthesis route to the pyridine OPV methyl thiol **3**. 4-vinylpyridine (Aldrich, 566 mg, 5.38 mmol, 1 equiv.) was coupled to 4-bromobenzaldehyde (Aldrich, 996 mg, 5.38 mmol, 1 equiv.) using Heck reaction to synthesize compound **1** (50-75% yield), in the presence of triethylamine (Aldrich, 817 mg,
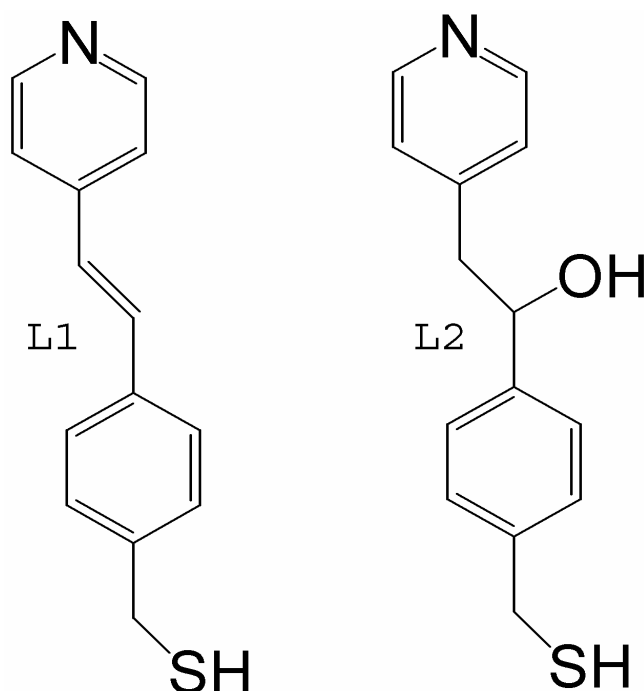
Figure 1. Diagram with the structures of the two molecules used in this paper, L1 - (S-{4-[(E)-2-pyridin-4-ylethenyl]benzyl}ethanethiolate) and L2 - (S-{4-[(2R)-2-hydroxy-2-pyridin-4-ylethyl]benzyl}. The thiol-protective acetyl group was removed during incubation with NH_4OH, or during synthesis by using $LiAlH_4$.
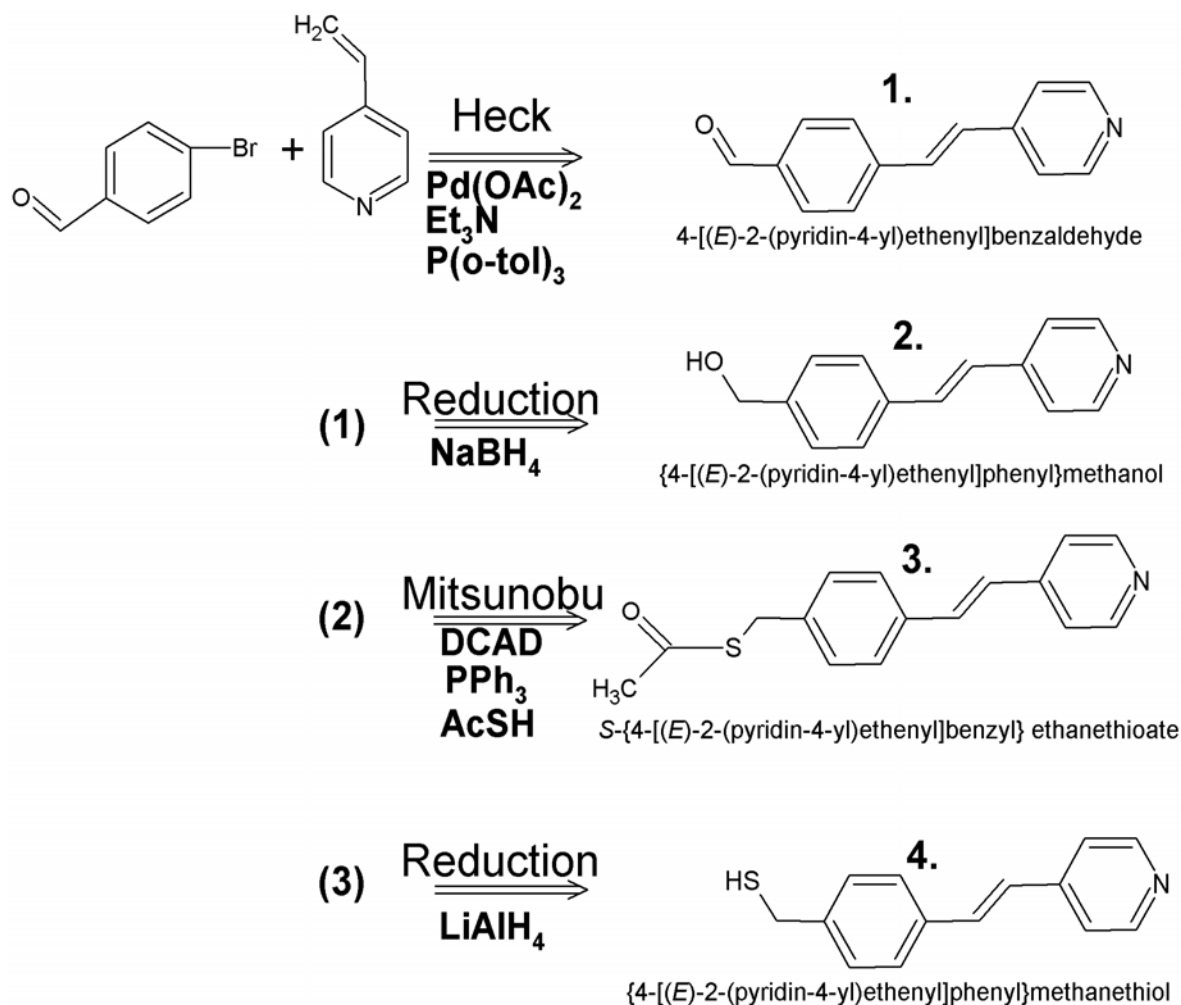
Figure 2: Synthesis scheme for linker 1.

8.07 mmol, 1.5 equiv.), tri-*o*-tolylphosphine (Aldrich, 164 mg, 0.54 mmol, 0.1 equiv.) and palladium(II) acetate (Acros Organics, 60 mg, 0.27 mmol, 0.05 equiv.) dissolved in dry *N,N*-dimethylformamide (5 ml). Molecule **1** was then reduced with sodium borohydride (Aldrich, 36 mg, 0.95 mmol, 1 equiv.) to create **2** with a yield of > 95%. For the synthesis of linker 1 (L$_1$), two equivalents of thioacetic acid and one equivalent of **2** were used, with the vinyl group being attacked by the negatively charged thioacetate. For the synthesis of linker 2 (L$_2$), thioacetic acid was coupled to **2**, using all reagents in two equivalents with respect to the concentration of **2**, and under the presence of DCAD (di-(4-(chlorobezyl) azodicarboxylate). ^{1}H NMR showed that the vinyl group was no longer present, while mass spectrometry analysis indicates that the weight of the molecule was 18 units higher compared to that of L$_1$ – evidence of the addition of H$_2$O (results not shown).

12
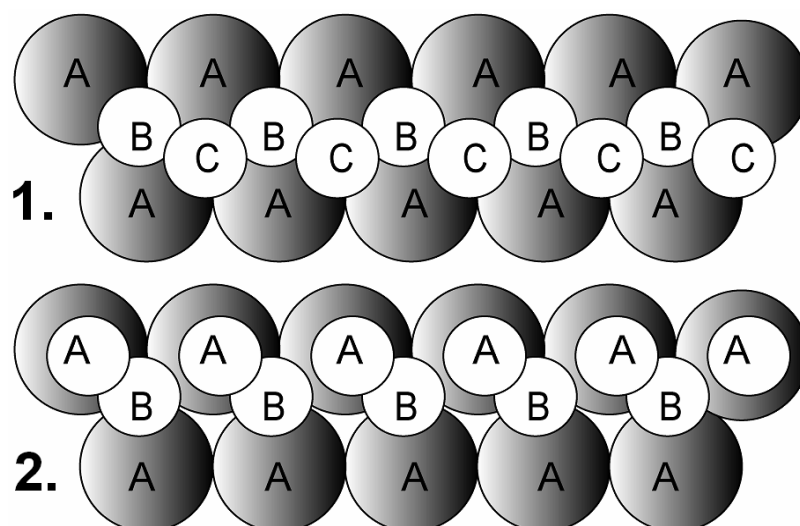
Figure 3: Different packing arrangements of the gold atoms (explanation in text).

Gold: Au surfaces were prepared *in-house* by RF sputtering 250-300 nm onto freshly cleaved mica V1-grade (Jeol B.V.) at a base pressure below 10^{-6} bars. Subsequently, annealing with a butane torch was performed so as to obtain flat, recrystallized Au (111) surfaces. The organization of the topmost Au layers is shown in Figure 3, and presents a model of the distribution of atoms in successive layers of the gold lattice. The centers of the gold atoms of the (bottom) first layer are marked as A, while the layer above it has its atoms denoted as B. The third, topmost layer can be situated either in position C (Fig. 3.1), hence the ABC packing or *fcc* crystals (face-centered cubic), or on top of A (Fig. 3.2), referred to as the ABA arrangement, corresponding to hexagonal-close packed crystals (*hcp*).

Sample preparation: Incubation procedures were similar for both molecular wires and consisted of a short (5') incubation time of 1mM 1-octanethiol (C_8, dissolved in ethanol), followed by addition of 100 μM of either molecular wire (dissolved in ethanol) for periods ranging from 44-48 hours, together with 2 μl of saturated aqueous ammonia hydroxide. NH_4OH has the role of hydrolyzing the acetyl protective group and thus exposing the thiolate. The functionalized gold surfaces were subsequently rinsed with ethanol and dried with N_2.

Ellipsometry: A M2000V Variable Angle Spectroscopic Ellipsometer (Woollam) was used for the thin films' characterization with the incident light at a fixed angle (65°). Data analysis was performed with the WVase software package (Woollam). The film thickness was calculated assuming a refractive index n = 1.55.

STM: Ex-situ STM measurements were performed with either a Digital Instruments Microscope (Veeco) equipped with a Nanoscope IIIa Controller or with an Pico LE Microscope (Agilent) equipped with a Picoscan II controller; both microscopes had a current-to-voltage preamplifier of 1 nA/V. STM tips (0.25mm diameter) were purchased from Veeco and mechanically cut prior to use. Unless otherwise noted, all images and STS curves were taken at a bias U = −1.4 V and set-point current I = 20 pA in constant-current mode at room temperature.

2.3 Results

2.3.1 Assembly on gold of the mixed monolayers

2.3.1.1 Organization of C_8 self-assembling monolayers

Because the molecular wires are assembled on gold surfaces and embedded within the octanethiol SAM, it is important to differentiate between the attachment on the surface of each linker and the surrounding alkanethiol matrix. To this end, we have first characterized the attachment of molecular films consisting solely of C_8 that serves as an insulating background against which the wires are compared (Figure 4).

Figure 4a. typifies the topographical disposition on gold of the alkanethiol C_8, consisting of regions with long-range lateral order, delimited by domain boundaries (black arrows). Of note is also the presence of the film defects that disrupt the continuity of alkanethiol domains, in the form of etched gold areas (white arrow in Figure 4.a). A closer inspection of a C_8 domain from Fig. 4b reveals the orderly disposition of alkanethiol molecules, along with the punctuated lack of C_8 molecules at individual spots, possibly because of the continuous reorganization of the octanethiol domains; the markers indicate the distance between adjacent molecules. On average, the distances between neighboring alkanethiols, as measured by 2D spectra (Fast Fourier Transforms of different images, as exemplified in Figure 4c) and by height profiles (Fig. 4d) are between 0.45-0.5 nm. These values are consistent with a prevailing model in the literature (2, 24-26), that assigns the thiols to both *hcp*-hollow sites and/or the bridge between two gold lattice atoms (see also Discussion). We thus support the ($\sqrt{3}a \times \sqrt{3}a$) R30° adlayer model (2, 23) (where $a = 0.288$ nm, is the distance between two adjacent gold atoms) (27).

14
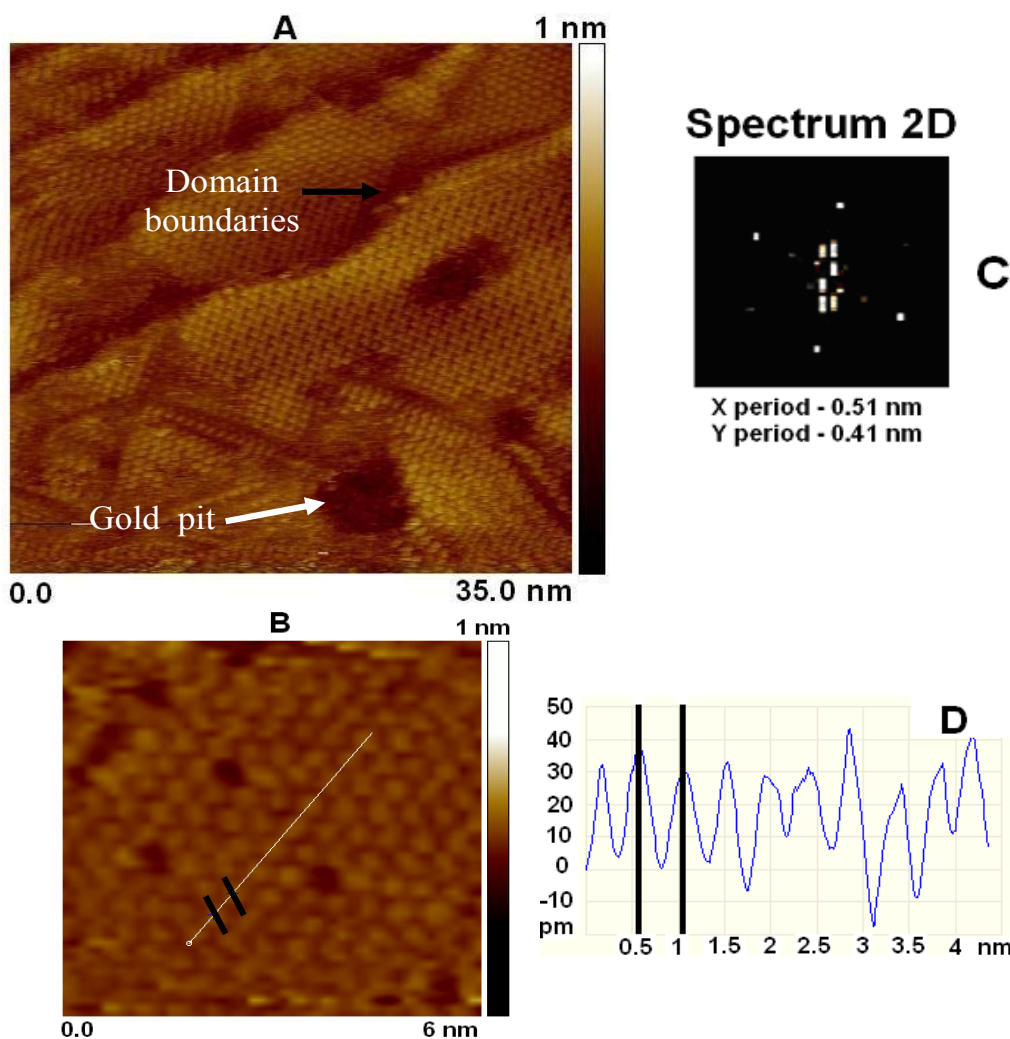
Figure 4. a) STM Height image of C_8 after 24 h incubation. b) Close-up of a 6 x 6 nm domain of C_8, highlighting in the cross-section the distance between two adjacent sulfurs. c) 2D spectrum of the image b, marking the periodicity along the X,Y axes. d) Height profile within a C_8 domain, with an average distance between markers of 0.467 nm. U = 0.54V, I = 70pA, constant current mode.

2.3.1.2 Presence of L_1 and L_2 aggregates

As the STM measurements on pure L_1 or L_2 films have not revealed any ordered structure on the surface, we assume that the molecular wires are randomly adsorbed on gold and that they may adopt a flat-lying position with respect to the substrate, possibly with the benzene rings horizontally π-stacked, as has been previously observed with other systems (45, 65, 66). This view is confirmed by the ellipsometrical data that indicate a thickness of about 0.4 ± 0.2 nm (results not shown). In order to ascertain the presence of the linkers in a "standing-up" configuration, use has been made of the 1-octanethiol (C_8) monolayers to serve as both molecular "props" for our wires and as contrasting background in STM (as they are expected to be much less conductive). In contrast to the prevalence of the C_8 on the surface, both L_1 and

15

L_2 were found to be sparsely interspersed within the SAM domains, and present in three distinct dispositions: as single molecules (Chapter 3 of this thesis), as disorganized aggregates and as ordered domains.

The disorganized states of L_1 and L_2, respectively, were measured in order to assess their relative height, and in order to estimate the surface roughness of the domains formed by either molecular wire. Representative STM images are shown in Fig. 5, highlighting the presence of disordered domains of various sizes produced by either linker on the surface. It is interesting to examine not only the height difference of each molecular wire when compared to the C_8 matrix, but also between L_1 and L_2 (Fig. 5c vs. Fig. 5d). Cross-sections averaged over approximately 20 different spots show a measurable, albeit small difference in height between the two molecular wires and the alkanethiol domains of 0.31 ± 0.04 nm for linker L_1 and 0.25 ± 0.08 nm for linker L_2, respectively. We suggest that, as the STM feedback control keeps the operating set-point current constant by moving the tip in Z-direction, molecular
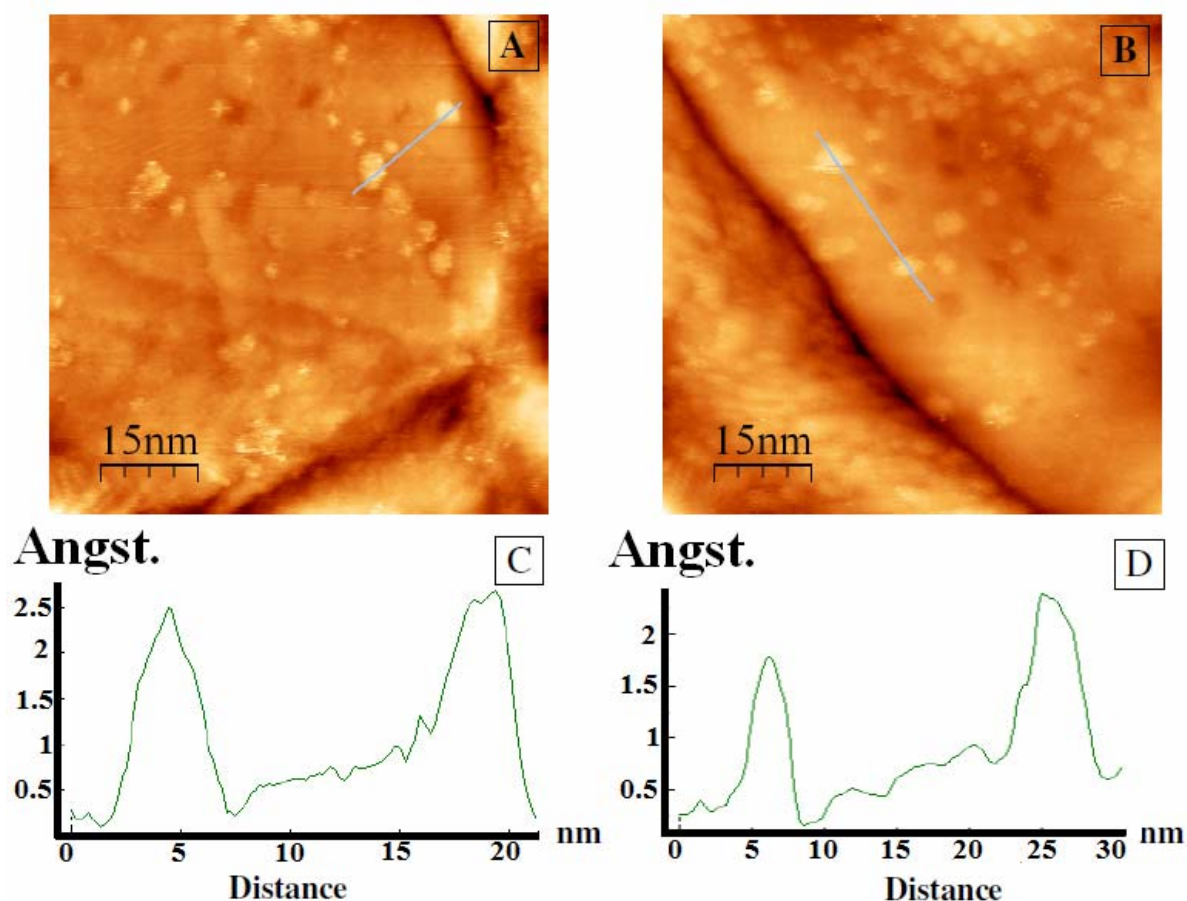
Figure 5. Large scale STM images and cross-sections of aggregates of L_1 (a, c) and L_2 (b,d). For details, see text. Analysis of the images was performed using WSXM 4.0 (Nanotec, Spain) (63)

16

species of different conductivity will produce different piezo-travel responses (and consequently discrepant apparent heights), even though the physical height of the molecular wires is here similar. Aside from disordered aggregates, we have also observed relatively large domains (in the order of 500 nm^2) of either linker, organized with a high degree of 2D order on gold terraces.

We will consider the case for each molecular wire separately, while noting that either molecular wire, present in organized structures or unresolvable aggregates (by STM) were measured on the same (heterogeneous) samples.

Figure 6. A) STM height image of extended, nondescript L_1 domains. B) STM close-up image (with an L_1 unit cell) and height profile (D) of a small L_1 domain consisting of molecular rows. C) model of L_1 π-stacking on gold.

17

2.3.1.3 Orderly disposition of linker L_1 on gold

Relatively large L_1 domains (up to 100 x 100 nm) were observed on the gold terraces, suggestive of robust adsorption. An example thereof is presented in Figure 6. The most common organization of L_1 was in the form of narrow, linear arrays, reminiscent of a stacked arrangement of the molecules involved (Fig. 6a). Such rows were often part of large, nondescript domains containing multiple parallel rows in close proximity. Occasionally two-dimensional ordering was observed as shown in Fig. 6b. Distances between adjacent molecules, and between molecular rows of 0.44 ± 0.06 nm (indicated by the striped arrows/bars in Figs. 6b and 6d), and 0.8 ± 0.1 nm, respectively (as pointed out by the black arrows/bars in Figs. 6b and 6d). The $(3 \times \sqrt{3})$ cell is proposed as the basic lattice unit, commensurate to the gold surface, and is shown as the parallelogram in Fig. 6b., a side view of which is presented in Fig. 6c.
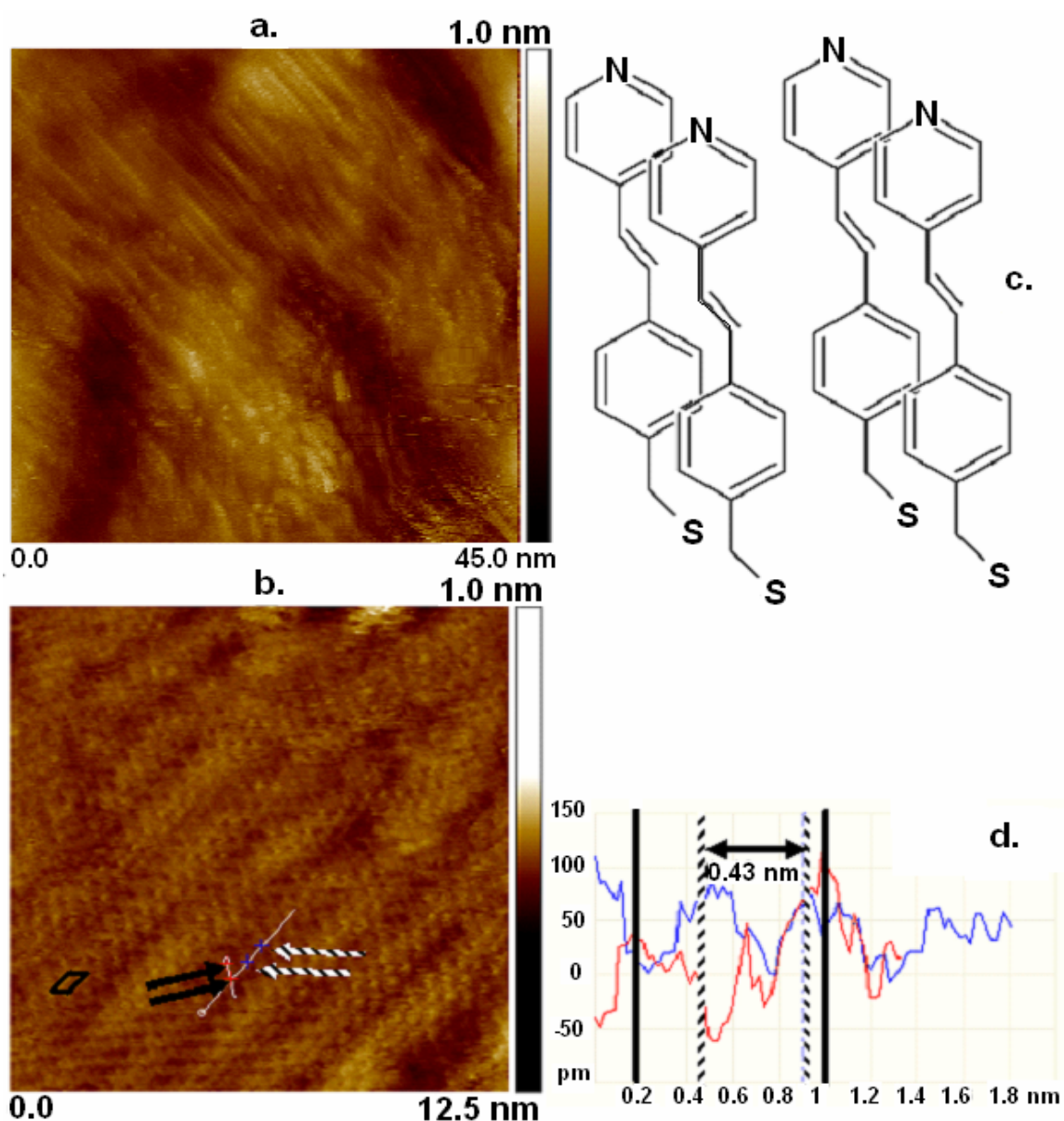
2.3.1.4 Orderly disposition of linker L_2 on gold

While single L_2 molecules were also found within the C_8 domains (result not shown), most of L_2 was present in large scale organizations (up to 1000-1500 nm^2), arrayed in single or double molecular rows. Figure 7 reveals the distribution of L_2 molecules organized in either single rows of molecules (Fig. 7a) or, most dominantly, paired. Fig. 7b. presents a close-up image with cross-sections representative of the average distances found along the rows (dark arrows), and between them (striped arrows) of 0.28 ± 0.03 nm and 0.29 ± 0.04 nm, respectively. The former set of values are consistent with interplanar intervals between aromatic moieties that have been both measured (69) or DFT-calculated (70), with the average π-π stacking distance of 0.32 nm.

We note here that these values are different than the distances measured for the cognate L_1, and the packing is much tighter within the L_2 structures. We propose that the rotational flexibility at the −CH$_2$− groups, located between the aromatic rings, may contribute to the decrease of the steric hindrance and minimization of the intermolecular distances. This flexibility of L_2 molecules contrasts to the rigidity of L_1 molecules, brought by both the rigidity of the coplanar aromatic moieties and the presence of the C=C bond. A suggested model of lateral interaction for L_2 molecules is presented in Fig. 7d, whereby π-stacking interactions are responsible for the orderly disposition along the observed molecular rows, and hydrogen bonds connect molecules across the rows.

18
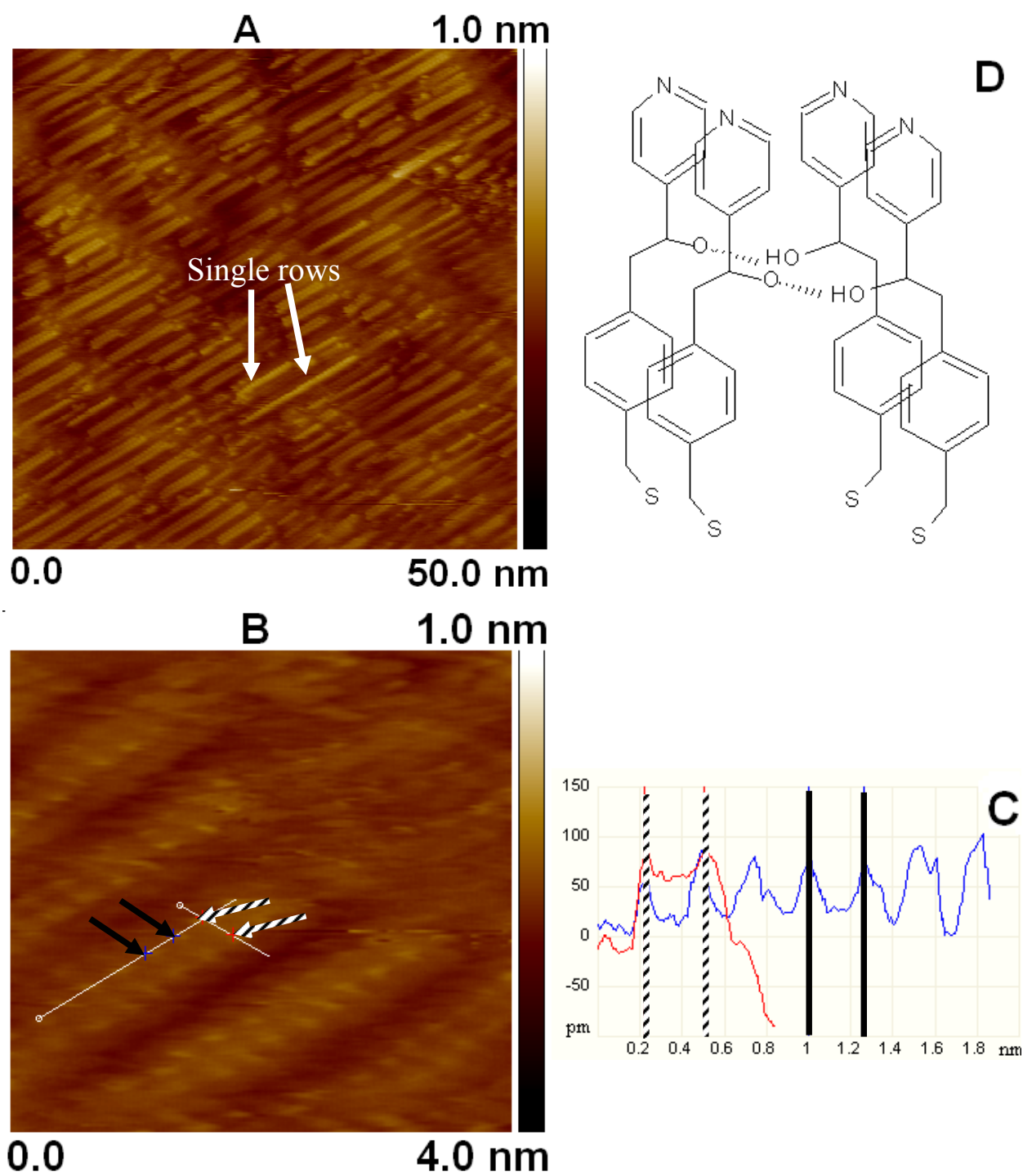
Figure 7. a, b) STM height images of L_2 organized in structures consisting (generally) of two molecular rows. c) Height profile of the representative distances along the L_2 rows (black arrows in Fig. 7.b, black lines in the cross-section) and across L_2 rows (striped arrows/lines). d) proposed model of interaction between L_2 molecules within the molecular rows (π-stacking and H-bonding along, and, respectively, across the molecular rows)

2.3.2. *I(V)* Spectroscopy

In order to further assess the conductance properties of the molecular wires, point current-voltage spectroscopy has been performed on the mixed monolayers (not on isolated spots). Since the STM tip is supposed to be atomically sharp, based on the atomic resolution obtained before acquiring the *I(V)* curves, we assume that the individual *I(V)* curves reflect the electron transfer of single, or at most a few, molecules. An example of the current response under variation of applied bias, for each molecular species, is presented in Figure 8.
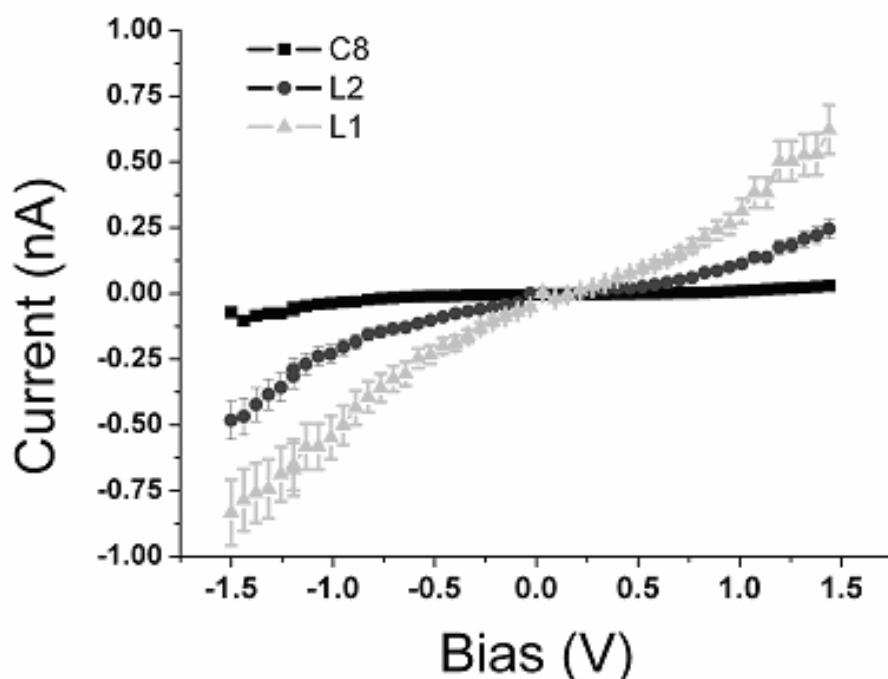
Figure 8. *I(V)* curves obtained over various spots within L_1, L_2 and C_8 domains. The bars represent the standard deviation of the data around the mean values. Each curve shown is the average of 20 raw curves obtained over 20 different spots.

The asymmetrical shape of *I(V)* curves of each molecular wire may be due to the asymmetry of the tunneling junction, i.e. a chemical contact at the gold surface (via S-Au bonding) vs. a physical contact at the pyridine group, through the STM tip. Of note are also the higher current values observed in the case of L_1, an effect we attribute to the presence of its C=C conjugated bond that ensures a continuous path for the π – electrons. It is worth noting that because of the incertitude in the Z-position of the STM tip – either because the tip relies on the current it measures to fine tune the Z- approach when performing spectroscopy, or, equally important, because of the mechanical and thermal drift of the instrument, we cannot assume that the curves presented represent just the electron transfer through the molecules alone, and a variable gap also has to be considered between the tip and molecule

20

for each curve thus obtained. In the low bias regime, between -200 mV to 200 mV, the linear response thus measured can be used to estimate the tunneling junction resistances, as exemplified in Table 1:

Table 1. Resistance values (gigaohms) of the mixed monolayers

	Linker 1	Linker 2	Octanethiol
Resistance(GigaΩ)	0.014	0.034	0.14

These values indicate an higher electrical resistance of the alkanethiol matrix, as opposed to the molecular wires, in accordance to recent published values (64). The lower values obtained for either molecular wire is due to the delocalized π-electrons and the backbone conjugated system that facilitate electron transfer between the two metals; we also note a significant difference between the resistance values of the two linkers, as can be expected from their structure.

2.3.3 Single molecule conductance switching

In order to understand the interaction between individual molecular wires with the alkanethiol matrix and with the gold surface, we have also measured for prolonged intervals their presence on the electrodes. The activity of alkanethiol-embedded single linkers or clusters thereof can be followed under constant bias and in constant current mode, thus providing time lapses of their adsorption kinetics. A reasonable assumption that can be made *a priori* is that the aromatic moieties will weakly interact via van der Waals forces with the alkyl chains (43).

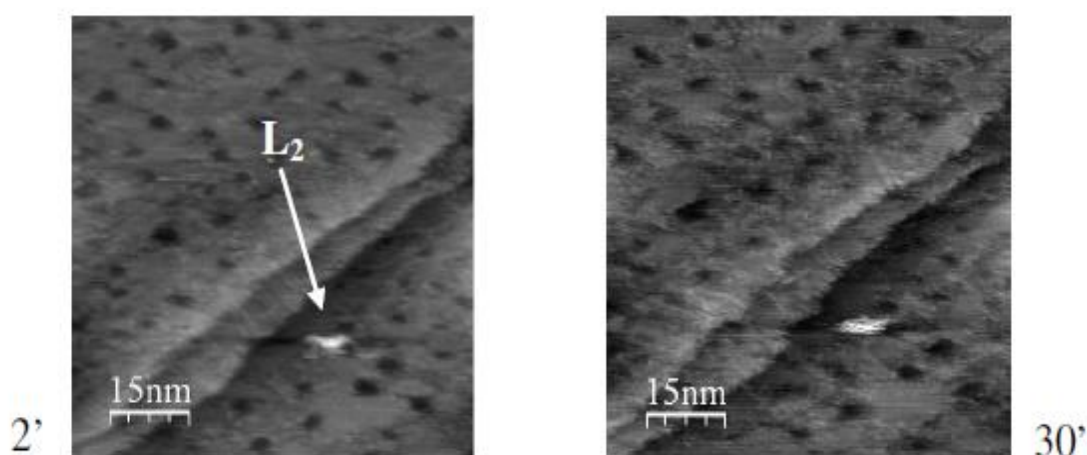**Figure 9**. STM height images of a bundle of L_2 molecules (indicated by the arrow in first image), highlighting their stability on the Au terraces. The interval between the two frames is 30 minutes. U = −1.4V, I = 20pA, constant current mode.

As such, one can expect that the electrical conductance of the molecular wires is determined by their structure, with an influence from the degree of structural disorder of the nearby matrix if tilting or rotations of the molecular wires are involved (15).

In terms of dynamical features in successive images the two linkers exhibited rarther contrasting behavior. We have not observed the dynamic distribution in the case of L_2 domains (i.e. no transitions on conductivity), in contrast to L_1. In particular, individual (or small clusters of) L_2 molecular wires, embedded in a SAM matrix, did not exhibit changes in conductance under applied bias for periods up to 30 minutes (before drift typically sets in), as exemplified in the Figure 9. This figure shows two STM images of a L_2 spot, taken during a measurement time of 30'; of note is the unchanged position of this spot, indicative of stable attachment on gold. Because of the size of this spot (~15 nm^2), it can be assumed that there may be several L_2 molecules clustered together, with no particular short range order.

When L_1 molecules were imaged, their behavior was rather different, marked by disappearance and reappearance in subsequent frames (Figure 10). Figure 10 presents the conductance "blinking" of individual L_1 spots. Panel A depicts the behavior of L_1 in the vicinity of a gold pit (white arrows), highlighting their stability (see also Discussion). In contrast, panel B indicates the "disappearance" of the conducting linker molecules (black circles) within the alkanethiol matrix. We remark here the opposite voltage signs used to acquire these images i.e. panel A vs. panel B (see Discussion). When analyzing these images, a first point that needs to be made is that one cannot attribute the influence of the STM tip in "picking-up" and later "writing-down" the molecules, as the switching events tend to be located close to the original spots (black arrows in panel B), while the STM scans from frame to frame across many film defects, where re-insertion could occur. Secondly, such an event is likely to perturb the imaging and render tunneling more difficult. Of note is also that it is difficult to assess whether all these conductive spots that appear to "blink" on the surface represent one or more molecules as exemplified by the relative size of the L_1 spot of ~3.12 nm^2 (inset in Fig. 10. panel B) vs. the calculated cross-sectional area of the volume occupied by a single L_1 molecule of 1.26 nm^2. Since the L_1 molecules are higher by about 0.4-0.5 nm than the 1-octanethiol matrix and sharper then the STM tip, the tip may not distinguish between one or few disordered molecules. It is likely that as the number of molecular wires from a particular spot increases, so does its brightness, i.e. their contribution to the tunneling current is additive. We therefore propose that the brighter spots for both molecular wires may correspond to more than one molecule, when they are inserted in the insulating matrix.
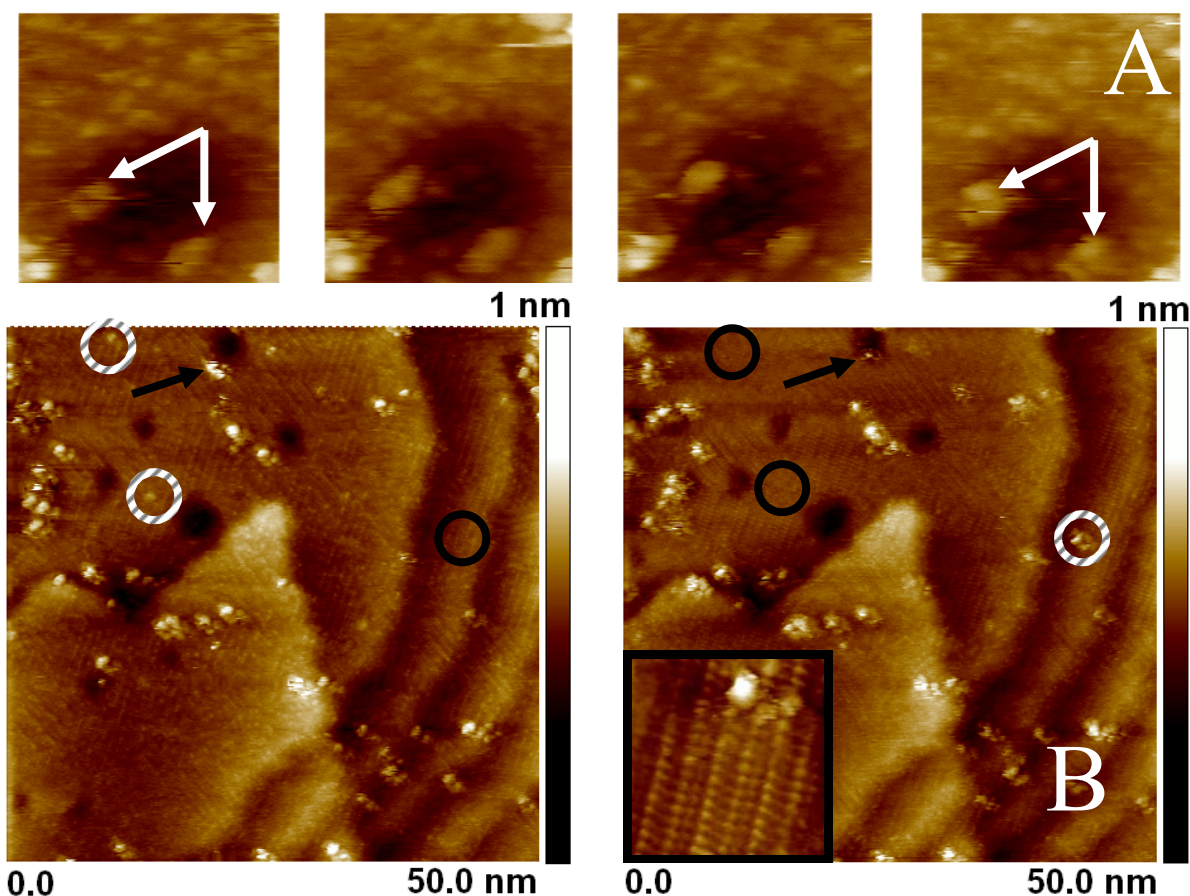
Figure 10. A) Consecutive STM images (6 x 6 nm) of embedded, non-diffusive L_1 molecules located when in the proximity of gold pits (white arrows); $U = -1.4$ V, $I = 20$ pA, constant current mode, time interval between frames is 2'. B) Consecutive STM images of diffusive L_1 molecules (bright spots); the patterned grey circles mark the presence of a conductive spot that is absent in the previous or the subsequent frame (black circles); the black arrows indicate the change in size of such a conductive spot, caused by the lateral diffusion in the alkanethiol matrix. The inset presents a high-resolution image (7 x 7 nm) of an embedded L_1 spot within the 1-octanethiol matrix; constant current mode, $U = 1.1$ V, $I = 20$ pA, time interval between frames is 2'.

2.4 Discussion

2.4.1 Contrasting assembly on gold of molecular wires

We first address the issue of the assembly kinetics of alkanethiols and molecular wires. Because the C_8 is first added to the gold and due to its fast adsorption kinetics (23), alkanethiols constitute the dominant component present on the surface. Upon attachment, most of the C_8 will initially organize into the so-called "striped-phase", whereby molecules are lying in parallel rows with the alkyl chains flat on gold, before adopting a standing-up position (2). Once either L_1 or L_2 has been added, a competition will ensue for the available gold surface between each molecular species, with the molecular wires either being inserted

individually in the film defects of the alkanethiol matrix (or, in fewer instances, within a C_8 domain), or collectively forming aggregates or ordered structures. We hypothesize that just as the alkanethiols move from a disordered phase, with the alkyl chains randomly oriented, to a highly ordered 2D phase, with dominant hydrophobic (lateral) interactions, the molecular wires transit from the disordered molecular aggregates that cannot be resolved with the STM, to the kind of structures presented in Figures 6 and 7. It is therefore possible that the aggregation stage is a thermodynamic step into the adsorption process, whereby the lateral chains will attempt to maximize their entropy by adopting random configurations.

The second aspect worth mentioning, which pertains also to the adsorption kinetics, is the distinct localization of the thiol head-groups of the molecular wires on the gold surface. It can be expected (28, 29) that because of the bulky moieties of these molecules, steric considerations will determine that the adsorption will be different than in the case of alkanethiols, in order to accommodate for the lateral chains. Even for the simpler case of alkanethiols, there is an on-going debate in the literature as to the exact location of the gold adsorption sites. The predictions made by the Density Functional Theory calculations conflict with the actual measurements (30-32), such that fcc, hcp, fcc-bridge, hcp-bridge, ''on top'' or combinations thereof, have been in turn proposed as dominant site. Especially in the DFT results, the calculations are generally limited to the methanethiol case, without including the van der Waals forces arising from the presence of the long alkyl chains, nor the presence of the lateral π-stacking in case of arenethiols. Hcp and fcc sites are often found to be isoenergetic (33), and generally it is agreed that the "on-top" site is the least favorable among the proposed adsorption sites (9, 27, 34, 35). A recent model based on Grazing incidence X-ray diffraction (36), tries to reconcile these discrepancies by introducing kinetic arguments into the adsorption process and considering it as a two-step phenomenon: in a first instance, the adsorption takes place at the ''on-top'' site and concomitantly the hydrogen from the –SH is lost; this is followed by a second stage, whereby the chemisorbed sulfur diffuses away (either on the gold surface to a more energetically favorable position such as fcc or hcp, or together with a gold atom (26, 37). This last step will depend, inter alia, on temperature – especially in the case where annealing is being used (26), but also on the length of the alkyl chains and therefore on the strength of the van der Waals forces, and is one of the reasons there may exist ''frozen'' domains, with molecules found on both the ''on-top'' sites and/or one of the hollow sites. It has been argued (26) that the strong Au-S bond with energies around 74 kJ/mol for alkanethiols and 46 kJ/mol for arenethiols is sufficient to perturb the

gold lattice and reconstruct its (22 × √3) surface, with subsequent formation of mono or bi-atomic deep gold pits and the formation of Au adatom islands (2). Such effect will be more pronounced in the alkanethiol case than for the arenethiols, due to their different diffusion barriers (26).

We emphasize that, within the ordered domains, the general arrangement in pairs of molecular rows, as well as the distances measured across these rows for either L_1 or L_2 are different than those corresponding to their aromatic moieties flat-lying on the surface, as we and others (45) have determined (e.g., trans-stilbene, that has a similar structure as L_1). The calculated distance of 0.65 nm between the aromatic centers contrasts with the measured average distances of 0.8 nm (L_1) and 0.3 nm (L_2). We therefore propose that while occasionally few L_1 molecules may still be π-stacked on gold, the observed majority thereof is in a "standing-up" disposition with respect to the surface and that both configurations can be found on Au (1,1,1). Such 2D polymorphism may be caused by the reorganization on the surface of various domains . We hypothesize that the higher conductivity is an effect of the increased lateral conduction, as noted in other cases (67, 68). It is also possible that these conductively dissimilar regions may have distinct physical and chemical properties, as observed with other systems (41, 42).

Further evidence that the observed molecular distances are mainly caused by the lateral interactions, for both L_1 and L_2, is supported by comparison with STM results on the adsorption of benzylmercaptan (BM) on gold (29). BM assembles into orderly domains on gold, with a lattice unit of 0.57 ± 0.02 nm, commensurable to gold, without any observed flat-lying domains. The presence of an extra aromatic ring, (and the extra −OH group of L_2) and the flexibility or rigidity between the aromatic rings causes therefore a marked difference in the adsorption and assembly of our molecules i.e. a tight packing for L_2 and a dynamic topographical distribution for L_1 on gold.

2.4.2 Conductance switching

In order to understand the origin of the observed "blinking" on the surface, it is useful to succinctly list the principal hypotheses put forth to explain the conductance switching, as the modulation of the current by these OPV is crucial in the design of future electronic devices. These proposed mechanisms involve the application of a reducing potential that can increase conductance (45), the rotational plane of the lateral groups (i.e. a hydroxyl group for L_2 or a nitro-group from a functionalized OPE - oligo(phenylene-ethynylenes) (46), the free rotation

of the middle OPE phenyl ring (47), bond fluctuations between the sulfur and the gold (48), changes in hybridization states of the Au-S bond (49), changes in the rigidity of the surrounding alkanethiol matrix (50, 51), hopping on-off gold steps (52) and voltage-induced conductance switching (53, 54, 60). Currently, it is accepted that the last four explanations have most experimental support (15). However, we propose that the above-mentioned explanations are not sufficient to account for the molecular conductance switching observed in this study.

In the hypothesized mechanism of a change in the hybridization state i.e. a change in the molecular tilt or in the reconstruction of the substrate (15, 55, 56) between the molecule and the gold substrate, it would be expected that both L_1 and L_2 will have the same tilt with respect to the surface, and that any change imposed on such single molecules by the electric field would lead to switching in both molecular wires; however we have only observed "blinking" in the case of L_1. Another mechanism involves a position exchange across the gold steps − as the molecular wires are likely to insert themselves preferentially along the gold terraces (52); however Figure 10. (panel A, white arrows) clearly indicates the stability of L_1 close to the gold pits for the whole duration (30') of the measurements; as mentioned, L_2 did not exhibit conductance switching regardless of its location on the terraces or on the edges along the terraces. As the degree of rigidity of the alkanethiol matrix is assumed to be similar for both L_1 and L_2 we cannot also invoke rotations of the aromatic moieties, as L_2 should exhibit even more switching events (15). The last proposed mechanism suggests a change in polarizability under imposed bias (54, 57) of the molecule when the voltage sign is reversed: depending on the dipole moment of the molecule, and the positive/negative potential applied, the molecule would be OFF if there is an electrostatic repulsion between the tip and the molecule, and ON if there is an electrostatic attraction. However L_2 does not "switch" even though it contains a polarizable –OH group, and L_1 does switch regardless of the sign of the imposed voltage bias (Figure 10, panel A with -1.4 V applied voltage versus panel B with 1.1 V bias). We suggest therefore that the mechanism behind the switching of L_1 is lateral diffusion in the 1-octanethiol matrix. Such process is indicated in Figure 10, panel B, by the black arrows. It is also likely that L_1 molecules will form through diffusion small aggregates of various sizes. The random orientation and weaker bonding within such spots − when contrasted to the contribution of about 5 kcal/mol brought about by the presence of the H-bonding in the case of L_2 − can be surpassed by a combination of thermal energy excitation (58) and in-plane relaxation of gold lattice upon thiol adsorption (37, 59), with the subsequent

26

formation of a gold adatom and a gold vacancy. The amount of energy released upon adsorption could thus be either dissipated, or used to diffuse on the surface, provided that the energy barriers for diffusion can be overcome (60).

2.5 Conclusions

We have measured the assembly onto gold and the conductive properties of two molecular wires, and described the critical influence that the lateral interactions and Au-S adatom formation may have on the conductance behavior of these molecules. The linkers show enhanced conductivity compared to the thiolalkane matrix, and it is highest for the fully conjugated linker L_1. In contrast with the view that stochastic (random) conductance switching is a general phenomenon in OPEs and OPVs (61,62), this work emphasizes a more nuanced approach with an accent on the structure of the molecular wires, as evidenced by both $I(V)$ spectroscopy and conductance switching events. Similar, yet not identical structures produce differential structural arrangements on the gold lattice, divergent properties as to the lateral dynamics on the surface and markedly different behaviors in conductance modulation. The tailoring of chemical functionalities of such candidates can thus have important consequences for the future rational design of switches that can be successfully integrated into electronic circuitries.

References

1. A. Aviram and M.A. Ratner (1974) *Molecular Rectifiers*. Chem. Phys. Lett., 29, 277-283.

2. J.C. Love, L.A. Estroff, J. K. Kriebel, R.G. Nuzzo and G.M. Whitesides (2005) *Self-Assembled Monolayers of Thiolates on Metals as a Form of Nanotechnology*. Chem. Rev., 105, 1103-1169.

3. F. Chen, J. Hihath, Z.F. Huang, X.L. Li and N.J. Tao (2007) *Measurement of single-molecule conductance*. Ann. Rev. Phys. Chem., 58, 535-564.

4. K.S. Kwok and J.C. Ellenbogen (2002) *Moletronics: future electronics*. Mater Today, 5, 28-37.

5. R.G. Nuzzo (2005) *The future of electronics manufacturing is revealed in the fine print*. Proc. Natl. Acad. Sci. USA, 98, 4827-4829.

6. C.M. Whelan, M. Kinsella, H.M. Ho and M. Karen (2004) *Corrosion Inhibition by Thiol-Derived SAMs for Enhanced Wire Bonding on Cu Surfaces* . J. Electrochem. Soc., 151, 33-38.

7. W. Wang, T. Lee and M.A. Reed (2005) *Intrinsic Electronic Conduction Mechanisms in Self-Assembled Monolayers*. Proc. IEEE, 98.

8. M.A. Reed, W. Wang and T. Lee (2005) *Electron tunnelling in self-assembled monolayers*. Rep. Prog. Phys, 68, 523-544.

9. Y. Yourdshahyan, H. K. Zhang and A.M. Rappe (2001) N-*alkyl thiol head-group interactions with the Au(111) surface*. Phys. Rev. B, 63, 081405.

10. J. Lahan and R.Langer (2005) *Smart materials with dynamically controllable surfaces*. MRS Bull., 30, 185-188.

11. D. Kafer, G. Witte, P. Cyganik, A. Terfort and Ch. Wöll (2006) *A comprehensive study of self-assembled monolayers of anthracenethiol on gold: solvent effects, structure, and stability*. J. Am. Chem. Soc., 128, 1723-1732.

12. P. Cyagnik and M. Buck (2006) *Competition as a Design Concept: Polymorphism in Self-Assembled Monolayers of Biphenyl-Based Thiols*. J. Am. Chem. Soc. 128, 13868-13878.

13. P. Cyagnik, M. Buck, W. Azzam and Ch. Woll (2004) *Self-Assembled Monolayers of -Biphenylalkanethiols on Au(111): Influence of Spacer Chain on Molecular Packing*. J Phys. Chem. B, 108, 4989-4996.

14. W. Azzam, P. Cyganik, G. Witte, M. Buck and Ch. Wöll (2003) *Pronounced Odd-Even Changes in the Molecular Arrangement and Packing Density of Biphenyl-Based Thiol SAMs: A Combined STM and LEED Study*. Langmuir, 19, 8262-8270.

15. A.M. Moore, A.A. Dameron, B.A. Mantooth, R.K. Smith, D.J. Fuchs, J.W. Ciszek, F. Maya, Y.Yao, J.M. Tour and P.S. Weiss (2006) *Molecular Engineering and Measurements To Test Hypothesized Mechanisms in Single Molecule Conductance Switching*. J. Am. Chem. Soc. 128, 1959-1967.

16. R.F. Heck and J.P. Nolley (1972) *Palladium–catalyzed vinylic hydrogen substitution reactions with aryl, benzyl and styryl halides*. J. Org. Chem., 37, 2320-2300.

17. T. Mizoroki, K. Mori and A. Ozaki (1971) *Arylation of olefin with aryl iodide catalyzed by palladium*. B. Chem. Soc. Jpn, 44, 581.

18. I.P. Beletskaya and A.V. Cheprakov (2000) *The Heck Reaction as a Sharpening Stone of Palladium Catalysis*. Chem. Rev., 100, 3009-3066.

19. L.Yin and J.Liebscher (2007) *Carbon-Carbon Coupling Reactions Catalyzed by Heterogenous Palladium Catalysts*. Chem. Rev., 100, 133-173.

20. P.D. Dudek, H.D. Sikesm and C.D. Chidsey (2001) Synthesis of Ferrocenethiols Containing Oligo(phenylenevinylene) Bridges and Their Characterization on Gold Electrodes. J. Am. Chem. Soc., 123, 8033-8038.

21. O. Mitsunobu and M. Yamada (1967) Preparation of esters of carboxylic and phosphoric acid via quaternary phosphonium salts. M. Bull. Chem. Soc. Jpn, 40, 2380-2382.

22. B.H. Lipshutz, D.W. Chung, B. Rich and B.R. Corral (2006) Simplification of the Mitsunobu reaction. Di-p-chlorobenzyl azodicarboxylate: a new azodicarboxylate. Org. Lett, 8, 5069-5072.

23. F. Schreiber (2004) *Self-assembled monolayers: from 'simple' model systems to biofunctionalized interface*. J Phys: Condens. Matt, 16, 881-900.

24. C. Vericat, M.E. Vela, G.A. Benitez, J.A.M. Gago, X. Torrelles and R.C. Salvarezza (2006) *Surface characterization of sulfur and alkanethiol self-assembled monolayers on Au(111)*. J Phys: Condens. Matt, 18, 867-900.

25. H. Park (2006) *PhD thesis,* Columbia University.

26. G. Yang and Gang-yu Liu (2003) *New Insights for Self-Assembled Monolayers of Organothiols on Au(111) Revealed by Scanning Tunneling Microscopy*. J Phys. Chem. B, 107, 8746-8759.

27. C. Vericat, M.E. Vela and R.C. Salvarezza (2005) *Self-assembled monolayers of alkanethiols on Au(111): surface structures, defects and dynamics*. Phys. Chem. Chem. Phys, 7, 3258.

28. W. Azzam, A. Bashir, A. Terfort, T. Strunskus and Ch. Wöll (2006) *Combined STM and FTIR characterization of terphenylalkanethiol monolayers on Au(111): Effect of alkyl chain length and deposition temperature*. Langmuir, 22, 3647-3655.

29. L. Hallmann, A. Bashir, T. Strunskus, R. Adelung, V. Staemmler, Ch. Woll and F. Tuczek (2008) *Self-Assembled Monolayers of benzylmercaptan and p-cyanobenzylmercaptan on Au(1,1,1) surfaces: Structural and spectroscopical characterization*. Langmuir, 24, 5726-5733.

30. M.G. Roper (2004) *Atop adsorption site of sulphur head groups in gold-thiolate self-assembled monolayers*. Chem. Phys. Lett., 87-91.

31. H. Kondoh, M. Iwasaki, T. Shimada, K. Amemiya, T. Yokoyama and S. Kono (2003) *Adsorption of Thiolates to Singly Coordinated Sites on Au(111) Evidenced by Photoelectron Diffraction*. Phys. Rev. Lett, 90, 066102.

32. V. de Renzi, R. Di Felice, D. Marchetto, R. Biagi, U. del Pennino and A. Selloni (2004) *Ordered (3 × 4) High-Density Phase of Methylthiolate on Au(111)*. J Phys. Chem. B, 108, 16-20.

33. M. Tachibana, K. Yoshizawa, A. Ogawa, H. Fujimoto and R. Hoffmann (2002) *Sulfur-Gold Orbital Interactions which Determine the Structure of Alkanethiolate/Au(111) Self-Assembled Monolayer Systems*. J Phys. Chem. B, 106, 12727-12736.

34. J. Gottschalck and B. Hammer (2002) *A density functional theory study of the adsorption of sulfur, mercapto, and methylthiolate on Au(111)*. J Chem. Phys., 116, 784.

35. Y. Akinaga, N. Takahito and H. Kimihiko (2001) *A density functional study on the adsorption of methanethiolate on the (111) surfaces of noble metals*. J Chem. Phys, 114, 8555.

36. X. Torrelles, C. Vericat, M.E. Vela, M.H. Fonticelli, M.A. Daza Millone, R. Felici, T. L. Lee, J. Zegenhagen, G. Muñoz, J.A. Martín-Gago and R.C. Salvarezza (2006) *Two-Site Adsorption Model for the (3 × 3)-R30 Dodecanethiolate Lattice on Au(111) Surfaces*. J. Phys. Chem. B, 110, 5586-5594.

37. M. Yu, N. Bovet, C. J. Satterley, S. Bengio, K. R. J. Lovelock, P. K. Milligan, R. G. Jones, D. P. Woodruff and V. Dhanak (2006) *True nature of an archetypal self-assembly system: Mobile Au-thiolate species on Au(111)*. Phys. Rev. Lett, 97, 166102.

38. D. Travor, C. E. D. Chidsey and D. N. Loiacono (1989) *In Situ Scanning-Tunneling-Microscope Observation of Roughening, Annealing, and Dissolution of Gold (111) in an Electrochemical Cell*. Phys. Rev. Lett, 62, 929-932.

39. F. Cunha, N.J. Tao, X.W. Wang, Q. Jin, B. Duong and J. D'Agnese (1996) *Potential-Induced Phase Transitions in 2,2 -Bipyridine and 4,4 -Bipyridine monolayers on Au(111) Studied by in Situ Scanning Tunneling Microscopy and Atomic Force Microscopy*. Langmuir, 12, 6410-6418.

40. L. Grill (2008) *Functionalized molecules studied by STM: motion, switching and reactivity*. J. Phys. - Condens. Mat, 20, 053001.

41. P. Jiang, A. Nion, A. Marchenko, L. Piot and D. Fichou (2006) *Rotational Polymorphism in 2-Naphthalenethiol SAMs on Au(111)*. J Am. Chem. Soc. 128, 12390-12391.

42. T. Ishida, W. Mizutani, N. Choi, U. Akiba, M. Fujihira and H. Tokumoto (2000) *Structural Effects on Electrical Conduction of Conjugated Molecules Studied by Scanning Tunneling Microscopy*. J. Phys. Chem. B, 104, 11680-11688.

43. L.A. Bumm, J.J. Arnold, M.T. Cygan, T.D. Dunbar, T. P. Burgin, L. Jones II, D. L. Allara, J. M. Tour and P.S. Weiss (1996) *Are single molecular wires conducting?* Science, 271, 1705-1707.

44. E.J. Sturrock, Q. Chen, P.H. Borchardt and N.V. Richardson (2004) *Coverage dependent change in orientation for the adsorption of benzyl mercaptan on Au(1 1 1)*. J Electron Spectrosc, 135, 127-134.

45. C.S. Tsai, C. Su, J. Wang and J.C. Lin (2003) *STM Study of trans-Stilbene Self-Organized on the Ag/Ge(111)-(v3 x v3)R30° Surface*. Langmuir, 19, 822-829.

46. M. DiVentra, S.G. Kim, S. T. Pantelides and N. D. Lang (2001) *Temperature Effects on the Transport Properties of Molecules*. Phys. Rev. Lett, 86, 288.

47. J. Cornil, Y. Karzazi and J. L. Brédas (2002) *Negative differential resistance (NDR) in phenylene ethynylene oligomers*. J Am. Chem. Soc., 124, 3516-3517.

48. G.K. Ramachandran, T.J. Hopson, A.M. Rawlett, L.A. Nagahara, A. Primak and S.M. Lindsay (2003) *A Bond-Fluctuation Mechanism for Stochastic Switching in Wired Molecules*. Science, 300, 1413-1415.

49. H. Sellers, A. Ulman, Y. Shnidman and J. E. Eilers (1993) *Structure and binding of alkanethiolates on gold and silver surfaces: implications for self-assembled monolayers.* J Am. Chem. Soc. 130, 9389-9401.

50. Z.J. Donhauser, B.A. Mantooth, T.P. Pearl, K. F. Kelly, S.U. Nanayakkara and P. S. Weiss (2002) *Matrix-Mediated Control of Stochastic Single Molecule Conductance Switching.* Jpn. J app. phy, 41, 4871-4877.

51. Z.J. Donhauser, B.A. Mantooth, K. F. Kelly, L.A. Bumm, J.D. Monnell, J. J. Stapleton, D. W. Price Jr., A.M. Rawlett, D.L. Allara, J.M. Tour and P.S. Weiss (2001) *Conductance Switching in Single Molecules Through Conformational Changes.* Science, 292, 2303-2307.

52. A.M. Moore, B.A. Mantooth, Z.J. Donhauser, F. Maya, D.W. Price, Y. Yao, J. M. Tour and P.S. Weiss (2005) *Cross-Step Place-Exchange of Oligo(phenylene-ethynylene) Molecules.* Nano Lett., 5, 2292-2297.

53. S.W. Wu, N. Ogawa, G.V. Nazin and W. Ho (2008) *Conductance Hysteresis and Switching in a Single-Molecule Junction.* J Phys. Chem. C, 112, 5241-5244.

54. A. Szuchmacher-Blum, J.G. Kushmerick, D.P. Long, C.H. Patterson, J.C. Yang, J.C. Henderson, Y. Yao, J.M. Tour, R. Shashidhar and B.R. Ratna (2005) *Molecularly inherent voltage-controlled conductance switching.* Nat. mater, 4, 167-172.

55. J. Choi, M Chipara, B. Xu, C. S. Yang, B. Doudin and P. A. Dowben (2001) *Comparison of the π-conjugated ring orientations in polyaniline and polypyrrole.* Chem. Phys. Lett, 343, 193-200.

56. P.E. Kornilovitch and A.M. Bratkovsky (2001) *Orientational dependence of current through molecular films.* Phys. Rev. B, 64, 195413.

57. P.A. Lewis, C E. Inman, F Maya, J M. Tour, J E. Hutchison and P. S. Weiss (2005) *Molecular Engineering of the Polarity and Interactions of Molecular Electronic Switches.* J Am. Chem. Soc., 127, 17421-17426.

58. S. Wakamatsu, S. Fujii, U. Akiba and M. Fujihira (2004) *The dynamical behavior of a single molecule inserted in a self-assembling monolayer matrix at room temperature.* Nanotechnology, 15, 137-141.

59. F.T. Arce, M.E. Vela, R.C. Salvarezza, and A.J. Arvia (1998) *The dynamic behavior of butanethiol and dodecanethiol adsorbates on Au(111) terraces.* J Chem. Phys, 14, 5703-5706.

60. K. Seo and E. Borguet (2007) *Potential-Induced Structural Change in a Self-Assembled Monolayer of 4-Methylbenzenethiol on Au(111).* J Phys. Chem. C, 111, 6335-6342.

61. R.A. Wassel, R.R. Fuierer, N. Kim and C.B. Gorman (2003) *Stochastic Variation in Conductance on the Nanometer Scale: A General Phenomenon.* Nano Lett., 3, 1617-1620.

62. A. Rochefort, M. Richard and A. Phaedon (2002) *Electrical Switching in ð-Resonant 1D Intermolecular Channels.* Nano Lett. 2, 877-880.

63. I. Horca, R. Fernández, J. M. Gómez-Rodríguez, J. Colchero, J. Gómez-Herrero and A. M. Baro (2007) Rev. Sci. Instrum., 78, 013705.

64. D. Kockmann, B. Poelsema and H.J.W. Zandvliet (2009) *Transport through a Single Octanethiol Molecule.* Nano Lett. 9, 1147-1151.

65. Z.Y. Hua and W. Xu (1997) *Imaging, polymerization, and reconstruction of polystyrene films with a scanning tunneling microscope*. J Vac. Sci. Technol. B, 15, 1353-1358.

66. R.W. Zehner (1998). *PhD thesis*, Chicago University.

67. A. Landau and A.Nitzan (2009) *Cooperative Effects in Molecular Conduction II: The semiconductor-Metal Molecular Junction*. J Phys. Chem. A, 113, 7451-7460.

68. Y. Yokota, K. Fukui, T. Enoki and M. Hara (2007) *Strong Intermolecular Electronic Coupling within a Tetrathiafulvalene Island Embedded in Self-Assembled Monolayers*. J Am. Chem. Soc., 129, 6571-6575.

69. D. Tor (1994) *The Nature of Stacking Interactions between Organic Molecules Elucidated by Analysis of Crystal Structures*. Acta Chem. scand, 48, 95-105.

70. X. Ye, Zhen-Hua Li, W. Wang, K. Fan, W. Xu and Z. Hua (2004) *The parallel π-π stacking: a model study with MP2 and DFT methods*. Chem Phys. Lett, 397, 56-61.

Chapter 3:

Scanning Probe Microscopy of alkanethiol-embedded conductive wires

Razvan C. Stan[1], Ben Peters[2], Frank G.M. Wiertz[3], Jason J. Davis[2], Hendrik A. Heering[3], Gerard W. Canters[3], Thijs J. Aartsma[1]

[1] Department of Biophysics, Huygens Laboratory, Leiden University, 2300 RA, Leiden, The Netherlands
[2] Department of Chemistry, Oxford University, OX1 3TA, Oxford, United Kingdom
[3] Department of Chemistry, Gorlaeus Laboratory, Leiden University, 2333 CC, Leiden, The Netherlands

Abstract: *The distribution and the electron transfer properties of a conductive molecular wire embedded within a supportive alkanethiol matrix on a gold substrate have been investigated by Scanning Tunneling Microscopy and Conductive-Atomic Force Microscopy. The molecule itself has the potential of binding to an engineered redox protein cavity such that it can mediate its attachment onto a supportive electrode. The current-voltage spectroscopy of the molecular wire presents reversible peak-shaped I(V) characteristics, suggestive of a HOMO-LUMO mediated electron transfer mechanism and are well-fitted to the Simmons equation for tunneling through an insulating barrier. The results also point to specific adsorption sites within the insulating matrix, according to the use of different surface functionalization protocols.*

3.1 Introduction.

Self-assembling monolayers (SAM) are important models in understanding the electrical, optical and mechanical properties of the adsorbed organic films, due to their stability and highly-ordered 2D structures they form onto appropriate metals (Au, Ag, Cu etc) or semi-conductor surfaces (InP). The quintessential alkanethiol SAM films have been extensively studied with various surface science techniques such as Scanning Probe Microscopy, electrochemistry, ellipsometry, IR and Raman spectroscopy etc., and by Density-Functional Theory based approaches. Aside from investigating the topographical details of the self-assembly on surfaces, the understanding of the electron transfer through organic layers is important in the future design of single molecule or single electron devices and in the optimization of current molecular devices (i.e. organic light emitting diodes).

Main research objectives have been the uncovering of the mechanisms involved in the electron transfer (ET) occurring via the alkanethiols, the influence of the molecular structure (in terms of molecular length, existence of lateral chemical groups or alternating single and double bonds etc.) and the presence of adjacent molecules in mediating electrical conduction, the nature of contact with the underlying surface and its influence on the ET through the films. It has been determined that their insulating properties depend not only on the length of the alkyl chain and the relative energy positions of the Highest Occupied and Lowest Unoccupied Molecular Orbitals (HOMO-LUMO band gap), but also on the electrode work function, conformational changes and molecular orientation. Consequently, in recent years, there has been an increasing interest in using aromatic molecules instead of alkanethiols to create SAMs, for a number of reasons amongst which the superior structural quality of the films (in terms of film defects) and their higher electrical conductivity (due to the delocalized electrons present in their π-moieties) stand out.

In this study, the work described in chapter 2 regarding the specific attachment of two molecular wires onto gold surfaces is extended to include the electron transfer characteristics of single-molecules in more detail, as measured with the Scanning Tunneling Microscope (STM) and Conductive-Atomic Force Microscope (C-AFM). The aim is to understand the electrical properties of such individual hot-wires with the goal of further using them as 'linkers' that can intermediate a protein metal center to an underlying electrode, via a molecular conductive pathway (1, 2). Moreover, this study is unique in that C-AFM is used to directly study the ET properties of OPV (oligo-phenylenevinylenes) conductive wires,

without the mediation of a "marker" gold nanoparticle, such that reliable electrical current characteristics and applied force values can be directly determined.

3.2 Experimental section

Gold surfaces: Freshly cleaved V-1 grade mica (SPI) was used as a substrate to RF sputter 250-270 nm thick gold films. The polycrystalline gold was subsequently annealed so as to obtain recrystalized terraces, with roughness (rms) values of 0.5-0.7 nm on 500×500 nm^2 large surfaces, as determined by AFM measurements (result not shown).

Linkers: The molecular wire (Fig. 1) was kindly provided by Dr. Alexander Kros. Its synthesis was described in Chapter II.
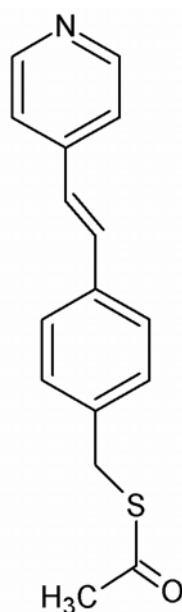

Figure 1. Structure of the *S*-{4-[(*E*)-2-pyridin-4-ylethenyl]benzyl} ethanethiolate used in this study. The acetate group is removed during incubation by addition of 2 μL aqueous ammonia.

Sample preparation: A series of alkanethiols have been used, ranging from hexanethiol (C$_6$) to undecanethiol (C$_{11}$) with main focus on octanethiol (C$_8$). Both the linker and the alkanethiol Self-Assembling Monolayers (SAM) were dissolved in NMP (N-methyl pyrrolidone). We have used two incubation methods, based on whether the linkers were added together with the alkanethiols (co-assembly) or prior to incubation with alkanethiols (pre-assembly). For the co-assembly method the freshly prepared Au(1,1,1) surfaces were incubated with a mixture of alkanethiols (throughout this study at 1mM concentration) and linkers (with concentrations

ranging from 0.1 to 0.001 mM) for 22-24 h at room temperature and washed afterwards with NMP. Alternatively, the Au surfaces were first incubated with linkers for 1 h, followed by rinsing with solvent and subsequent addition of alkanethiols and then incubating for another 22 h, also at room temperature.

STM/ C-AFM: A PicoSPM I (Agilent Technologies) equipped with a S-scanner and a Digital Instruments Multimode Microscope (Veeco) with a Nanoscope IIIa controller were used for the Scanning Tunneling Microscopy (STM) work, while a PicoLE microscope (with a current to voltage converter of 1VnA-1 sensitivity) was used for Conductive Atomic Force Microscopy (C-AFM) measurements. The conductive AFM probes (Cont-E-10, Nanoandmore, Germany) were coated with Pt (25nm) or Au (25nm, RF sputtered in house) and Cr (adhesion layer ~ 2nm) and had a nominal spring constant of 0.2N/m, while mechanically cut Pt/Ir tips (Veeco, USA) were used for STM and STS (scanning tunneling spectroscopy) work. To reduce the water and oxygen content, all conductive measurements were acquired while continuously flushing with N2 in a home-made environmental chamber.

UV-Vis measurements: Optical absorption spectra of linkers (0.1 mM, dissolved in ethanol). were collected using a Shimadzu spectrophotometer (UV-3101, PC) at room temperature.

3.3 Results

3.3.1 Topographical measurements

3.3.1.1 STM measurements.

Proximal probe techniques like STM and C-AFM are important in analyzing the self-assembly and electrical properties of single molecules or clusters of few molecules, in contrast with other techniques that involve comparatively much larger areas, as in the use of ellipsometry or electrochemistry (5, 6). STM is highly sensitive in obtaining the best molecular resolution in plane (xy), generally at the expense of the unknown z-position, whereas C-AFM ensures the vertical control of the tip, due to its force-feedback, but with a decreased resolution (because of the sheer size of the scanning tip with respect to the feature being probed). Since STM measurements of samples incubated with solutions containing only linkers on gold have not shown any recognizable domains (results not presented), we have attempted to use the alkanethiol SAM as structural props for our molecular wires. These alkanethiol-based SAMs are known to self-assemble within minutes in small, densely-packed,

36

ordered domains (8, 9). The goal is to ensure that the linkers are mainly present on the gold terraces, so that the imaging with a C-AFM scanning probe is facilitated. Figure 2 shows representative STM micrographs of C_8-SAM prepared in the absence of linkers or along with linkers, according to the two incubation methods employed (fig 2b-d).

Figure 2a shows the domains formed by octanethiol monolayer assembly on gold, with the monoatomic gold vacancies (pits) created by the thiols' adsorption indicated by arrows. Barring the presence of impurities, the surface is homogenously covered with alkanethiols, with exposed gold available only along the step edges, or at the congruence between octanethiol domains (12, 13). Figures 2b and 2c present a mixed-phase molecular film
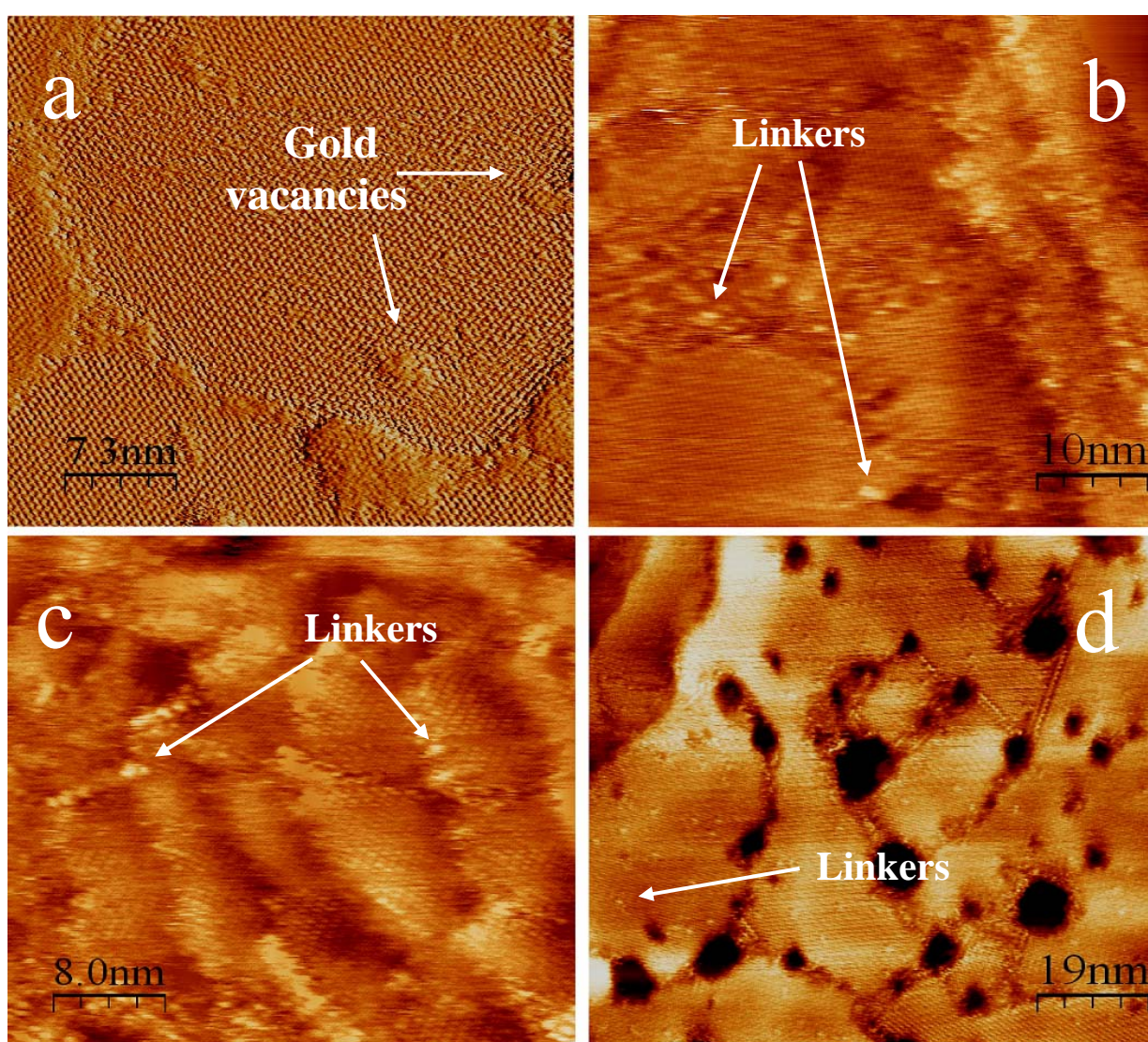

Figure 2. a) STM Current image of pure octanethiols on Au(1,1,1); constant height mode, I = 200pA, V = 375mV. b) STM Height image of a heterogeneous film prepared by the pre-assembly procedure; linker concentration is 0.1 mM; constant current mode, c) STM Height image of a mixed SAM prepared by pre-adsorption; linker concentration is 0.01 mM; constant current mode d) STM Height image of mixed SAM prepared by the co-assembly protocol, with the linker concentration at 0.1mM. Tunneling parameters in Fig. 2 b-d are I = 86pA, V = 860mV.

prepared by pre-assembling the linkers (at 0.01 and 0.1mM concentration, respectively), followed by alkanethiol adsorption. The relatively few spots observed contrast with the increase in number of linkers observed when the heterogeneous films were prepared by co-assembly, as shown in Figure 2.d. Furthermore, we note the differential distribution of the linkers on the surface according to the incubation method: when pre-assembled, the linkers tend to be located close to the film defects/step edges, while when co-adsorption protocol was used, the molecular wires are "trapped" within alkanethiol domains (Figure 2c. versus Figure 2d.). Although we prepared solutions whereby the linker concentration varied by orders of magnitude, the STM images did not show a corresponding increase in number of conductive spots, similar with STM measurements on other systems (32). We propose that the reason for this discrepancy lies with the faster adsorption kinetics of alkanethiols that will obscure the increase in concentration of the molecular wires; we also note the difficulty of assessing whether a bright spot observed with STM consists of one or several clustered linkers.

3.3.1.2 Conductive-AFM measurements

Conductive-AFM experiments were aimed at obtaining topographical information related to the linker distribution within the SAM, and at acquiring current-voltage spectra of individual spots, once stable scanning had been achieved. Two representative examples of the same discrepant topographical assembly observed for the molecular wires with STM are shown in Figure 3, presenting current images of mixed monolayers prepared by co-assembly and pre-
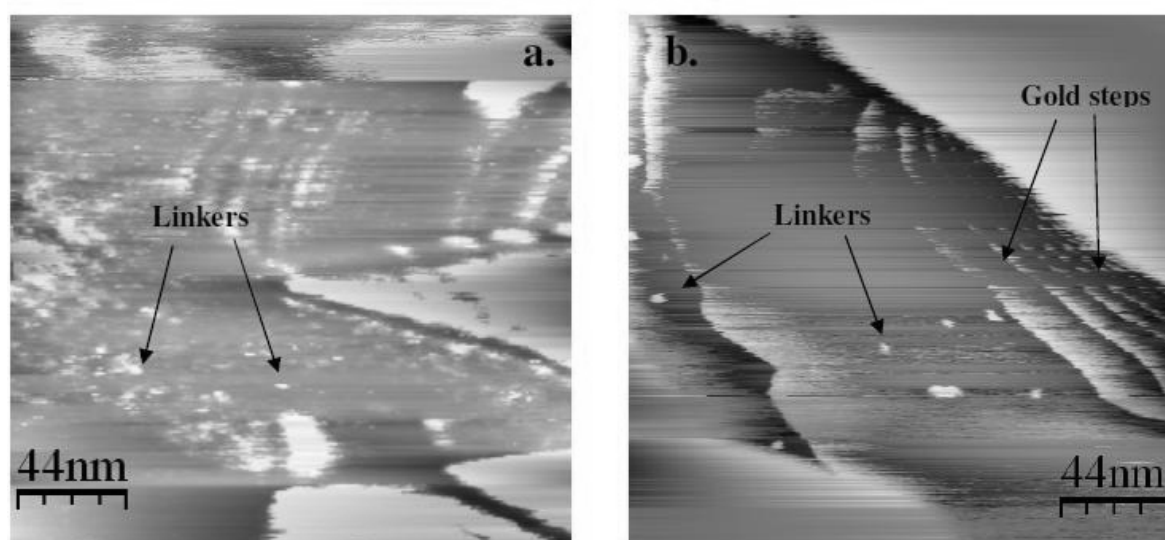

Figure 3. Left: C-AFM current image of a mixed SAM prepared by co-assembly; a multitude of bright (conductive) spots are visible. Right: C-AFM current image of a heterogeneous surface prepared by linker pre-adsorption; few conductive spots are present, along with visible gold steps. Both images taken at ~ 4nN applied force.

38

adsorption, respectively. Numerous bright (i.e., more conductive) spots of various sizes are noticeable; we assume that these are the physically higher, more conductive linkers (indicated by arrows). In turn, figure 3.b. presents fewer bright spots on a sample prepared with linker pre-assembling method, in line with the STM observations, the different nature of the contact with the functionalized surface notwithstanding. We note that the lower number of conductive features differs from the STM results, possibly because of the large C-AFM tip that cannot probe linkers situated in the deep trenches between Au terraces – as large as 10 nm (results not shown), or when present along the steps of the gold terraces.

3.3.2 Conductance measurements

Once the presence of the molecular wires was assessed on the alkanethiol-functionalized gold surface, spectroscopic measurements were performed with both the STM and C-AFM by positioning the scanning probe on top of the point of interest, disengaging the feedback and then recording a current while sweeping the bias. For STM, since the tunneling should ideally only occur at the outermost atom of the tip, the *I(V)* spectra were only acquired once the alkanethiol atomic lattice had been resolved. This approach may ensure the conductance measurements of only a single molecule in the tunneling gap. Since such resolution is not possible in C-AFM, we have acquired the *I(V)* spectra of the conductive spots when the gold steps/pits were also present in the images so they could serve to verify the integrity of the tip and assess the adequacy of image resolution, based on the STM/C-AFM topographical images (Fig. 2 and 3). Within the instrument's limitations (mainly the thermal drift) the *I(V)* spectra were reproducible, regardless of the incubation method. When using the Current-sensing AFM for *I(V)* measurements, care has been taken that the forces applied did not perturb the films, as evidenced from the images taken after the acquisition of *I(V)* curves. All the reported force values shown in Figure 4 have a 10 - 15% uncertainty, due to the uncertainty of the nominal spring constants of the tips (the noise in the individual *I(V)* curves is < 0.2 pA). Sets of *I(V)* curves acquired at different applied forces are shown in Figure 4, along with the STS data on the linkers.

Figure 4 summarizes the *I(V)* data obtained with both C-AFM and STM. The insert in Fig. 4b shows that the current response of the C8 SAM is an order of magnitude lower compared to the values observed when the tip is positioned on top of the linker molecule. Of note are the Negative Differential Resistance (NDR) features (exemplified by the arrow in Fig. 4.a.) present in most *I(V)* spectra at 0.65 - 0.8 V substrate bias, for each value of applied force.
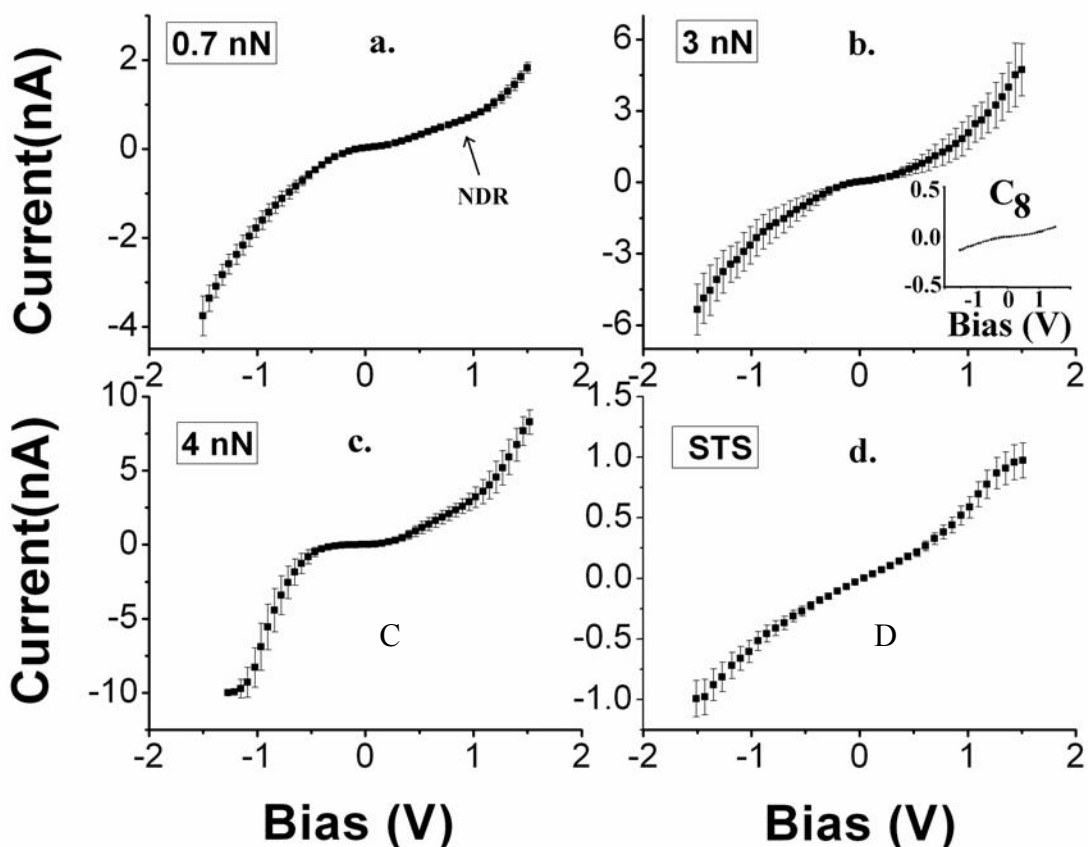
Figure 4. a-c) C-AFM I(V) spectra of various linker spots at different values of applied forces; inset in Fig.4b presents a typical response obtained over different C8 spots d) STS IV measurements of linkers (105 curves, averaged); I = 120 pA, U = −0.4 V. Noise in all I(V) curves is < 0.2pA.

NDR features are not observed in the *I(V)* spectra obtained on the C_8 SAM (result not shown), which suggests that theyr are associated with intronsici properties of the linker molecule.

These NDR characteristics represent a decrease in detected current with the increased bias, and are due to the modulation of the charge transport by various molecular mechanisms (i.e. conformational changes, charging effects, bond fluctuation etc). We also note here the increase in current magnitude with applied force, which translates into a shorter barrier length. Figure 4d shows the average of the *I(V)* data obtained with the STM on linkers. By comparing the spectra obtained with STM versus those obtained by C-AFM, it is evident that the magnitude of the current is lower, probably due to insulating air gap that exists between the C-AFM tip and molecules being probed.

Based on the STM constant current operating mode, the conductance in the tunneling gap over each molecular phase can be used to estimate both the decay constant value β and
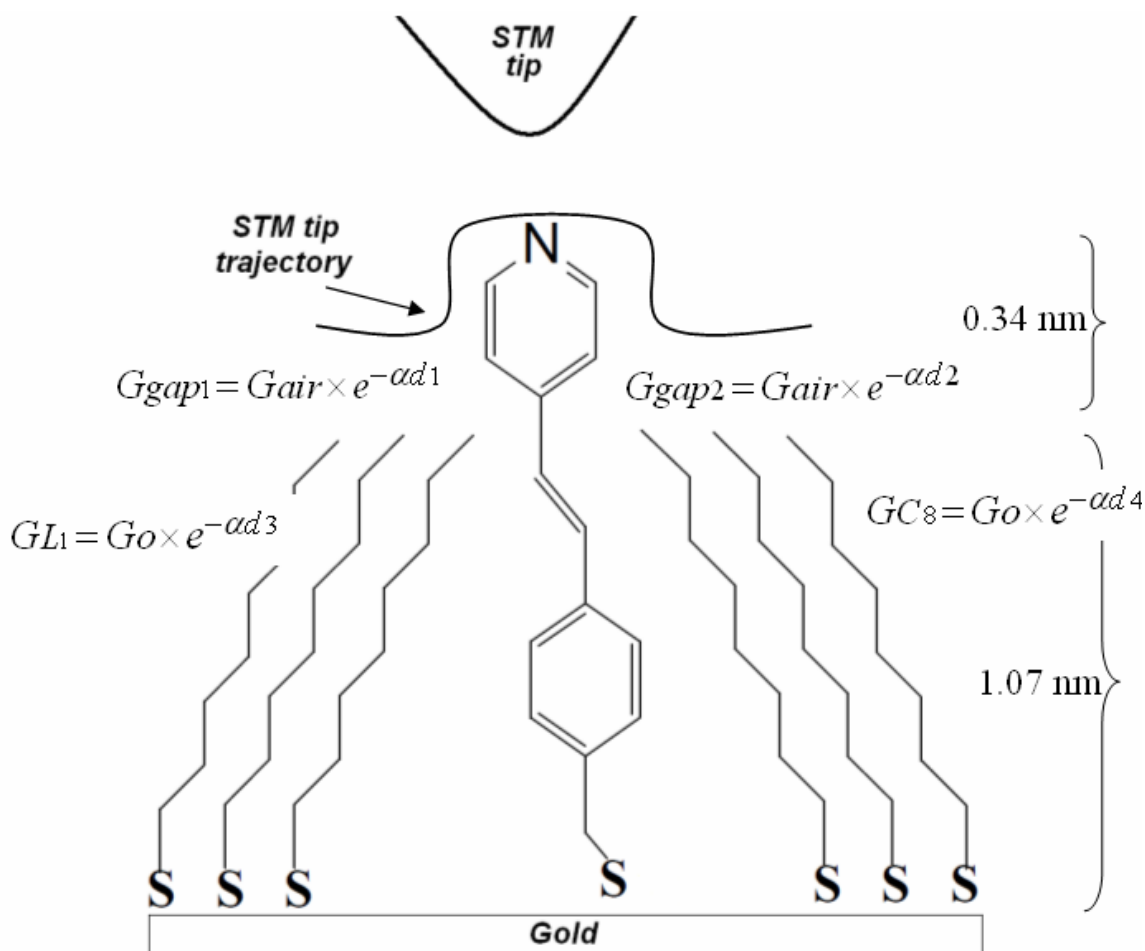
Figure 5. Proposed model of L_1 and C_8 attachment on Au (111). Distances were calculated using HyperChem 7 from HyperCube, Inc. STM tip (not drawn to scale) is shown in its trajectory on top of the film, when operated in constant current mode. The conductance in the tunneling junction is the product of the conductance of either molecular phase multiplied by that of the air gap between the STM tip and film (explanations in text)

the distance atop the film, as depicted in Figure 5. It presents the proposed model of interaction between L_1 and the C_8 along with their relative heights above the surface; L_1 is shown in a "standing-up" configuration on the gold lattice, based on the angle that the Au-S-C atoms encompass of approximately 100° (24). The alkanethiol molecules are tilted by ~ 30°, hence their lower heights on the surface compared to a standing-up configuration; the pyridine ring from L_1 protrudes above the SAM matrix.

Because the transconductance across the barrier is dependent on the probability of electrons tunneling from the tip to the gold surface (22, 23), its value is a product of the conductances of the air gaps and molecules:

$$G_T = G_{films}G_{air} \tag{3.1}$$

41

Each conductance term can be expressed as $G = G_0 e^{-\beta L}$ where G_0 is the contact conductance, β is the decay constant and L is the molecular height/ gap distance between STM tip and molecules. Values for β of the air gap ($\beta_{1,4} = 2.3$ Å^{-1}) and C_8 ($\beta_3 = 0.95$ Å^{-1}) are available from literature (22), while the height profiles for linkers ($L_2 = 1.42$ nm) and C_8 ($L_3 = 1.04$ nm) were calculated. It follows from (3.1) that

$$G_T = G_{Linker}G_{gap\ 1} = G_{C8}G_{gap\ 2} \qquad (3.2)$$

As the G_T can be calculated from the tunneling conditions used prior to *I(V)* data acquisition (I = 20 pA, V = −1400 mV), it is possible to estimate the decay constant of a linker molecule $\beta = 0.49$ Å^{-1}.

3.3.3 Optical absorption measurements of the linker constructs

UV-Vis spectra were collected in order to estimate the band gap energy, as shown in Figure 6. From the onset of the absorption (344 nm), as determined by the tangent to the abscissa, we determine a value of the energy band gap of 3.6 eV (see Discussion).

3.4 Discussion

The current model for tunneling through π-conjugated systems and saturated molecules is based on the theoretical work of Simmons (14, 15), that is best applied to the Metal-Insulator-Metal (MIM) structures with gaps between 0.6 - 2 nm, which is within the range of our molecules. Because of the large variations in reported data possible conduction mechanisms
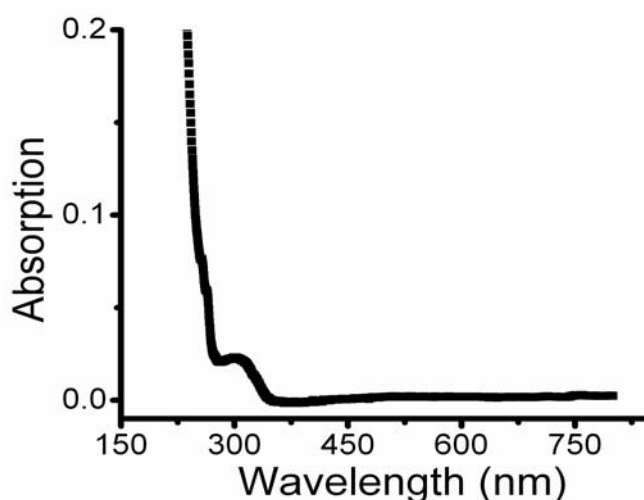

Figure 6. Absorption spectrum of 100 μM linkers (in EtOH).

are the subject of ongoing debate (3,4,16), however, based on whether the electron transfer is thermally activated or not, they fall into two main categories (for the low-bias regime): 1) thermionic (hopping) conduction and 2) direct, temperature-independent tunneling. It has been shown (17) that for alkanethiols, at a temperature ranging from 80K to 300K and a bias range of 0.0 to 1.0 V there is no tunneling dependence on temperature, and direct tunneling is likely to be the mechanism of electron transfer in such MIM. Moving from the conventional one-dimensional case of an electron of energy E tunneling through a potential barrier of a height V and length L, where the transmission probability will be proportional to $e^{-\beta L}$ and $\beta(\text{Å})$ = 1.02 $\sqrt{(\varphi/eV)}$ with φ being the barrier height $V - E$ (the electron energy), onto the case where an electron tunnels through an organic molecule, we note that the potential barrier is replaced by the molecular orbitals of the molecules in the tunneling gap (assuming uniform electron distribution over the molecules involved). In using the Simmons model for this mechanism, the $I(V)$ curves must contain both the slope in the low-bias regime (ohmic behavior) and the exponential increase in current at higher bias, as observed for our system, while excluding the dielectric breakdown (17).

For small voltages the Simmons equation (20) writes as:

$$I = I_0 \left\{ \overline{\varphi} e^{-LA\sqrt{\overline{\varphi}}} - (\overline{\varphi} + eV) e^{-LA\sqrt{\overline{\varphi}+eV}} \right\} \tag{3.3}$$

where I is the detected current, V is the applied bias, L is the barrier width (molecular height for C-AFM), I_0 is a constant, $A = 2(2m)^{1/2}/\hbar$, and $\overline{\varphi}$ is the mean height of the energy gap between the Fermi level and the band edge (HOMO, or LUMO) [21]. If one assigns $\beta = A\varphi^{-1/2}$
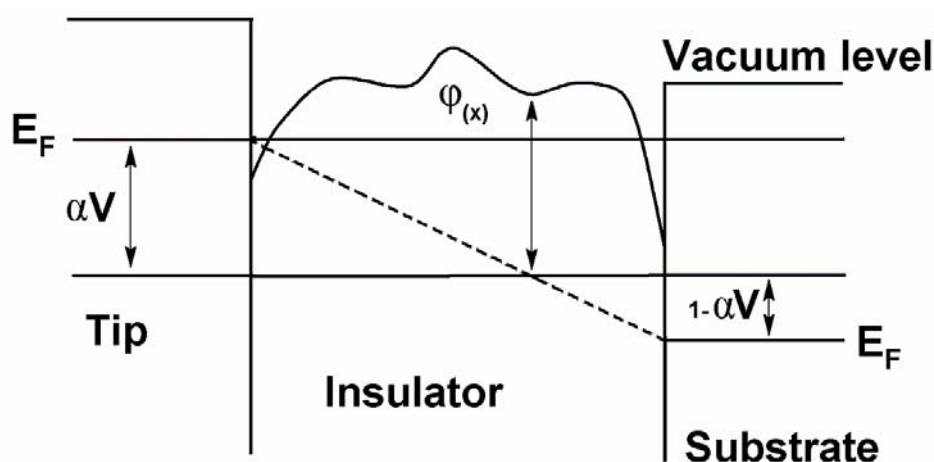

Figure 7. Band diagram of a molecular junction when ramping the bias. Adapted from (25).

the equation above should indicate a direct proportionality between *I* and *V* and an exponential dependence with distance. Because of both the asymmetrical molecule (L_1) and the asymmetry in the tip-substrate junction (i.e. a chemical contact established via the thiol head-group, and a physical contact made with the STM/C-AFM tip), the symmetrical equation (1.4) can be modified (25-26) such that the dissimilar voltage drop across the molecules can be divided in two components as follows:

$$V = \alpha V + (1 - \alpha V) \tag{3.4}$$

where αV is the elevated tip potential, and $(1 - \alpha V)$ the reduced potential of the substrate, as depicted in Figure 7. The current density across the molecules can now be expressed as:

$$I = \frac{e^2}{2\pi h L^2}\left\{(\varphi - \alpha V)e^{-K(\varphi - \alpha V)^{1/2}} - (\varphi + (1 + \alpha)V)e^{-K(\varphi + (1 - \alpha)V)^{1/2}}\right\} \tag{3.5}$$

where $K = 4\pi L/h \, (2me)^{1/2}$, *m* is electron mass, *e* is the electron charge and α is an asymmetry factor (when it equals 0.5, eq. (1.5) reverts to (1.3)) . It is conceivable that when performing *I(V)* spectroscopy with the C-AFM, because of the large size of the (coated) tips and the forces applied, the supporting alkanethiol matrix is also being probed, especially if the tip penetrates the monolayer, and this contribution in lateral conduction to the overall shape and amplitude of the current-voltage response has to be addressed. For each *I(V)* curve obtained on a linker 'spot' we have measured *I(V)* responses of the surrounding matrix; these were uniform and reproducible for a specific force applied (as shown in Figure 4b - inset). After subtracting the measured current response of the alkanethiols, better fittings could be obtained, an example of which is presented in Figure 8. The solid lines present fits to the modified
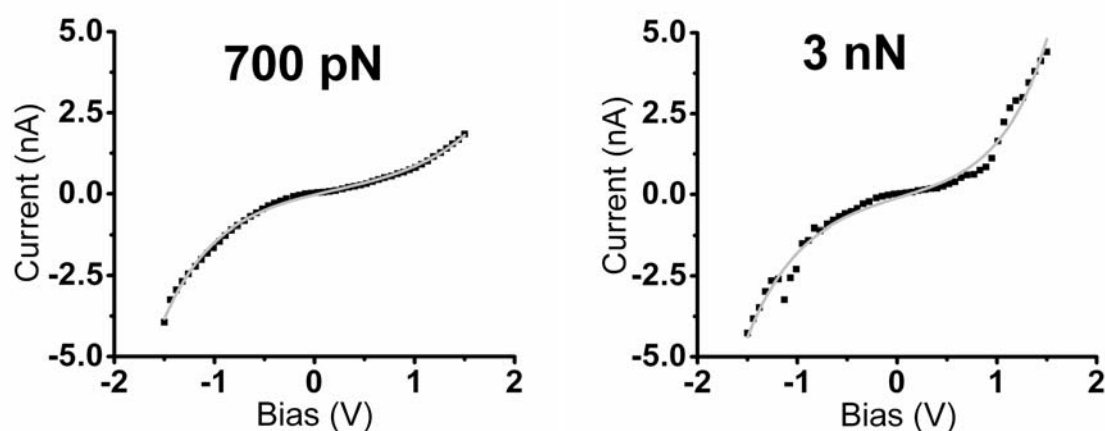

Figure 8. Examples of Simmons fits to individual C-AFM IV spectra obtained at 0.7nN (left) and 3nN (right). For the fitting to Simmons equation, L, φ_0 and β were treated as adjustable parameters.
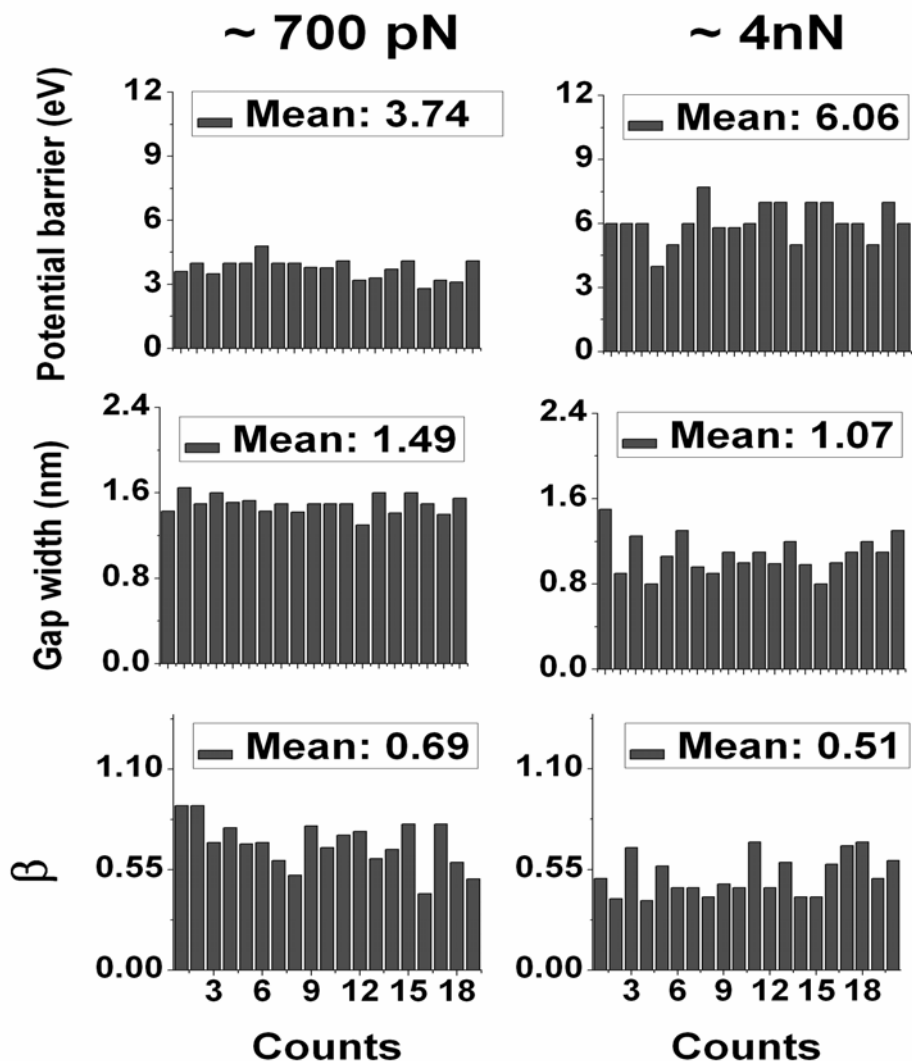
Figure 9. Overview of the decay constant β (Å^{-1}), tunneling barrier heights (nm) and barrier width (eV) obtained after fitting to Simmons equation.

Simmons equation; we note that in these examples, as well as in all spectra with current steps, NDR events are not particularly well fitted, and the decay constants thus obtained do not wholly reflect the effect of molecular structure on electron transfer.

An overview of the fitting parameters of individual traces is presented Figure 9, at the lowest and highest applied force respectively. It summarizes the relevant quantities (decay constant, barrier length and width) resulting from fitting the *I(V)* spectra to the modified Simmons equation, as obtained in the high (4 nN) and low (0.8 nN) force regimes. We emphasize that each bar in the histogram corresponds to an individual linker molecule (or spot). The heterogeneity from molecule to molecule in the noted values, even within the same force range, may be due to different contact geometries between tip and molecular adsorbates.

The potential barrier and the gap widths vary with the increase in applied force, as can be expected. We note that the average decay constant β is similar in the high force regime to the one calculated from STM data (0. 51 Å^{-1} vs. 0.49 Å^{-1}), and that both values are smaller than β = 0.95 Å^{-1} obtained from C$_8$. It is important also to note from the fitting procedure that the variations in the detected current under applied force are deconvoluted into contributions from changes in both tunneling distance and barrier height. The high potential barrier observed at ~ 4 nN applied force, higher than that obtained at ~0.8 nN (3.74 eV vs. 6 eV) may relate to the higher indentation of the C-AFM tip into the monolayers. This may result in both the perturbation of the structure of the molecular wires and/or contact with the insulating alkanethiol SAM.

It is interesting to analyze the presence of the current steps present in the *I(V)* spectra, by considering the molecular orbitals HOMO/LUMO of linkers as mediators of the electron transfer from the two metals (Au/Pt). Resonant tunneling through LUMO, which may also be involved in a redox process, has been previously observed with both STM and inelastic tunneling spectroscopy on other systems (27). The correlation of reduction potentials, LUMO, and NDR peaks was considered when an electron is injected into the molecule's LUMO, if the applied voltage corresponds to the LUMO energy, resulting in a current spike (28). However, the alignment of the Fermi levels of the contact with the energy levels in the molecule is generally unknown, as is the electric field distribution through the junction – it can take place at the molecule/contact interface(s) or within the molecular layer (29).

We can accentuate the observed current steps by plotting the differential conductance quantity dI/dV versus the applied bias V, according to the equation:

$$g_0(V) = dI/dV = \left(2e^2 \middle/ h \right) T(E_F + eV)$$

(3.6)

where T is the transmission factor and E_F the Fermi level, as shown in Figure 10.

Figure 10 presents the disposition of the linker molecular orbitals, with a band gap HOMO-LUMO of 2.34 eV. We note that this value is much smaller than the ~ 7 eV band gap of alkanethiols, but closer to the 3.1 eV value of trans-stilbene with a similar structure as that of our molecular wire (30). An estimation of the band gap and the pinning of the molecular energy levels, as calculated semiempirically (after geometry optimization) with HyperChem 7 (Austin Model 1), reveals a LUMO = −2.75 eV, HOMO = −5.16 eV and a band gap of 2.41 eV. When comparing this result to the 3.6 eV value obtained from optical absorption spectra,
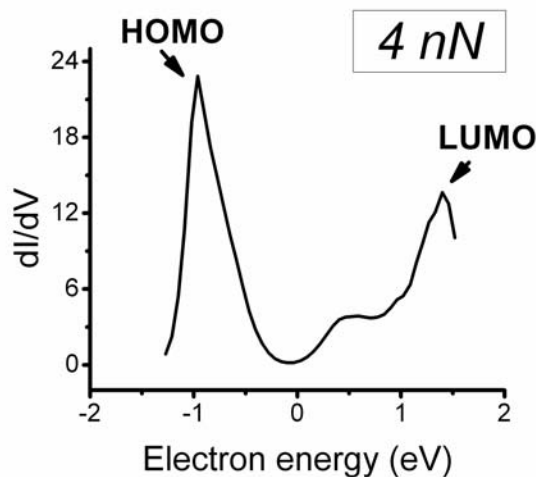
Figure 10. Differential conductance for the IV spectrum of the data obtained at 4 nN (averaged spectrum).

we note that the band gap will be diminished when the molecule is in a solid-state environment (31), compared to that in solution (Fig. 6) or when computed in vacuum. Because of the presence of the surrounding alkanethiol matrix, we assume that the trans-cis transitions of the molecular wires are precluded, and that the molecule is planar, such that the current steps are not reflective of conformational changes. Since the potential profile of the surface is not known, and only a potential difference is applied in the ex-situ STM/C-AFM setup, we assume that by ramping the bias the E_F of the gold surface matches the LUMO of the linkers, and electron transfer is feasible; the electron from LUMO is thereafter transferred onto the HOMO and further on to the other metal, thus achieving resonant electron transfer. We envision that independent determination, by electrochemical means (including electrochemical STM or C-AFM) of the redox potential of linkers (and hence of the HOMO-LUMO band gap), can help further establish the origin of the observed NDR.

3.5 Conclusions

In conclusion, we have described and compared two methods by which a conductive molecular wire can be inserted into an insulating alkanethiol matrix, amenable to probing by both STM and C-AFM and we have also measured the conductance of such wires. We have described a dependence of the current with applied force in C-AFM and also noted a decrease in the current measured in C-AFM with increased bias (NDR), the mechanism of which deserves further investigation. We propose here that the resonance tunneling via the molecular

orbitals of the linkers occurs. However, independent values of HOMO, LUMO and band gaps should also be obtained (e.g. electrochemically). Finally, we note that these assembled structures can be further used to attach appropriate proteins, thus providing them both a defined orientation and a conductive path with respect to a metal surface.

References

1. T. E. de Jongh (2006) *PhD Thesis*, Leiden University.

2. T. den Blaauwen, M. van de Kamp and G.W. Canters (1991) *Type I and II copper sites obtained by external addition of ligands to a His117Gly azurin mutant*. J Am Chem. Soc., 113, 5050-5052.

3. J. van Ruitenbeek (2005) *Lecture notes in physics*. Springer-Verlag, 680, 253-274.

4. W. Wang, T. Lee, M. Kamdar, M.A. Reed, M. P. Steward, J. J. Huang and J. M. Tour (2003) *Electrical Characterization of Metal-Molecule-Silicon Junctions*. Ann. N. Y. Acad. Sci., 1006, 36-47.

5. S. Sachs, S.P. Dudek, R.P. Hsung, L.R. Sita, J.F. Smalley, M.D. Newton, S.W. Feldberg and C.E.D. Chidsey (1997) *Rates of Interfacial Electron Transfer through π-Conjugated Spacers*. J Am Chem. Soc., 119, 10563-10564.

6. C.E.D. Chidsey, C.R. Bertozzi, T. M. Putvinski and A.M. Mujsce (1990) *Co-adsorption of ferrocene-terminated and unsubstituted alkanethiols on gold: electroactive self-assembled monolayers*. J Am Chem. Soc., 112, 4301-4306.

7. M. Tachibana, K. Yoshizawa, A. Ogawa, H. Fujimoto and R. Hoffmann (2002) *Sulfur-Gold Orbital Interactions which Determine the Structure of Alkanethiolate/Au(111) Self-Assembled Monolayer Systems*. J Phys. Chem. B, 106, 12727-12736.

8. H.J. Kim, Y.S. Kim, B.I. Seo, E.R. Kim and H. Lee (1998) *Adsorption kinetics of alkanethiols studied by quartz crystal microbalance*. Thin solid films, 327-329, 191-194.

9. H. Park (2006) *PhD Thesis*, Columbia University.

10. L. Li, S. Chen, and S. Jiang (2003) *Molecular-Scale Mixed Alkanethiol Monolayers of Different Terminal Groups on Au(111) studied by low-current STM*. Langmuir, 19, 3266.

11. B. Luessem, L. Meskamp, S. Karthäuser, R. Waser, M. Homberger and U. Simon (2006) *STM study of mixed Alkanethiol/Biphenylthiol Self-Assembled Monolayers on Au(111)*. Langmuir, 22, 3021-3027.

12. R.W.Zehner (1998) *PhD Thesis*, Chicago University.

13. J.C. Love, A. Estroff, J.K. Kriebel, R.G. Nuzzo and G.M. Whitesides (2005) *Self-assembling monolayers of thiolates on metals as a form of nanotechnology*. Chem. Rev., 105, 1103-1169.

14. J. Simmons (1963) *Electric tunnel effect between dissimilar electrodes separated by a thin insulating film*. J app. Phys., 34, 2581-2590.

15. A. Vilan (2007) *Analyzing Molecular Current-Voltage Characteristics with the Simmons Tunneling Model: Scaling and Linearization*. J Phys. Chem. C, 111, 4431-4444.

16. S. Sze (1981) *Physics of semiconductor devices*. John Wiley & sons.

17. W. Wang, T. Lee and M. Reid (2003) *Mechanism of electron conduction in self-assembled alkanethiol monolayer devices*. Phys. Rev. B, 68, 035416.

18. S. Lindsay (2006) *Molecular Wires and Devices: Advances and issues*. Faraday Discuss., 131, 403-409.

19. A. Salomon, D. Cahen and S. Lindsay (2003) *Comparison of electron transfer measurements on organic molecules*. Adv. Mater., 15, 1881-1890.

20. D.J. Wold and C.D. Frisbie (2001) *Fabrication and Characterization of Metal-Molecule-Metal Junctions by Conducting Probe Atomic Force Microscopy*. J. Am. Chem. Soc., 123, 5549-5556.

21. X.D. Cui, X. Zarate, J. Tomfohr, O.F. Sankey, A. Primak, A.L. Moore, T.A. Moore, D. Gust, G. Harris and S.M. Lindsay (2005) *Making electrical contacts to molecular monolayers*. Nanotechnology, 13, 5-14.

22. K. Moth-Poulsen, L. Patrone, N. Stuhr-Hansen, J.B. Christensen, J.P. Bourgoin and T. Bjornholm (2005) *Probing the effects of conjunction path on the electronic transmission through single molecules using STM*. Nano lett., 4, 783-785.

23. L.A. Bumm, J.J. Arnold, T.D. Dunbar, D.L. Allara and P.S. Weiss (1999) *Electron transfer through organic molecules*. J Phys Chem B, 103, 8122-8127.

24. J.A. Seminari, A.G. Zacarias and J.M. Tour (2000) *Theoretical Study of a Molecular Resonant Tunneling Diode*. J Am. Chem. Soc., 122, 3015-3020.

25. J. Zhao, J.J. Davis, M.P. Samson and A. Hung (2004) *Exploring the Electronic and Mechanical Properties of Protein Using Conducting Atomic Force Microscopy*. J Am Chem. Soc., 126, 5601-5609.

26. W. Tian, S. Datta, S. Hong, R. Reifenberger, J. Henderson and C.P. Kubiak (1998) *Conductance Spectra of Molecular Wires*. J Chem. Phys., 109, 2874-2882.

27. L. Scudiero, D.E. Barlow, U. Mazur and K.W. Hipps (1997) *STM, Orbital-Mediated Tunneling Spectroscopy and UV Photoelectron Spectroscopy of Metal(II) Tetraphenylporphyrins deposited from vapor*. J Am Chem. Soc., 123, 4073-4080.

28. W. Ha, E. N. Durantini, T.A. Moore, A.L. Moore, D. Gust, P. Rez, G. Leatherman, G.R. Seely, N. Tao and S.M. Lindsay (1997) *STM contrast, electron-transfer chemistry and conduction in molecules*. J Phys. Chem. B, 101, 10719-10725.

29. R. McCreery (2004) *Molecular electronic junctions*. Chem. Mater., 16, 4477-4496.

30. C. Jiang, R. Xie, F. Li and R.E. Allen (2009) *Trans-to-cis isomerization of stilbene following an ultrafast laser pulse.* Chem. Phys. lett., 474, 263-267.

31. S. Kubatkin A. Danilov, M. Hjort, J. Cornil, J.L. Brédas, N. Stuhr-Hansen, P. Hedegård and T. Bjørnholm (2004) *Single electron transistor with a single conjugated molecule*. Curr. appl. Phys., 4, 554-550.

32. J. Wei, H. Liu, A.R. Dick, H. Yamamoto, Y. He and D. Waldeck (2004) *Direct Wiring of Cytochrome c's Heme Unit to an Electrode: Electrochemical Studies*. J Am Chem. Soc., 124, 9591-9599.

Chapter 4

Conductive – Atomic Force Microscopy of hot-wired azurins

Razvan C. Stan[1], Nusrat J. M. Sanghamitra[1], Gerard W. Canters[2], Thijs J. Aartsma[1]

[1] Department of Biophysics, Huygens Laboratory, Leiden University, 2300 RA, Leiden, The Netherlands
[2] Department of Chemistry, Oxford University, OX1 3TA, Oxford, United Kingdom
[3] Department of Chemistry, Gorlaeus Laboratory, Leiden University, 2333 CC, Leiden, The Netherlands

Abstract: *The reconstitution of azurin H117G with external ligands capable of interfacing the protein core to an underlying metal surface has been studied with Conductive-Atomic Force Microscopy, ellipsometry and UV-Vis absorption techniques. The two cognate molecular wires display an improved electron transfer, over the mediation by the protein framework, and all complexes (including the wild-type azurin) show the signature of a redox active metal, i.e. Cu, versus the optically and electrically inactive azurin Zn-mutant. These results point to the feasibility of constructing and assembling proteins on the surfaces, directly and in a precise conformation wired onto appropriate electrodes.*

4.1 Introduction

There is considerable interest in the design of current bio-electronical devices to incorporate metallo-proteins, owing to their ability to form structured arrays onto appropriate surfaces and to facilitate electron transfer to and from electrodes. Moreover, the redox active metal from such protein films can be replaced, with minimum change in the overall structure, and reversible switching between different ionic states can be accomplished. This study is concerned with azurin, an electron transfer, mononuclear metallo-protein, with a characteristic type-1 copper site, wherein the metal is coordinated by a Sγ from a cysteine, the Nδ of two histidines, the Sγ of a methionine (that serves as an axial group) and, uniquely, by a second axial group − the C=O from a glycine, in a geometry resembling a distorted trigonal bipyramid (1-3). This configuration renders the structure amenable to mutations whereby one of the histidines can be replaced by a smaller amino acid like glycine. Such a mutation produces a cavity (Figure 1) that makes the Cu^{2+} accessible to coordination by external ligands, thus reconstituting the overall structure of the redox activity. Various techniques such as NMR, EPR, UV-Vis and electrochemical studies have demonstrated that the structural properties of the wild-type protein can be restored when a mutant such as azurin H117G (Figure 1.) is being reconstituted with appropriate ligands (imidazole, pyridine, etc) (4-6). We have explored the reconstitution of azurin H117G with external ligands able to attach both to the protein (via a pyridine) and to an electrode (by means of thiol functionality), while separated by an aromatic linker.
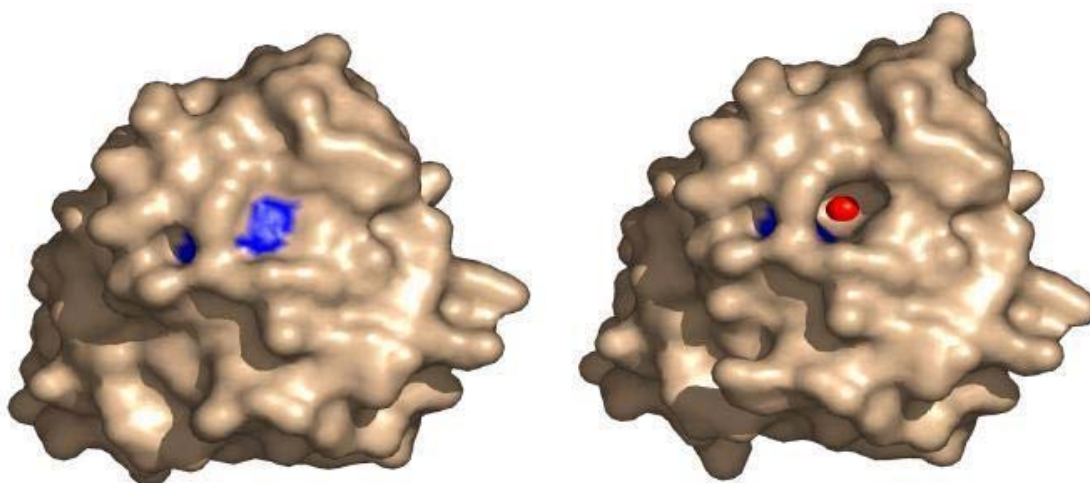

Figure 1. Top-view of models of the native azurin (left) and the H117G cavity mutant (right) used in this study; copper is depicted in red.

Once such construct has been assembled there are two important advantages in its potential use as a protein biosensor: 1) the protein is "shielded" from the bare electrode by the "tail" of a long molecular wire, thus preventing its denaturation/loss of biological activity and 2) the copper distance and orientation with respect to the surface is defined by its direct coupling to the head-group. Such beneficial arrangement prevents the unspecific attachment of the protein onto functionalized surfaces, for instance onto alkanethiol-based Self-Assembling Monolayers (SAM); moreover, the aromatic backbone of the molecular wires are conducive to higher electron transfer rates from the electrode to the metal core, due to presence of the delocalized electrons. We present here our investigations into the structural and electron transfer properties of azurin H117G films on Au (1,1,1), when reconstituted with two molecular wires, as studied with Conductive-Atomic Force Microscope and ellipsometric spectroscopy. We envision that such work will be relevant for the controlled assembly of more complex proteins onto appropriate electrodes, by means of molecular wires, such that film stability and enhanced electron transfer mediation can be achieved.

4.2 Experimental section

Gold preparation: Commercial gold-on-glass chips (Arrandee) were annealed by using a butane torch (prior to protein attachment), followed by quenching in Milli-Q grade water and drying under N_2 flow. The surface flatness was regularly checked with AFM and only surfaces with terraces on the order of $1\mu m^2$ were used.

Conductive-AFM (C-AFM): Ex-situ topographical and conductance studies were performed at room temperature with a Pico LE (Agilent) or with a Digital Instruments Multimode microscope (with a Nanoscope IIIa controller). Each *I(V)* spectrum consisted of 50 data points. The conductive tips were either prepared by RF sputtering commercial AFM cantilevers (Olympus, spring constant 2.0 N/m, 10-15 nm quoted radius) with 5 nm of Ti, followed by ~ 25 nm layer of Au; alternatively, commercial cantilevers were used (ContE, Budget Sensors, Innovative Solutions, Bulgaria) with a nominal spring constant of 0.2N/m and a Cr/Pt coating. Analysis of the *I(V)* spectra was performed using Origin 7.5. (OriginLab, Massachusetts, USA)

Reconstitution of H117G: One equivalent of $Cu(NO_3)_2$ was added to 50-100 μM of apo-azurin (50mM MES, pH 6.0) for 1', followed by addition of equimolar concentrations of either Linker 1 or Linker 2.

UV-Vis: Absorption spectra of the reconstitution of H117G were collected using a Shimadzu spectrophotometer (UV-3101, PC) at room temperature.

Gold functionalization: Reconstituted H117G azurins (50-100 μM, in 50 mM MES buffer, pH 6.0) were incubated on gold surfaces for periods ranging from 10'' to 10' in order to determine the optimum incubation time/coverage for electrical measurements. The protein films, once assembled on the gold surfaces, were rinsed with the buffer, and thereafter with Milli-Q grade (18 MΩ) water.

Hot-wires: The molecular linkers (Figure 2) were kindly provided by Dr. Alexander Kros. Their synthesis was described in chapter II. These hot-wires incorporate a thiol group able to covalently attach to a gold surface, while at the other end, the pyridine head-groups couple to the metal from the exposed redox center. Of note is also the presence of the –OH lateral group in Linker 2, that breaks the π-conjugation, thus providing a "bottle-neck" for the electron transfer from the electrode to the Cu centre (in contrast to the conjugated system present in Linker 1). The acetyl-protective groups for the thiol functionality are removed upon the interaction with the gold surfaces (7-9).

Ellipsometry: A M2000V Variable Angle Spectroscopic Ellipsometer (Woollam) was used for thin films' characterization with the incident light at a fixed angle (65°). The illuminating
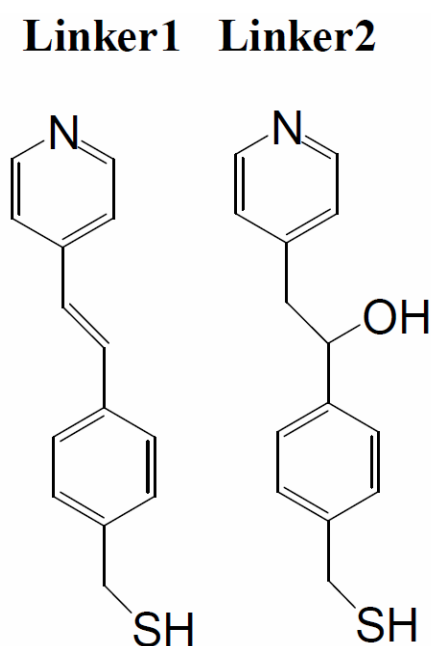

Figure 2. Structures of the molecular wires, linkers L_1 and L_2, used in this study.

arm consisted of a 50W quartz tungsten halogen lamp, while the detection arm permits spectroscopical measurements within the 390-1000 nm range. Freshly cleaned gold substrates (unmodified) were used for determining the optical constants of gold. The ellipsometric data for the azurins were modeled by use of optical constants obtained from clean gold substrates and adding a Cauchy layer to model the protein complexes. To fit the experimental data, we have assumed a refractive index n = 1.5 (14). The analysis of the data was performed with the WVase software package (Woollam, Lincoln, NE).

SEM: Because of the inherent issues involved when scanning with coated cantilevers (wear, damage, contamination etc) Scanning Electron Micrographs of the C-AFM cantilevers employed were necessary. Images were obtained using a FEI Nova *NanoSEM*200 at a base pressure below 10^{-6} bars, examples of which are shown in Figure 3.

The coated cantilevers, after *I(V)* measurements, were also used to calibrate the force imposed on a hard, clean substrate (freshly cleaved mica). The SEM images of these
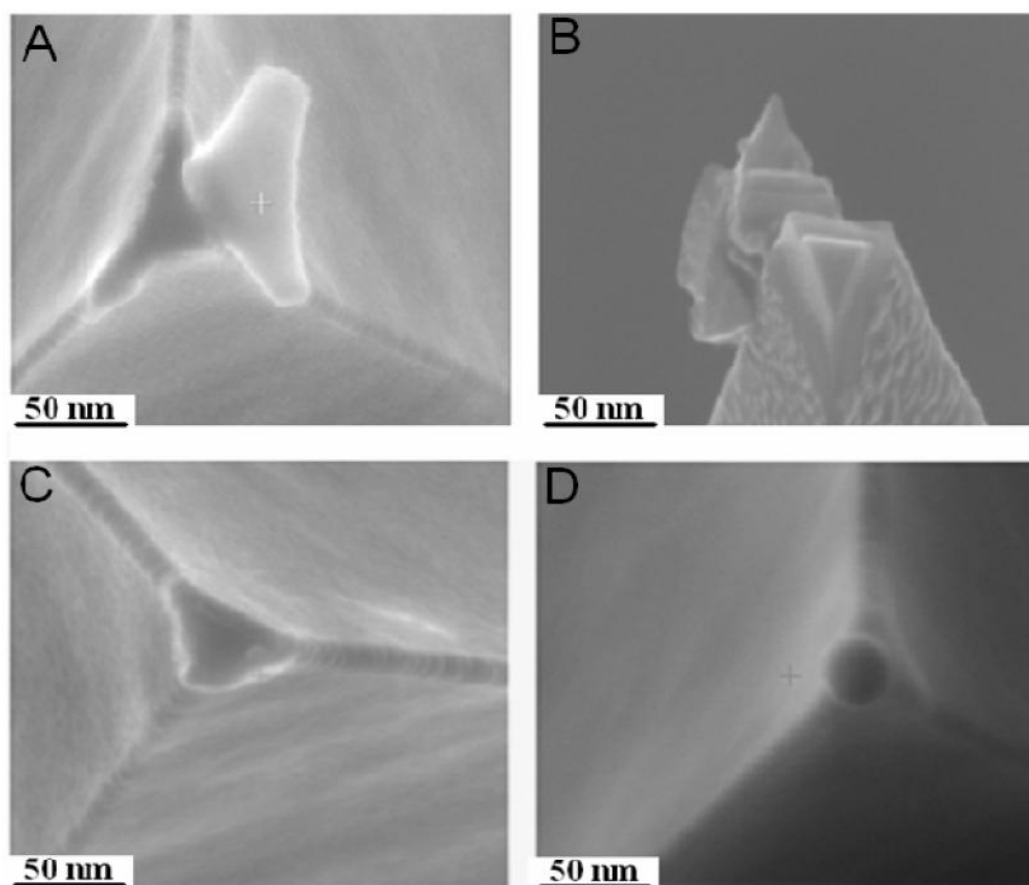

Figure 3. Top-view SEM images of C-AFM cantilevers used for scanning and performing current-voltage spectroscopy. a), b) micrographs of damaged, non-conductive tips after scanning the functionalized surfaces, with a lifetime of usually below 10'; c), d) conductive C-AFM tips after

cantilevers after these types of measurements allow the determination of the contact area of the tips, and thus an estimate on the number of proteins probed by the tip apex can be obtained (assuming an uniform coverage on the surface in the form of a protein monolayer). Figure 3. depicts typical images of C-AFM cantilevers after imaging protein films on gold and performing *I(V)* spectroscopy. It is evident from Fig. 3a-b, that scanning functionalized surfaces has adverse effects on the integrity of the tip's conductive coating, which results in unstable imaging and unreliable *I(V)* spectra; as such, no data obtained with such cantilevers were used for analysis. In contrast, Fig. 3c, d. show intact, conductive cantilevers after having only been used for force-curve measurements and *I(V)* spectroscopy.

4.3 Results

4.3.1 Optical measurements of apo-azurin reconstitution

In order to first assess the insertion of the pyridines into the azurin redox cavity, optical spectra of the apo-azurin and the holo-azurin were taken. Coordination of the pyridine involves a single binding event and occurs by removal of a H_2O molecule from the protein cavity (1, 2). The pK of individual linkers are considered similar to that of pyridine (pK = 5.2), hence at the pH 6.0 used for the optical measurements, the linkers are deprotonated, a requirement for copper coordination. The configuration upon binding of either linker to the metal is shown in Figure 4.
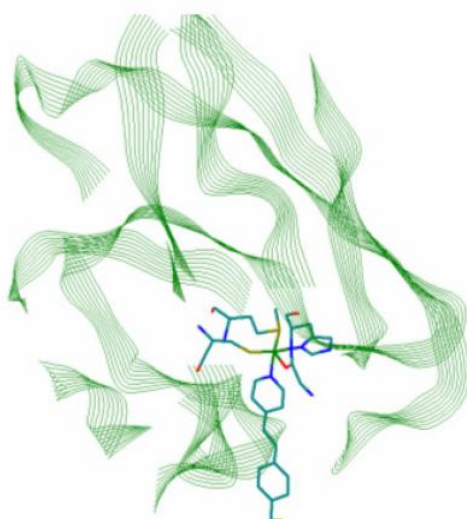

Figure 4. Proposed model of interaction between either hot-wire and the H117G-Cu(II) cavity. Copper is depicted in green. The complex is shown from a side-view, with the sulfur from the linker facing down towards the Au surface. Image created using Hyperchem (Hypercube).
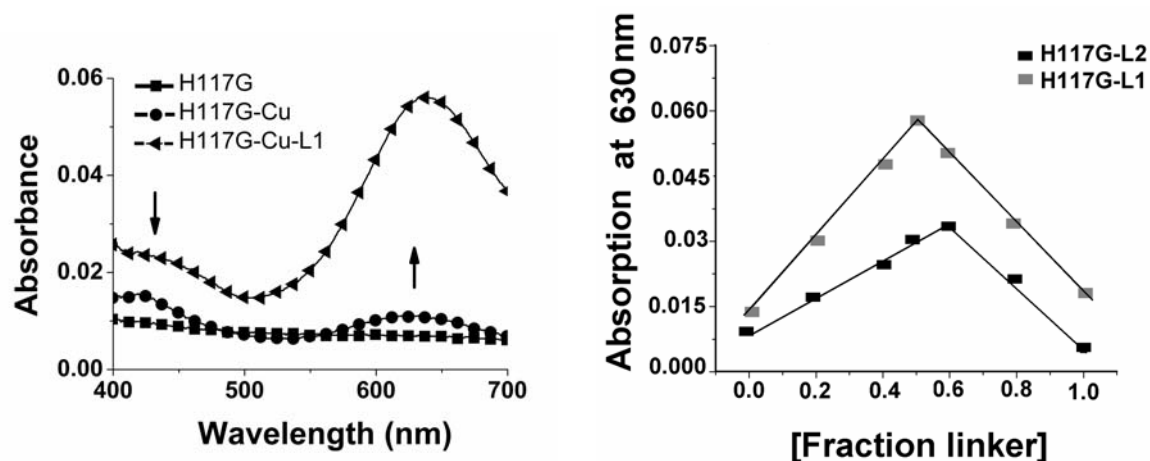
Figure 5. Left: H117G-Cu(II) (black) reconstituted with L_1 (red). The arrows indicate the changes in absorption at 420 nm and 630 nm respectively, upon increasing the concentration of ligand. Right: Job's plots for coordination of $L_{1/2}$ to H117G-Cu(II) azurin; the x-axis is the ratio of [Linker]/[H117G-Cu(II)] + [Linker]

In the absence of external ligands, the H117G-Cu(II) protein (apo-azurin) is green with a maximum absorption peak at around 420 and a smaller one at 630 nm. Upon addition of external ligands the protein turns blue with the 420 nm absorption peak decreasing in intensity, whilst the 630 nm peak increases (Figure 5). Figure 5. presents the variation in reconstituted azurin absorption (measured at 630 nm) versus the molar fraction of linker yielding the stoichiometry between the protein and the molecular wires, as determined by Job's method of continuous variation (1). This method consists of keeping the total molar concentration of the protein and the linker constant, while the ratio between them is varied. This allows for the optimum stoichiometry of the binding to be determined, and consequently, the maximum optical absorption of the H1117G-linker complex. For linkers 1 and 2 the protein/linker stoichiometry is 1.1 and 1:2 respectively, as measured at the intersection points between the positive and negative slopes [x/(1 − x)] of the fraction of linker used versus change in optical absorption measured at 630 nm. Also shown is an example of the absorption spectra of H117G-Cu(II) before and after addition of linker L_1, when the characteristic blue color of wt-type azurin is being restored. The reconstituted complexes in oxidized state were stable and measurable for periods up to 4h; once the copper is in reduced form, the linkers tend to detach from the cavity and the complex becomes colorless.
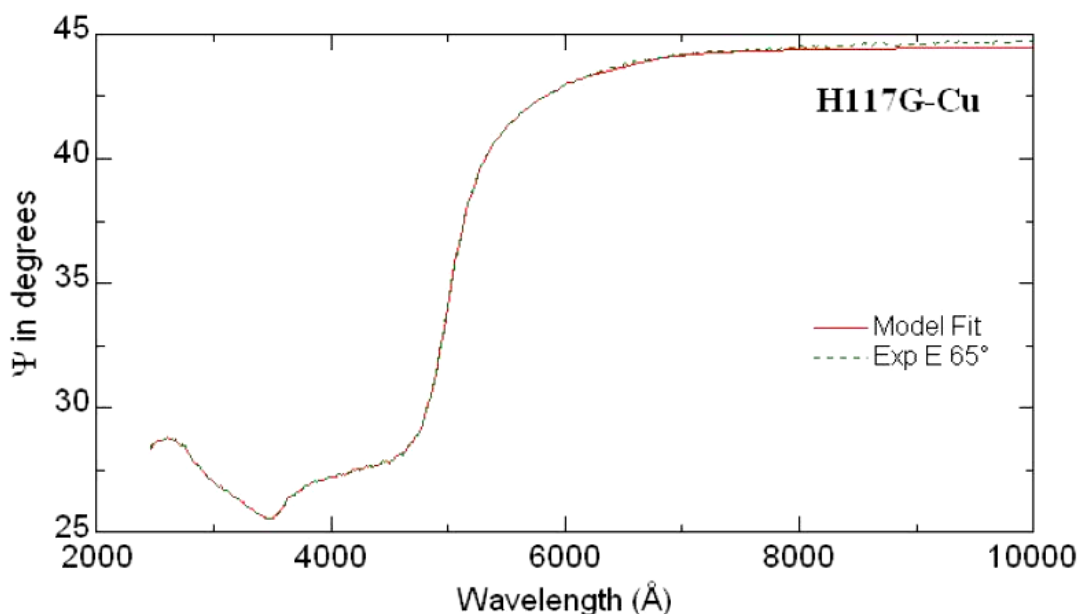
Figure 6. Ellipsometrical measurement (dotted line) and data fitting of the apo-azurin assembled on gold (MSE below 1).

4.3.2 Ellipsometry of adsorbed protein films.

In order to first characterize the attachment of the reconstituted complexes on the gold surface, we have measured the thickness that such films may present on gold. Because of the presence of the linkers, even when inserted into the protein cavity, we assumed that the height of the complexes may be higher than the height of either the wild-type azurin or that of H117G-Cu (II) azurin on Au (1,1,1). To verify this assumption, we have prepared protein films on the annealed gold surface consisting of H117G-Cu(II) or H117G-Zn reconstituted with either linker and measured their ellipsometrical signature, as exemplified in Figure 6.

The protein film thickness was determined by using a 3-layer model (11-15) involving air, the protein complexes and the gold substrate, and a point-by-point fit was applied until the Mean Squared Error parameter was minimized. Such measurement revealed a marked difference between the protein films assembled with or without the molecular wires, as summarized in Table 1.

Table 1. Thickness values for various azurin films, as ellipsometrically determined. Each value is the average of approximately 15 spots from 3 different samples.

H117G-Cu(II)	H117G-Zn-L_1	H117G-Cu-L_1
3.67 ± 0.1 nm	4.52 ± 0.18 nm	4.68 ± 0.13 nm

58

The value obtained for the wt-azurin (~3.7 nm) corresponds well with the crystallographic data of 3.5 x 3.5 x 4.4 nm^3 (22) and with other AFM results (8). The values obtained for H117G reconstituted with either Zn or Cu and with L$_1$ are consistently 0.9nm ($\pm$ 0.2 nm), higher than the wild-type form or the apo-azurin. We hypothesize that the pyridine group is inserted into the protein cavity, and that the attachment to the gold surface occurs via the thiol head-group, such that stable films of the reconstituted azurin are assembled on the gold in a "standing-up" configuration.

4.3.3 AFM topographical measurements of adsorbed azurins.

The molecular conductance of protein arrays can be measured at single molecule level with either Scanning tunneling microscope (STM) or the Conductive-atomic force microscope. While the resolution attainable with STM can be exquisite, gathering reliable *I(V)* data can be problematic, because no independent assessment of the force imparted on the surface-confined features can be obtained, nor can the vertical distance on top of the molecule of interest be accurately determined (the STM tip may be "buried" inside the protein layer, in contact or separated by a small air/vacuum gap). For this reason, we have focused on performing the *I(V)* measurements with a conductive-AFM, as the vertical deflection of the conductive cantilever can be measured at all times, and the force imposed on the functionalized surfaces can be thus controlled . Conductive-AFM has been used to probe the electrical properties of various proteins e.g. ferritin (16), wild-type azurin (17, 18) or
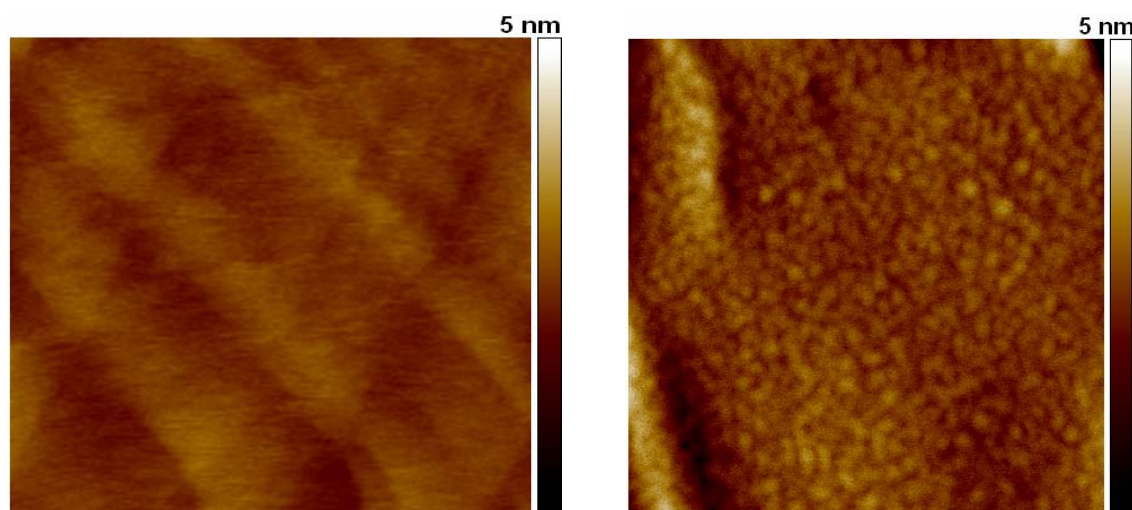
Figure 7. TM-AFM image of a flat gold surface (left), before the addition of the H117G-Cu reconstituted with either linker (right). When protein complexes are incubated, the featureless surface is completely covered with globular features (i.e. with azurin H117G-L$_1$/L$_2$). No such features are observed when the surface is incubated with buffer (AFM result not shown). We also note the lack of aggregation of the surface, a condition for performing *I(V)* spectroscopy on protein monolayers

plastocyanin (19) under anisotropic applied forces, with an emphasis on determining the mediation of electron transfer by the oxidation state of the metal contained within the protein. All these studies were based on directly attaching the proteins on the bare electrodes, with possible adverse effects on the molecular properties (e.g. denaturation). To circumvent this problem, our assembling approach for the azurin mutant relies on its attachment to a surface via a molecular wire. However, it is important to determine that such complexes do not aggregate on surfaces and that complete coverage is attained, before C- AFM measurements can be performed. In order to reveal the topographical features of the assembled films, we have first performed *ex-situ* tapping mode (TM)-AFM, (Fig. 7), before performing point spectroscopy on the assembled films.

4.3.4 Conductive-AFM and *I(V)* spectroscopy on protein films.

In order for the *I(V)* measurements to be meaningful, the properties of the tunnel junction in the absence of the proteins have to be determined. We found that the gold surfaces produce generally an ohmic response (result not shown). On functionalized surfaces, different IV responses were obtained, as a function of the tip-induced stress. At very low forces (below 1 nN), the tip is making weak contact with the film, and, regardless of whether the Cu or Zn-azurin is being used, no detectable electron flow apart from the noise levels (0.2 pA) could be measured. Alternatively, at very high forces (> 60 nN), the tip likely penetrates through the monolayer and metal-metal contact is being established, with subsequent loss of tip integrity and saturation of the current pre-amplifier. Two representative examples of these two extremes are shown in Figure 8.

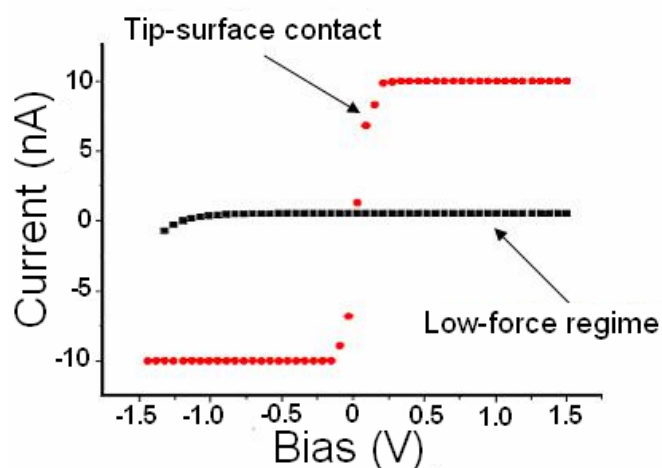In order to verify the influence on the electron transfer from the protein cavity when the active

Figure 8. Different operating regimes of the C-AFM cantilever and the corresponding I(V) curves

metal is changed (Cu>Zn) or when the conductive path is modified (L_1>L_2), we have performed C-AFM *I(V)* spectroscopy on different protein films assembled on gold, after having obtained topographical information with TM-AFM. The results are shown in Figure 9 which presents a summary of of the main I(V) results obtained on various azurin films, reconstituted with either of the two linkers and in the presence or absence of copper. Fig. 9 a-b presents I(V) spectra obtained on H117G reconstituted with Zn and L_1 (a), and on native azurin respectively (b). We note here that we assumed the electron transfer occurs via multiple azurins presented to the coated cantilever, with the proteins arranged in a monolayer with minimum gaps between them.

4.4 Discussion

From the analysis of the *I(V)* curves, two important aspects are worth discussing. First, the amplitude of the overall measured current increases from the H117G reconstituted with Zn and L_1 to the wild-type azurin and the H117G-Cu reconstituted with L_2 and L_1. It is remarkable, when comparing the *I(V)* spectra from Fig. 9 a-b-c with those from Fig. 9. d, that
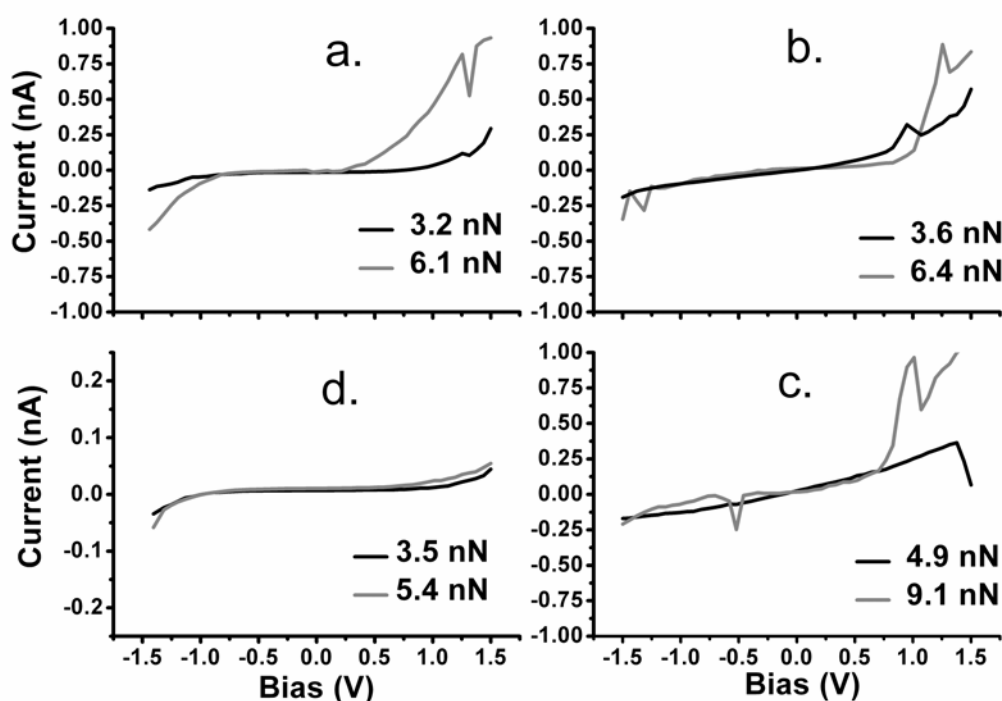

Figure 9. Representative I(V) curves obtained at various moderate forces ont: a) wild-type azurin b) H117G-L_1 ; c) H117G-L_2; d) H117G-Zn-L_1.

the currents measured are on average an order of magnitude larger when reconstitution involves both the copper and either linker, evidence of efficient electronic coupling to the gold electrode (within generally similar applied forces regimes). Because of the presence of negative differential resistance (NDR) features, and because of their shifting position (see infra), fitting of the I(V) data to a model that can account for the influence on electron transfer of a redox active metal (i.e. Cu) and of a more efficient electron path such as our linkers is not possible. As such, determination of the decay constants for these protein films was not feasible. It is therefore worth comparing the current values at fix bias values and across similar applied force for all samples, as presented in Table 2:

Table 2. Current values obtained at ± 1V at ~ 5 nN applied force, normalized against the approximate number of proteins, as determined from the SEM images of the tip

	Current(pA), at +1V	Current(pA), at −1V
H117G-Cu-L_1	60	30
H117G-Cu-L_2	27	24
H117G-Zn	1.9	0.34
Wt-azurin	13	9

We note from both the Table 2 and from Fig. 9 the presence of current rectification (i.e. the higher measured current at positive bias values than at negative voltages), due to the dissimilar voltage drops across the tunneling barrier, imposed by the configuration within the tunneling junction, as has been previously proposed (21). The contact resistances within such a barrier, as is the case with (reconstituted) azurins, are likely to be different (chemisorbed thiols and covalent attachment at one side, physical bonding to the C-AFM tip, manifested by unspecific, van der Waals forces at the other end). We can make use of the linear current response (within ± 200 mV) to estimate the resistances of the tunneling junctions (Figure 10).

Figure 10 presents a semi-logarithmic plot of the measured resistances within the protein tunneling junctions, with the linear decrease in resistance upon increase of applied force. Such linear response, within the indicated 3-10 nN force range, indicates that: 1) the protein structure may be elastically deformed by the C-AFM tip, such that dielectric breakdown does not occur; 2) the neighboring proteins participate *en masse*, within the area probed by the cantilever, to the electron transfer; 3) electrical resistance through the protein monolayers decreases by one order of magnitude from the H117G reconstituted with Zn to the
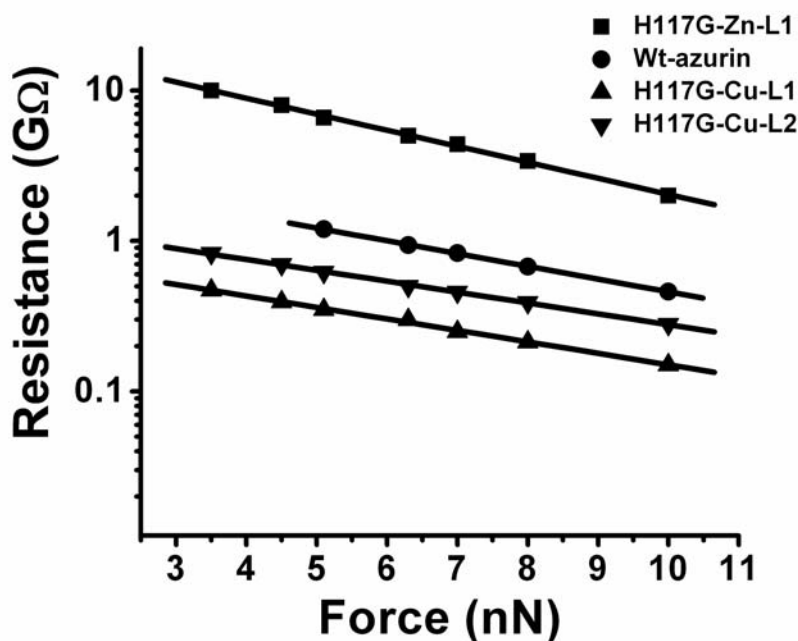
Figure 10. Resistance values of the protein junctions (Gigaohms, not normalized)

H117G reconstituted with Cu (both assembled thereafter with L_1 on gold); 4) the wild-type azurin and the H117G-Cu reconstituted with L_2 have resistance values in between the above mentioned extremes, indicative of the importance of the structure of the conductive path from the metal onto the electrode. We note here that the values obtained for the native azurin within the quoted force range (3-10 nN) of around 1 GΩ are within the same order of magnitude with previous observations (18).

The second aspect that stands out in the *I(V)* response obtained for the protein films is the absence of current spikes (NDR) in the H117G-Zn-L_1 sample, possibly related to its lack of redox activity. This feature contrasts with the spectra obtained for both wild-type azurin and H117G-$L_{1/2}$ (Fig.9 c-d). The presence of these current peaks in all of the samples reconstituted with the linkers may point to the involvement of the copper in mediating electron transfer through resonance tunneling between the two metals (tip-substrate). We emphasize that not all *I(V)* data obtained on wt-azurin exhibit the resonant tunneling, possibly due to different attachment configurations (apart from the expected binding to gold via the disulfide bridge Cys 3 - Cys 26. We also note that the position of the current peaks shifts noticeably, within a range of 400-500 mV, among different *I(V)* curves, as has been previously observed in other systems (20). These NDR events were only observed within a certain force range, typically between 3-15 nN, similar to measurements performed on native azurin (18); other data contradict this observation (22), albeit at a more restricted bias range of

± 1V. However, whilst the resonance peaks measured in the former work centered around -2.2 ± 0.7 V and 2.8 ± 1V, we in turn observed NDR events at 1 V ± 0.15 V, with some symmetrically positioned peaks at − 1V ± 0.1 V. Examples of NDR peaks shifting collected for H117G-Cu reconstituted with $L_{1/2}$ are presented in figure 11, within the 3-10 nN force regime.

The shifts towards lower bias position in our systems as opposed to the C-AFM measurements on wt-azurin chemisorbed on gold suggests a better electron coupling to the surface, as mediated by the molecular wires. Small variations in position (on the order of tens of mV) within the same force range have been observed – possibly indicating the heterogeneity in the contact geometry among various cantilevers (in terms of integrity of conductive coating, differences in spring constants, presence of impurities etc) and suggestive of the importance of mechanical coupling of the tip-protein system for the electron transfer. The corresponding voltage position generally shifts toward higher values in direct proportionality with the increase in applied force. We hypothesize that as the protein-linker structure is denatured by compression, conduction through the molecular wires will be affected and the tunneling barrier height will increase (even though the tunneling length will decrease).

This observation may highlight the importance of defined electron transfer "pathways" (25) as opposed to the treatment of protein as an "organic glass", where the electron transfer is solely determined by the atomic packing density (26). The resonance observed can be attributed to the reduction of the Cu centre; however, because of the variations in the positions
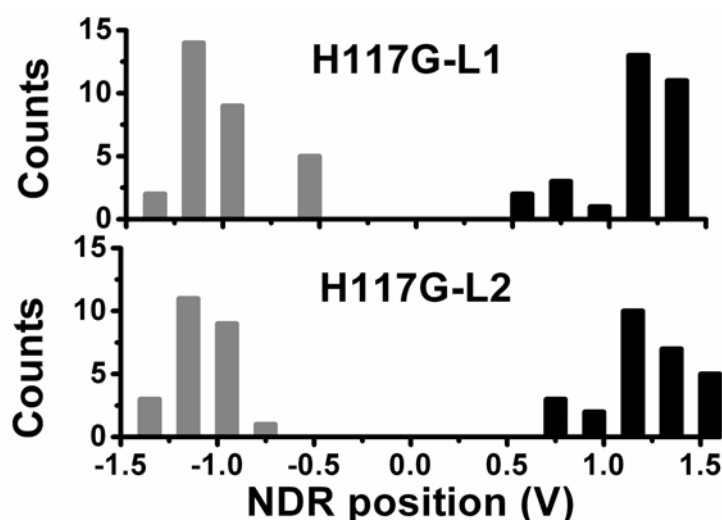

Figure 11. Histograms presenting the variation of NDR peak locations (V)
for H117G-Cu reconstituted with either linker.

of the current peaks and due to the uncertainty as to the absolute potential on the substrate, it is impossible to precisely correlate the electrochemical potential of the thus-reconstituted azurins (chapter 5 of this thesis) to the Fermi level of the tip-substrate system (23). We envision that, performing Electrochemical C-AFM in situ with a coated nanotube mounted on an AFM cantilever, exposed only at its apex by laser ablation, will be the next step in characterizing the current response under both controlled forces and voltages.

4.5 Conclusions

In summary, we have characterized the reconstituted H117G azurins by a variety of techniques, and we have demonstrated that the proteins can be reconstituted with two cognate hot-wires, that they assemble on appropriate surfaces and form stable monolayers, while exhibiting both conductance switching and higher electron transfer than the wt-azurin or than the the Zn-containing reconstituted H117G. Such study may help design prospective protein sensors assembled via conductive molecular wires onto electrodes, that will be both stable and more effective at relaying electrons.

References

1. T.E. de Jongh (2006) *PhD thesis*, Leiden University

2. L. Jeuken (2001) *PhD thesis*, Leiden University

3. A. Messerschmidt, R. Huber, K. Wieghardt, T. Poulos (ed.) (2001) *Handbook of Metalloproteins*, Wiley.

4. T. den Blaauwen and G.W. Canters (1993) *Creation of Type-1 and Type-2 Copper Sites by Addition of Exogenous Ligands to the Pseudomonas aeruginosa Azurin Hisl 17Gly Mutant*. J Am Chem. Soc., 115, 1121-1129.

5. T. den Blaauwen, M. van de Kamp and G.W. Canters (1991) *Type I and Il Copper Sites Obtained by External Addition of Ligands to a Hisll7Gly Azurin Mutant*. J Am Chem. Soc., 113, 5050-5052.

6. L. Jeuken, P. van Vliet, M. Ph. Verbeet, R. Camba, J. P. McEvoy, F. A. Armstrong and G. W. Canters (2000) *Role of the Surface-Exposed and Copper-Coordinating Histidine in Blue Copper Proteins: The Electron-Transfer and Redox-Coupled Ligand Binding Properties of His117Gly Azurin.* J Am Chem. Soc., 122, 12186-12194.

7. O.P. H. Vaughn, M. Turner, F.J. Williams, A. Hille, J.K. Sanders and R.M. Lambert (2006) *Direct observation of surface-mediated thioacetyl deprotection: covalent tethering of a thiol-terminated porphyrin to the Ag(100) surface*, J Am Chem. Soc., 128, 9578-9579.

8. J.M. Tour, L. Jones, D.L. Pearson, J.J.S. Lamba, T.P. Burgin, G.M. Whitesides, D. L .Allara (1995) *Self-assembling monolayers and multilayers of conjugated thiols, α, ω – dithiols, and thioacetyl-containing adsorbates,* J Am Chem. Soc., 117, 9529-9534.

9. M.G. Badin, A. Bashir, S. Krakert, T. Strunskus, A. Terfort and C. Woll (2007) *Kinetically stable, flat-lying thiolate molecules*, Angew. Chem. Int. Ed., 46, 3762-3764.

10. L. Cai, Y. Yao, J. Yang, D.W. Price, Jr. and J.M. Tour (2002) *Chemical and Potential-Assisted Assembly of Thiolacetyl-Terminated Oligo(phenylene ethynylene)s on Gold Surfaces.* Chem. Mater., 14, 2905-2909.

11. E.P. Friis, J.E.T. Andersen, L.L. Madsen, P. Moller and J. Ulstrup (1997) *In situ STM and AFM of the copper protein Pseudomonas aeruginosa azurin.* J electroanal. Chem., 431, 35-38.

12. M. Sastry (2000) *A note on the use of ellipsometry for studying the kinetics of formation of self-assembled monolayer* . B Mater. Sci., 23, 159-163.

13. H. Arwin (2000) *Ellipsometry on thin organic layers of biological interest: characterization and applications*. Thin Solid Films, 377, 48-56.

14. J. Voros (2004) *The Density and Refractive Index of Adsorbing Protein Layers.* Biophys. J, 87, 553-561.

15. H. Elwing (1998) *Protein absorption and ellipsometry in biomaterial research,* Biomaterials , 19, 397-406.

16. D. Xu (2004) *PhD thesis*, Brigham Young University.

17. J.J. Davis, C.L. Wrathmell, J. Zhao and J. Fletcher (2004) *The tunneling conductance of molecularly ordered metallo-protein arrays.* J Mol. Recognit., 17, 167-173.

18. D. Axford, J.J. Davis, N. Wang, D. Wang, T. Zhang, J. Zhao and B. Peters (2007) *Molecularly resolved protein electromechanical properties*. J Phys. Chem. B, 111, 9062-9068.

19. L. Andolfi and S.Cannistraro (2005) *Conductive Atomic Force Microscopy study of plastocyanin molecules adsorbed on gold electrode*. Surf. Sci., 598, 68-77.

20. C. Gorman, R.L. Carroll and R.R. Fuierer (2001) *Negative Differential Resistance in Patterned Electro-active Self-Assembled Monolayers*. Langmuir, 17, 6923.

21. J.G. Kushmerick, C.M Whitaker, S.K Pollack, T.L Schull and R. Shashidhar (2004) *Tuning current rectification across molecular junctions*. Nanotechnology, 15, 489-493.

22. B. Bonanni, D. Alliata, L. Andolfi, A.R. Bizzarri and S. Cannistraro (2005) *Redox metalloproteins on metal surfaces as hybrid systems for bionanodevices: An extensive characterization at the single molecule level*. Surf Sci Res Develop, 1-73.

23. W. Han (1997) *STM Contrast, Electron-Transfer Chemistry, and Conduction in Molecules*. J Phys. Chem. B, 101, 10719-10725.

24. B. Schnyder, R. Kötz, D. Alliata and P. Facci (2002) *Comparison of the self-chemisorption of azurin on gold and on functionalized oxide surfaces*. Surf. Interface Anal., 34, 40-44.

25. D.N. Beratan, J.N. Onuchic, J.R. Winkler and H.B. Gray (1992) *Electron-Tunneling Pathways in Proteins*. Science, 258, 1740-1741.

26. C.C. Page, C.C. Moser, X. Chen and P.L. Dutton (1999) *Natural engineering principles of electron tunnelling in biological oxidation-reduction*. Nature, 402, 47-52.

Chapter 5:

Electrochemistry of hot-wired azurins on gold and carbon electrodes

Razvan C. Stan[1], Hendrik A. Heering[2], Nusrat J. M. Sanghamitra[1], Jeroen Appel[2], Alexander Kros[2], Frank G.M. Wiertz[2], Gerard W. Canters[2], Thijs J. Aartsma[1]

[1]   Department of Biophysics, Huygens Laboratory, Leiden University, 2300 RA, Leiden, The Netherlands
[2]   Department of Chemistry, Gorlaeus Laboratory, Leiden University, 2333 CC, Leiden, The Netherlands

Abstract: *The assembly, interfacial electron transfer rate and coverage of azurin H117G on gold and carbon electrodes have been electrochemically determined. The mutant protein has a cavity that can be reconstituted with a series of "hot-wire" molecules that also mediate the direct attachment to underlying electrodes, with increased electron transfer rates compared to the wild-type. Such an approach, by "click-on" chemistry, may have potential applications in designing future protein-based sensors, assembled onto appropriate surfaces in a precise orientation and able to shuttle electrons to and from electrodes.*

5.1 Introduction

Protein-film electrochemistry is a useful means to study the activity of redox proteins, and to characterize molecular sensing devices (1-8). Redox enzymes that are capable of molecular recognition couple this effect with electron shuttling to the surface of an electrode. The small electrical signals thus triggered are further relayed to electronic circuits that can be an integral part of a biofuel cell, a miniaturized lab-on-chip or a biosensor (9-12). However, in many proteins, including azurin, the cofactor is buried inside the proteins, such that, when assembled on surfaces, electrical communication with the surface is hindered, substrate access is precluded, proteins cannot be activated solely by the potential applied to the electrode and therefore fast electron transfer rates are difficult to achieve (13). Furthermore, direct attachment of proteins results in inactive protein-surface conjugates (18) or may lead to denaturation and poor data reproducibility (14). Attempts to embed the proteins in conductive polymers often result in random orientations of the proteins with respect to the surface, and in non-optimal electron transfer communication with the underlying electrode (mediated by the diffusional redox-active cofactors) (29). A different approach that has been employed consists of connecting the enzyme directly, via a conductive path, to the electrode. Such wiring may involve Au nanoparticles (16), carbon nanotubes (17) or long molecular wires that can probe deep-buried protein cavities (18, 19). In this report, we extend the concept of tethering the active site of a protein by making use of molecular wires of various structures, and we investigate the electrochemical properties of the thus reconstituted complexes on two of the common electrode surfaces, namely (annealed) gold and pyrolytic graphite electrodes (PGE). Such molecular wires ('hot-wires') have the ability to directly connect the redox cavity of the protein to an electrode ('click-on' chemistry). We also demonstrate the ability to create mixed self-assembling monolayers (SAM) on gold onto which we can specifically couple the azurin mutant and thus facilitate electron transfer to its metal centre.

5.2 Experimental section

AFM: Tapping Mode AFM was performed with a Digital Instrument Multimode microscope (Veeco) equipped with a Nanoscope IIIa controller. Olympus cantilevers (2N/m, 70kHz) were used for ex-situ imaging of the functionalized gold surfaces prior and after electrochemical measurements.

70

Au surfaces: Commercial Arrandee gold chips were annealed with a butane torch, thereafter rinsed with Milli-Q grade water and dried under N_2 flow. The surface flatness and cleanliness was checked regularly with AFM, prior to protein attachment.

PGE electrodes: Pyrolytic graphite "edge" (PGE) plane electrodes (4 mm^2) were constructed as described previously (24), and were polished successively in 1 μm, 0.3 μm, and 0.05 μm size alumina slurries (Buehler) and extensively sonicated with Milli-Q water, in order to remove most of the trapped alumina particles (21).

Electrochemistry: A 20-25 μl droplet of protein solution was inserted between the working electrode and the reference electrodes i.e. Ag/AgCl/3 M NaCl at +215mV vs. NHE, for experiments on gold. For the electrochemical experiments performed on PGE surfaces we used SCE (Radiometer, UK) as reference electrode, at + 244mV vs. NHE. In both cases the counter electrode was a platinum wire (22). The whole electrochemical cell was flushed before protein attachment with argon, and the gas flow was maintained throughout the experiments. Voltammetry was carried out at room temperature with a μ-Autolab electrochemical analyzer (EcoChimie, Utrecht, The Netherlands) equipped with a PGSTAT 30 potentiostat and a fast analogue scan generator (SCANGEN), in combination with an analog-to-digital converter (ADC750), at 2 mV potential steps. All measurements were performed inside a home-built Faraday cage. Electrochemical data were analyzed by using accessory software of the Autolab system.

Optical absorption measurements of H117G reconstitution: All UV-Vis experiments were performed on a Perkin Elmer λ spectrophotometer. One equivalent of $Cu(NO_3)_2$ was added to 100 μM of H117G apo-protein in 20 mM MES (2-(*N*-morpholino)ethanesulfonic acid), pH 6.0, at room temperature, resulting in the green-colored, Cu-reconstituted mutant-azurin. To this solution, either 1 equivalent of linker L_1 or L_4, or 2 equivalents of linker L_2, or 4 equivalents of linker L_5 respectively were added to reconstitute the spectral and functional properties of the wild-type azurin (see also chapter 4).

Linkers: Linkers 1 and 2 have been introduced in chapter 2; they were used to reconstitute the H117G azurin mutant on both gold and PGE. In addition, we have also made use of three additional molecular wires, for experiments on PGE alone (linker L_3 — pyridine, linker L_4 — {4-[(E)-2-pyridin-4-ylethenyl]phenyl}methanol and linker L_5 — 2[[(4-{2-amino-3-(1H-imidazol-4-yl)propanoyl]amino}butyl)amino]-3-sulfanylpropanoic acid. Figure 1 presents the various hot-wires employed in this study.
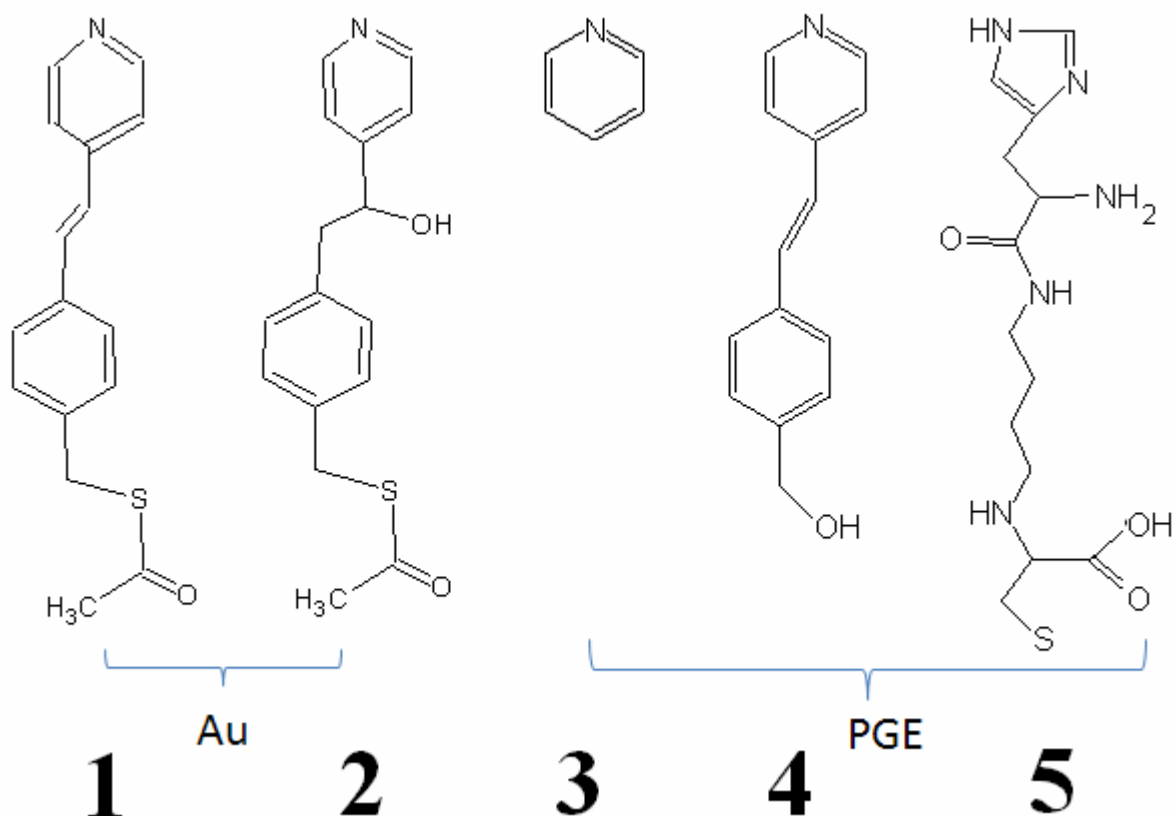
Figure 1. Molecular wires used to reconstitute azurin H117G. Linkers L_1 and L_2, because of their sulfur functionality, were used to attach a reconstituted azurin complex on gold. All linkers were solved in ethanol prior to surface attachment or optical absorption measurements. The thiol-protective acetyl group is removed upon gold adsorption.

Mixed SAM preparation on gold: 8-Hydroxy-1-octanethiol (HSC_8-OH), 99% purity, was purchased from Dojindo and dissolved in ethanol. 100 μM of linkers L_1 or L_2 (dissolved in ethanol) was incubated for 1h, followed by the addition of 1 mM HSC_8-OH for 22-24h on annealed-gold surfaces (at room temperature). Samples were rinsed with ethanol, dried under N_2 stream and readied for AFM/electrochemical measurements.

Immobilization of H117G-Cu on gold: In order to electrochemically probe the electron transfer properties of H117G-Cu azurins upon reconstitution with linkers L_1 and L_2, we have employed two incubation methods. First, the azurin mutant was assembled with either linker 1 or 2 in solution and the complex, after assessing its optical absorption spectrum, was incubated directly on gold for periods ranging from $30'' - 10'$. Alternatively, we have prepared mixed self-assembling monolayers (SAM) on annealed gold consisting of either linker L_1 or L_2 and a supporting molecular matrix of HSC_8OH, to which we have added H117G-Cu for periods of 10'-1h, followed by rinsing with MES buffer and deionized water.

72

5.3 Results

5.3.1 Optical measurements of H117G azurin reconstitution

The copper site of azurin H117G is accessible to external ligands that contain an appropriate head-group such as imidazole or pyridine (chapter 3 of this thesis). The properties of such a molecular construct can be measured by UV-Vis spectroscopy, in the presence or absence of the reconstituting linkers, in order to determine if the absorption spectrum resembles the wild type azurin's. We have already shown our optical measurements of the reconstitution of H117G with linkers L_1 and L_2 (Chapter 4 of this thesis). Figure 2b. presents the effect of reconstitution with linkers L_3-L_5, as determined from changes in optical absorption of H117G with or without the external linkers. Figure 2a. shows the arrangement of the five amino acids that form the active site of wt-azurin. Upon removal of the (bulky) histidine at position 117, copper becomes accessible to linkers L_1-L_5. This reconstitution can be followed spectroscopically, as shown in Fig. 2b, where the difference in absorbance between H117G reconstituted with Cu only and the additional reconstitution with linkers L_3-L_5 is presented. The absorption peak at around 415 nm, characteristic of the green-colored, type 2 H117G-Cu
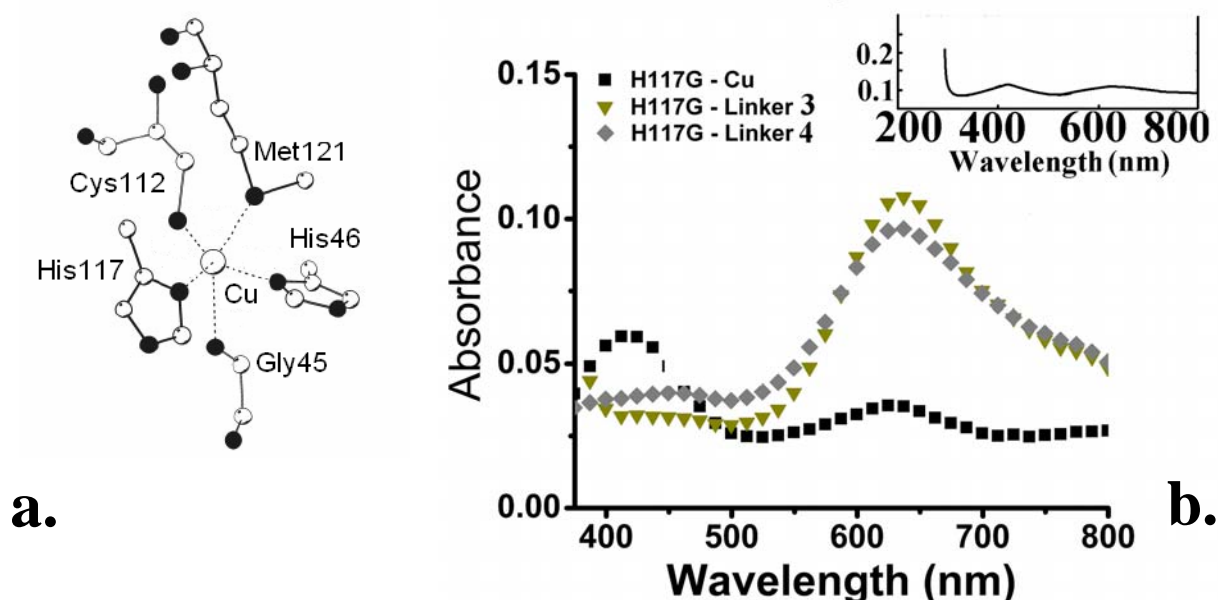

a.

b.

Figure 2. a) The geometry of the type 1 active site of wild type azurin; upon removal of His 117, imidazole or pyridine-based external ligands can reenter and re-coordinate the copper from the protein cavity (Figure adapted from ref. 30). b) Optical absorption spectra of H117G (20mM MES, pH 6.0, RT) reconstituted with linkers 3 and 4; the absorbance of H117G-Cu (black squares) is shown for comparison. Inset: reconstitution of H117G with linker 5. Protein: linker concentration ratio is 1:1, either of them at 100 μM concentration.

azurin decreases upon copper coordination with the linkers, while a simultaneous increase in absorption takes place at 625-632 nm (the source of the blue color in wt-azurin), due to a $S(Cys)\pi \rightarrow Cu\ d_{x^2-y^2}$ transition (20, 23).

We also note that, in the case of linker 5 (inset in Fig. 2b.), the so-called type 1.5 azurin is observed, that represents an intermediate between type 1 and type 2, with two bands of approximately equal magnitude at 430-450 nm and at 580-610 nm (31). This disparity may be related to a weaker binding of the ligand and a smaller displacement of the copper out of the NNS plane – as determined by the N^δs of His 46 and His117 and the S^γ of the Cys 112 (32). It is worth noting that the spectra were stable for up to 4 hours, before the copper is reduced, the linkers eventually detach and finally the reconstituted blue azurin H117G complexes become colorless.

5.3.2 AFM topographical measurements of protein-functionalized Au surfaces

Ex-situ tapping mode AFM measurements on H117G reconstituted with linkers 1-2 and adsorbed on annealed gold were performed prior to electrochemical measurements in order to determine the protein surface coverage and the optimum incubation times/concentrations needed to prevent the formation of aggregates. We have determined that concentrations of the reconstituted azurins in the range of 50-100 μM and incubation times of 1-10 minutes are necessary for protein monolayer formation and stable AFM imaging. Representative images of the H117G-L₁ protein film after performing electrochemical experiments are shown in Figure 3. The observed globular features (Figs. 3a. and 3c.) are neither present on freshly annealed gold, nor on the Au substrates incubated only with buffer (results not shown). Of note are the small height variations of the reconstituted complexes across the film (the mean height variation in Fig. 3a. is ~ 0.216 nm), as shown in Fig. 3b. We attribute the narrow distribution of protein heights to the small monoatomic height variations of the underlying gold substrate (on the order of 0.1-0.3 nm). At the same time, this distribution suggests the absence of aggregation of reconstituted azurins and the arrayal at uniform distances with respect to the surface. Based on the size of a single wild-type azurin (3.5 × 3.5 × 4.4 nm), as determined by X-ray crystallography (28, 30), we calculate a maximum coverage of ~ 63.000 proteins/μm², assuming a perfectly planar surface. From the AFM images we estimate a coverage of at least 15-20% of that of a monolayer. The actual number may be somewhat higher considering the limited AFM resolution and possible clustering of proteins.
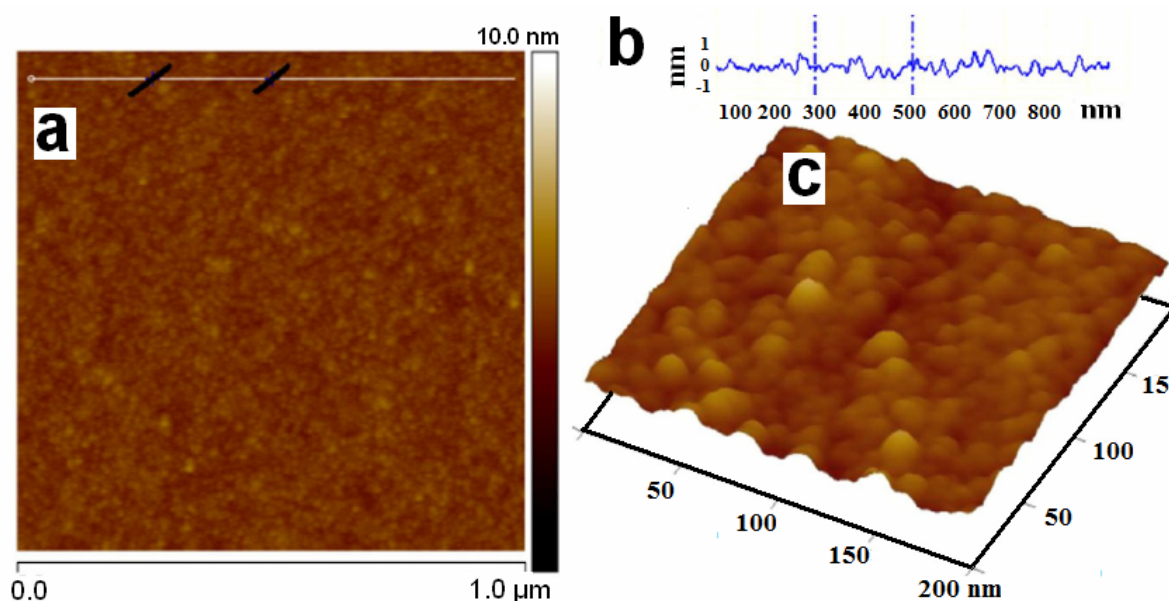
Figure 3. TM-AFM images of different H117G-L1 areas (a, c) and a height profile (b), as indicated by the two markers from image (a). The heterogeneity in height values of the proteins presented in the 3D image (c) is within 0.2-0.4 nm.

5.3.3 Electrochemical measurements

Since protein film voltammetry (PFV) is based on adsorption of redox active species on surfaces, it does not rely on the slow protein diffusion to and from electrodes for efficient electron transfer to occur, thus favoring the control of the redox state of the whole protein population. As such, PFV is a powerful tool to probe the potential dependence of enzymatic activity and the role of cofactors in relaying electrons, and to study chemical reactions coupled to electron transfer, i.e. proton transfer or active-site rearrangements (4, 24, 33). For wild-type azurin, a series of electrochemical studies have been performed, in order to determine the most efficient protein-electrode electronic coupling, on both carbon electrodes (25) and annealed gold (26). Quasi-reversible behavior was reported on gold through use of hydrophobic promoters such as bis(4-pyridyl) disulfide, diphenyl disulfide or hexanethiol (27, 28). To investigate the influence of structure of the molecular wires presented in Fig.1. (in terms of presence/absence of aromatic moieties, influence of the sulfur functionality etc), we have reconstituted the H117G azurin mutants and assembled the complexes on carbon and (SAM-functionalized) gold electrodes. In what follows, we will present the electrochemical results separately for each type of surface.

5.3.3.1 Electrochemistry of reconstituted azurins on carbon electrodes

Previous studies of the redox properties of azurin H117G have focused on the sole reconstitution with small ligands (Cl⁻, imidazole) on carbon electrodes, without the use of a molecular path able to directly connect the surface (20). A typical PGE surface presents upon abrasion various chemical groups i.e. alcoholic, phenolic, carboxylic etc (34). The behavior of adsorbed proteins onto these inhomogeneous surfaces is expected to be complex, reflecting the various interactions that can be established, e.g. between the positively charged amino groups and the negatively charged functional groups off the surface. The oxidative and reductive current peaks of wild-type azurin assembled on PGE do not overlap (in contrast to the ideal behavior of adsorbed species), and this separation in current peaks is present even at the lowest scan rates (1mV/s). Our aim here is to further research the influence on electron transfer of the attachment of azurin, as mediated by conductive wires with different structures: linker L_3 lacks a molecular "tail", being thus structurally the most similar with the native azurin; linker L_4 presents a contiguous conductive path for the π-electrons (double bonds and aromatic rings) while linker L_5 presents only σ-bonds and is not electrically conductive. Figure 4 presents the electrochemical response of azurins in wild-type form or reconstituted with these linkers.
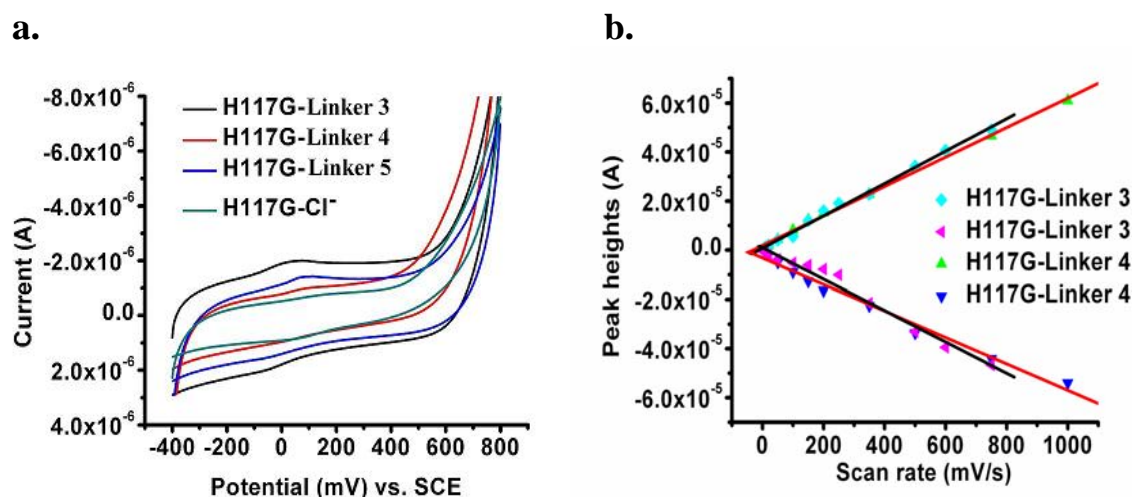

Figure 4. a) Cyclic voltammograms of 100 μM H117G-Cu reconstituted with linkers L_3, L_4, L_5 and Cl⁻ and assembled on PGE electrodes; scan rate for all scans is 10mV/s; measurements performed in 150mM Na2SO4 and 20mM MES pH 6.0, at room temperature b) Examples of the scan rate dependence of azurin H117G-Cu reconstituted with linkers 3 and 4, demonstrating the adsorbed nature of the complexes.

At the low scan rate presented (10mV/s) there is a noticeable peak separation of 50-70 mV, higher than the value for adsorbed wt-azurin of ca. 10mV (20).The half-height peak

widths (hhpw) are 30-40 mV higher than the literature values for the native form (90-100mV, versus the theoretical value of 90.6 mV at 298 K), indicating that the reaction is quasireversible (28). The broad peaks may indicate different adsorption configurations for azurins; it is also possible that some of the chemical groups produced upon polishing of PGE may themselves be electrochemically active (39). Figure 4B shows the linear dependence of the current peak heights with the scan rate for H117G-Cu reconstituted with linkers 3 and 4, thus confirming the adsorbed nature of the protein-surface conjugate (4). Of note is also the reconstitution of the H117G-Cu with anions such as Cl^-, as previously determined (20, 31) and the electrochemical activity of such complex on the carbon surface. Reconstitution with such anionic ligand was only possible by using excess of Cl^- of up to 100× (optical absorption spectrum not shown). The surface coverage, calculated by integration of the areas under the current peaks, yields ~2.1×10^{12}, ~7.4×10^{12} and ~1.4×10^{12} molecules/cm^2 for H117G reconstituted with linkers L_3, L_4 and L_5 respectively. We have obtained sub-monolayer coverage values with respect to the maximum coverage attainable ~ 10^{13} molecules/cm^2 (when considering the area of a single azurin of ~ 11 nm^2) for a complete monolayer and to the literature-reported values of ~ 4×10^{12} wt-azurins/cm^2 on PGE (25). We note however that we assume an ideally planar electrode when calculating the maximum theoretical coverage for a globular protein, despite the porous nature of the PGE electrode (21).

5.3.3.2 Electrochemistry of reconstituted azurins on (functionalized) gold electrodes

Representative cyclic voltammograms of surface-immobilized H117G-Cu pre-reconstituted with linker L_1 or L_2 in solution, followed by adsorption on gold, and by reconstitution *in situ* on a mixed SAM that is pre-adsorbed on Au(111) are shown in Figures 5A and 5B, respectively. The mixed SAM was obtained by incubating the Au electrode with a 10:1 mixture of HSC$_8$OH and linker L_1. Since AFM measurements show no adsorption of the H117G-Cu to a pure HSC$_8$OH SAM (result not presented), we assume that the electrochemical signal of the protein (Fig. 5B) reflects its coupling on the surface to the protruding L_1 or L_2 molecules and the establishment of a conductive path onto the gold surface (click-on chemistry). The linear scan rate dependence with the measured current (Fig. 5C) is indicative of surface-immobilized complexes. Assuming a one-electron transfer process, sub-monolayer coverages of reconstituted azurins on Au were calculated for H117G-L_1 and H117G-L_2, directly assembled on gold (~5×10^{12} and ~9×10^{12} molecules/cm^{-2}, respectively). These values are consistent with AFM estimates, and with data from the literature (28, 36). For H117G-Cu assembled on pre-adsorbed mixed SAM, we obtained ~2.8×10^{11} and ~$4.1 \times$
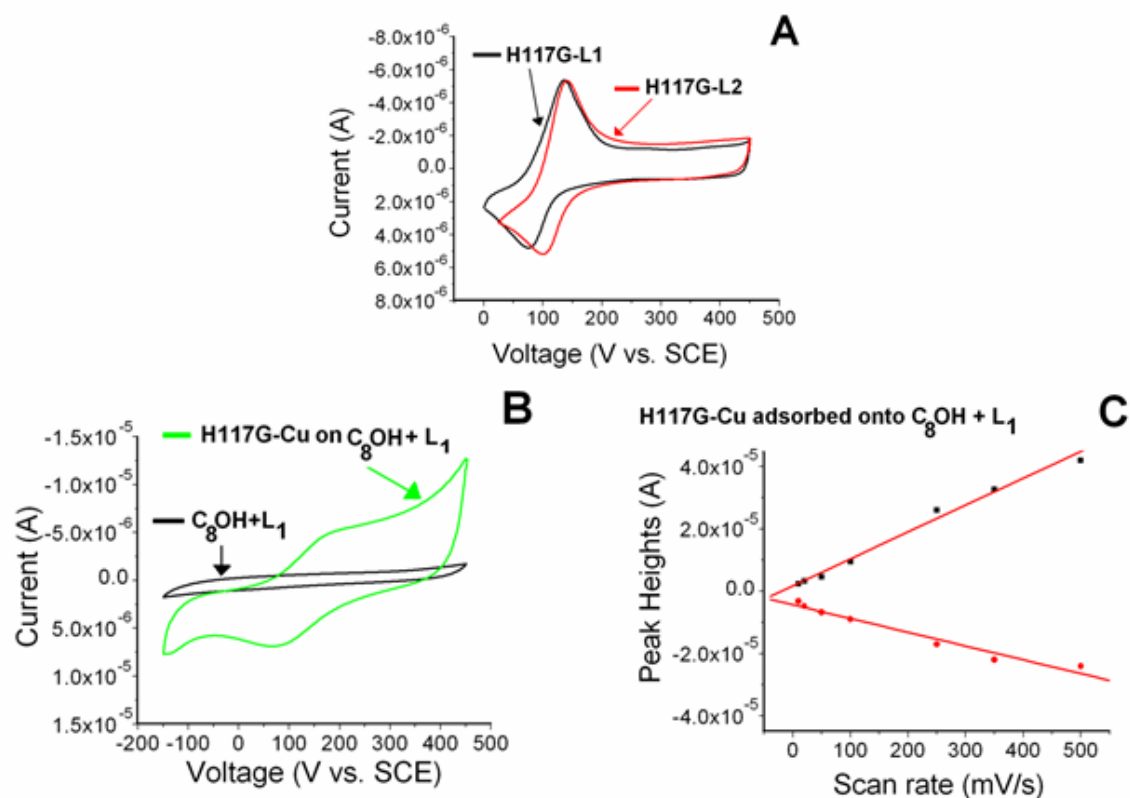
Figure 5. A) Cyclic Voltammograms of ~75 μM H117G-Cu azurin (in 50mM MES pH 6.0) reconstituted with linkers L_1 an L_2 and incubated for 1' on bare Au surfaces. Scan rate 5mV/s. B) Cyclic voltammogram of mixed SAM film consisting of C_8OH(1mM) and linker 1 (0.1mM) before H117G-Cu addition (black); in green, cyclic voltammogram obtained after addition of 200 μM H117G-Cu to the mixed self-assembling monolayer, incubation for 10' and rinsing with MES buffer and deionized water. Scan rate 50mV/s. All potentials are quoted vs. Ag/AgCl, NaCl (3M); wetted areas ~25 mm^2. C) Linear dependence of the scan rate with peak currents of H117G-Cu assembled on mixed HSC_8OH and linker 1 SAM (pre-chemisorbed on annealed gold)

10^{11} molecules/cm^{-2} for H117G-Cu adsorbed on L_1+HSC_8-OH and L_2+HSC_8-OH films, respectively. These lower values probably reflect the lower concentration of linkers within the mixed SAM which limits the surface coverage of wired proteins. These observations are indicative of a high retention of electrochemical activity for the reconstituted azurins upon Au adsorption.

5.4 Discussion

For modest peak separations (up to ~ 300mV) it is possible to make use of the Butler-Volmer formalism to fit the peak potentials versus scan rates and obtain the ET rates for oxidation-reduction of azurins (20, 38):

$$k_{red} = k_0 e^{-\alpha nF(E-E_0')/RT} \tag{5.1}$$

$$k_{ox} = k_0 e^{(1-\alpha)nF(E-E_0')/RT} \tag{5.2}$$

where k_0 is the standard rate constant at zero overpotential, E is the applied voltage bias, E_0' is the midpoint potential, α is the transfer coefficient ($\alpha = 0.5$), F is the Faraday constant, n is the number of electrons transferred ($n = 1$), R is the gas constant, T is the temperature (298 K). Figure 6 presents examples of the fitting to the Butler-Volmer equaton for H117G-Cu assembled on PGE with linker L_3 (left) or *in-situ* on functionalized Au surfaces with linker L_1 (right) with n=1, $\alpha = 0.5$, T = 298 K, E_0' (in the above examples) is + 315 mV (vs. NHE, on PGE) and + 340 mV (vs. Ag/AgCl, on Au). We have also observed a small current peak separation, even at low scan rates (exemplified also in Fig. 5A., at 5mV/s), as previously measured for wt-azurin or other proteins (37). This constant peak separation ("unusual quasi-reversibility", or UQR) is not caused by the interfacial electron transfer such that the rate constant for electron transfer (ET) between the Au surface and the azurins must be determined from additional peak separation at higher scan rates (35). The rate constants obtained after fitting to the Butler-Vomer equation, for both electrodes and all linkers, are shown in Table 1, that summarizes the electrochemical properties of H117G-Cu, reconstituted with linker L_1 or L_2 on Au, or with linkers L_3 to L_5 on carbon electrodes.
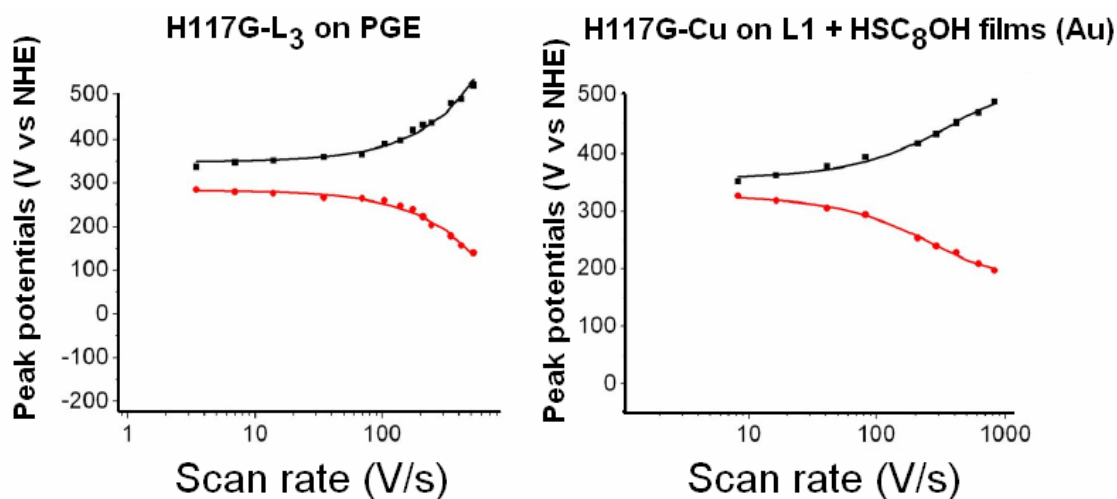

Figure 6. Left: Fit according to Butler-Volmer eq. of the peak potentials obtained for the H117G-Cu reconstituted with Linker L_3 on PGE; right: fitting of the H117G-Cu azurin peak potentials reconstituted on a Linker L1 + HSC$_8$OH functionalized gold surface.

Table 1. Electrochemical characteristics of H117G-Cu assembled on Au/PGE with linkers 1-5 (pH 6.0)

System:	$E_0^{'}$ (mV vs NHE)	k_o (s^{-1})
$H_{117}G$-L_1 (Au)	319	116 ± 9
$H_{117}G$-L_2 (Au)	335	92 ± 4
$H_{117}G$-Cu (L_1+C_8OH, Au)	340	33 ± 13
$H_{117}G$-Cu (L_2+C_8OH, Au)	344	21 ± 2
$H_{117}G$-L_3 (PGE)	315	24 ± 2
$H_{117}G$-L_4 (PGE)	312	9 ± 4
$H_{117}G$-L_5 (PGE)	319	8 ± 2

We note that the values for midpoint potential values are close to that of azurin in solution (~ 330mV vs NHE, pH 6.0), but that there are also notable differences. These differences may be attributable to the increased solvent accessibility (through loosening of the protein structure) caused by the mutation of the active cavity of the azurin H117G, that results in lowered reduction potentials, as observed for other azurin mutants (40). Two hypotheses may explain the peak broadening and the sluggish electron transfer measured on PGE: 1) the inhomogeneity of azurin populations assembled on carbon, in terms of orientation of the copper centre with respect to the surface and 2) anti-cooperative interactions that exist between redox centres that are located in proximity (protein molecules may form head-to-head dimers on the electrode) with the net effect that either mechanism should affect the oxidative and reductive peaks equally (25), as observed with our systems. On Au electrodes, direct, covalent bonding ensures stable scanning (~ 10% signal loss after 1h) and higher electron transfer rates than H117G-Cu physisorbed on carbon. Equally important, the azurin mutant is able to couple a functionalized gold surface ("click-on" chemistry), thus self-assembling into a protein-molecular wire construct from the "bottom-up". The k_0 values observed are intermediate between those observed for wt-azurin adsorbed on gold functionalized with alkanethiol monolayers: 4 - 12 e^-s^{-1} for azurin-hexanethiol system (28)or 70 e^-s^{-1} (J.M. Salverda, submitted) and 62 ± 2 e^-s^{-1} for azurin-dodecanethiol conjugate (39). These values are also higher than those observed for wt-azurin adsorbed on bare gold of $67 \pm$

6 e$^-$s^{-1} (J. M. Salverda, submitted). It is important also to note that other results (41) indicate much higher interfacial electron transfer rates (within 1-2 orders of magnitude), however the experimental conditions (pH, ionic strength etc) are not similar throughout. The k_0 values measured upon the reconstitution of H117G-Cu with linkers L_1 and L_2 are nonetheless higher than the values observed for other alkanethiol-functionalized gold surfaces, indicative of good electrical contact and increased conductivity upon adsorption. Moreover, *ex-situ* conductive-AFM measurements at various forces on apo-azurin reconstituted with linkers L_1 and L_2 and thereafter assembled on gold also point to a decreased tunneling resistance (or, conversely, to an increased conductance) of the azurin reconstituted with L_1 over the reconstitution with the structurally related L_2, by a mean factor of 2 difference (Chapter 4 of this thesis).

Further analysis of the electron transfer rates reveals that L_1 and L_2, after reconstitution of the H117G-Cu azurin, do not differ dramatically between themselves in terms of the conductivity of the protein (on gold surfaces). Their small difference of ~15 e$^-$/s and ~ 10 e$^-$/s for H117G-Cu reconstituted directly on gold, or on functionalized mixed SAM surfaces respectively reflects only a modest influence of the structure of the linkers on the values of k_0. Similarly, the values of k_0 observed for H117G-Cu reconstituted on PGE with linkers L_3, L_4 and L_5 suggest little influence on the electron transfer rates from the molecular wires, when compared to the wild-type adsorbed on similar surfaces. However, as previously observed (39), different sets of k_0 have been observed for wt-azurin attached to PGE surfaces, reflecting the non-ideal reproducibility among different electrodes after polishing. It is also likely that either poor electron coupling occurs between the mutant azurin and the surface (for instance H-bonding between the L_4 and the PGE's hydrophilic patches), or that the protein adsorbs randomly, irrespective of the presence of the wires. By comparison, better defined protein configuration, as obtained when the azurin mutant was reconstituted on gold with linkers L_1 or L_2 results in higher k_0 values (a factor of 5 difference).

5.5 Conclusions

In conclusion, we have characterized the topographical and electrochemical properties of azurin H117G-Cu cavity mutant, after the reconstitution with a variety of molecular wires, able to also couple to a metal surface. Stable protein films are observed with AFM and cyclic voltammetry when the complexes thus formed attach covalently to the appropriate electrode (i.e. gold), and reconstitution can also be performed on the functionalized Au surface. We envision that this approach may have impact in constructing enzymes assembled on surfaces,

with good ET to and from electrodes, electrochemically addressable by their physiological partners (metabolic substrates, other enzymes etc), in a stable, well-defined configuration.

References

1. F.A. Armstrong and G.S. Wilson (2000) *Recent developments in faradaic bioelectrochemistry*. Electrochim. Acta, 45, 2623-2645.

2. I. Willner and E. Katz (2000) *Integration of layered redox proteins and conductive supports for bioelectronic applications*. Angew. Chem. Int Edit., 39, 1180-1218.

3. C. Leger, J. Elliott, K. R. Hoke, L.J.C. Jeuken, A.K. Jones and F.A. Armstrong (2003) *Enzyme electrokinetics: using protein film voltammetry to investigate redox enzymes and their mechanisms*. Biochemistry, 42, 8653-8662.

4. F.A. Armstrong (2002) *Insights from protein film voltammetry into mechanisms of complex biological electron-transfer reactions*. J Chem. Soc. Dalton, 5, 661-671.

5. N. Chaki and K.Vijayamohanan (2002) *Self-assembled monolayers as a tunable platform for biosensor applications*. Biosens Bioelectron, 17, 1-12.

6. K. Reddy, M. G. Bothara, T. Barrett, J. Carruthers and S. Prasad (2008) *Nanomonitors: Protein Biosensors for Rapid Analyte Analysis*. Sens. J, IEEE, 8, 720-723.

7. B. Strehlitz, N. Nikolaus and R. Stoltenburg (2008) *Protein Detection with Aptamer Biosensors*. Sensors, 8, 4296-4307.

8. F. Lin, M. Mac Sweeney, M.M. Sheehan and A. Mathewson (2001) *A protein biosensor using Geiger mode avalanche photodiodes*. J Phys. Conf. Ser., 10, 333-336.

9. A.N. Shipway and I. Willner (2001) *Electronically transduced molecular mechanical and information functions on surfaces*. Acc. Chem. Res., 34, 421-432.

10. N. Mano, F. Maob and A. Heller (2004) *Electro-oxidation of glucose at an increased current density at a reducing potential.* Chem. Comm., 2116-2117.

11. E. Katz and I. Willner (2003) *A biofuel cell with electrochemically switchable and tunable power output*. J Am Chem. Soc., 125, 6803-6813.

12. A. Heller (2004) *Miniature biofuel cells* . Phys. Chem. Chem. Phys., 6 , 209-216.

13. H.A. Heering, F.G. Wiertz, C. Dekker and S. de Vries (2004) *Direct Immobilization of Native Yeast Iso-1 Cytochrome c on Bare Gold: Fast Electron Relay to Redox Enzymes and Zeptomole Protein-Film Voltammetry*. J Am Chem. Soc., 126, 11103-11112.

14. S. Cosnier (1997) Electropolymerization of Amphiphilic Monomers for Designing Amperometric Biosensors. Electroanalysis, 9, 894-901.

15. M. Zayats, E. Katz, R. Baron and I. Willner (2005) *Reconstitution of Apo-Glucose Dehydrogenase on Pyrroloquinoline Quinone-Functionalized Au Nanoparticles Yields an Electrically Contacted Biocatalyst.* J Am Chem. Soc., 127, 12400-12406.

16. Y. Xiao, F. Patolsky, E. Katz, J.F. Hainfeld and I. Willner (2003) *Plugging into Enzymes: Nanowiring of Redox Enzymes by a Gold Nanoparticle*. Science, 299, 1877-1880.

17. F. Patolsky, Y. Weizmann and I. Willner (2004) *Long-Range Electrical Contacting of Redox Enzymes by SWCNT Connectors*. Angew. Chem. Int. Ed., 43, 2113-2117.

18. C.R. Hess, G.A. Juda, D.M. Dooley, R.N. Amii, M.G. Hill, J.R. Winkler and H.B. Gray (2003) *Gold Electrodes Wired for Coupling with the Deeply Buried Active Site of Arthrobacter globiformis Amine Oxidase*. J Am Chem. Soc., 125, 7156-7157.

19. J. Wei, H. Liu, A.R. Dick, H.Yamamoto, Y. He, and D.H. Waldeck (2002) *Direct wiring of cytochrome C's heme unit to an electrode: electrochemical studies*. J Am Chem. Soc., 124, 9591-9599.

20. L.J. Jeuken (2001) *PhD Thesis*, Leiden University.

21. C.F. Blanford and F.A. Armstrong (2006*) The pyrolytic graphite surface as an enzyme substrate: microscopic and spectroscopic studies*. J Solid State Electr., 10, 826-832.

22. W.R. Hagen (1989) *Direct electron transfer of the redox proteins at the bare glassy carbon electrode.* Eur. J Biochem., 182, 530.

23. T. E. de Jongh (2006) *PhD Thesis*, Leiden University.

24. L.J. Jeuken and F.A. Armstrong (2001) *Electrochemical Origin of Hysteresis in the Electron-Transfer Reactions of Adsorbed Proteins: Contrasting Behavior of the "Blue" Copper Protein, Azurin, Adsorbed on Pyrolytic Graphite and Modified Gold Electrodes*. J Phys. Chem. B, 105, 5271-5282.

25. J. Hirst and F.A. Armstrong (1998) *Fast scan cyclic voltammetry of protein films on pyrolytic graphite edge electrodes: characteristics of electron exchange*. Anal. Chem., 70, 5062-5071.

26. Q.J. Chi, J.D. Zhang, J.U. Nielsen, E.P. Friis, I. Chorkendorff, G.W.Canters, J.T. Andersen and J. Ulstrup (2000) *Molecular monolayers and interfacial electron of Pseudomonas aeruginosa azurin on Au(111)* J. Am. Chem. Soc., 122, 4047-4055.

27. T. Sakurai, F. Nose, T. Fujiki and S. Suzuki (1996) *Reduction and oxidation processes of blue copper proteins, azurin, pseudoazurin, umecyanin, stellacyanin, plantacyanin, and plastocyanin approached by cyclic and potential step voltammetries*. Bull. Chem. Soc. Jpn., 69, 2855-2862.

28. G. Gaigalas and G. Niaura (1997) *Measurement of electron transfer rates between adsorbed azurin and a gold electrode modified with a hexanthiol layer*. J. Colloid Interf. Sci., 193, 60-70.

29. M. Zayats, B. Willner and I. Willner (2008) *Design of Amperometric Biosensors and Biofuel Cells by the Reconstitution of Electrically Contacted Enzyme Electrodes.* Electroanalysis, 20, 583-601.

30. H. Nar, A. Messerschmidt, R. Huber, M. v/d Kamp and G.W. Canters (1991) *Crystal Structure Analysis of Oxidized Pseudomonamsv aeruginosa azurin at pH 5.25 and pH 9.0.* J. Mol. Biol., 221, 765-772.

31. T. Den Blaauwen and G.W. Canters (1993) *Creation of type-l and type-2 copper sites by addition of exogenous ligands to the Pseudomonas aeruginosa mutant His117Gly*. J. Am. Chem. Soc., 115, 1121-1129.

32. J. Han, T. M. Loehr, Yi Lu, J.S. Valentine, B. A. Averill and J.S. Loehr (1993) *Resonance Raman Excitation Profiles Indicate Multiple Cys - Cu Charge Transfer Transitions in Type 1 Copper Proteins*. J. Am. Chem. Soc., 115, 4256-4263.

33. M.N. Hasan, C. Kwakernaak, W.G. Sloof, W.R. Hagen and H.A. Heering (2006) *Pyrococcus furiosus 4Fe-ferredoxin, chemisorbed on gold, exhibits gated reduction and ionic strength dependent dimerization.* J biol. inorg. Chem., 11, 651-662.

34. G.E. Cabaniss, A.A. Diamantis, W.R. Murphy Jr., R.W. Linton and T.J. Meyer (1985) *Electrocatalysis of proton-coupled electron-transfer reactions at glassy carbon electrodes*. J Am Chem. Soc., 107, 1845-1853.

35. S.W. Feldberg and I. Rubinstein (1988) *Unusual quasi-reversibility (UQR) or apparent non-kinetic hysteresis in cyclic voltammetry: an elaboration upon the implications of N-shaped free energy relationships as explanation*. J. electroanal. Chem., 240, 1-15.

36. J.J. Davis, D. Bruce, G.W. Canters, J. Crozier and H.A.O. Hill (2003) *Genetic modulation of metalloprotein electron transfer at bare gold*. Chem. Comm., 576-577.

37. F.G.M. Wiertz (2008) *PhD Thesis*, Delft University.

38. J. Hirst (2006) *Elucidating the mechanisms of coupled electron transfer and catalytic reactions by protein film voltammetry*. Biochim. Biophys. Acta, 1757, 225-239.

39. L.J. Jeuken and F.A. Armstrong (2002) *Insights into Gated Electron-transfer Kinetics at the Electrode-Protein Interface: A Square Wave Voltammetry Study of the Blue Copper Protein Azurin.* J. Phys. Chem. B, 106, 2304-2313.

40. A.J. Di Bilio, T.K. Chang, B.G. Malmstrom, B.H. Gray, B.G. Karlsson, M. Nordling, T. Pascher and L.G. Lundberg (1992) E*lectronic absorption spectra of M(II)(Met121X) azurins (M = Co, NI, Cu; X = Leu, Gly, Asp, Glu). Charge transfer energies and reduction potentials.* Inorg. Chim. Acta, 198-200, 145-148.

41. B.D. Fleming, S. Praporski, A.M. Bond and L.L. Martin (2008) *Electrochemical Quartz Crystal Microbalance Study of Azurin Adsorption onto an Alkanethiol Self-Assembled Monolayer on Gold.* Langmuir, 24, 327.

Summary

Proteins are the workforce of the cells. They catalyse biochemical reactions, have a key role in communicating with the environment, and control many biological processes. Because of their specific functionality, there is nowadays a growing desire to emulate or incorporate their evolutionarily fine-tuned features into modern devices and applications. A flurry of interest in the practical possibilities of this synergy has been in full swing and led to a number of potential applications. An example of a commercially viable device is the glucose sensors. Moreover, a great many studies on the adsorption and activity of small proteins or DNA on various surfaces have also a considerable theoretical interest, last but not least being a better understanding of the interplay between adsorption, surface catalysis and molecular self-assembly. However, as outlined in this thesis, numerous obstacles still hinder the practical implementations, chief among which being the control of the chemistry of attachment to the surfaces. Protein adsorption is sensitive to changes in pH, temperature, ionic strength or to surface charge and roughness. As such, control of both the protein's attachment sites and of surface chemistry and flatness is important.

For our studies, we have made use of engineered proteins (azurin H117G) with an open cavity and direct access to the redox active site; moreover, the attachment to surfaces has been designed such that a molecular wire could couple very specifically to the metal inside the redox cavity, while a thiol functionality lends covalent adsorption to (flat) gold surfaces feasible.

In order to attach the azurin-molecular wire complex onto surfaces, we have employed two approaches. One route consisted of adsorbing the molecular wires, and further attaching the azurins with the open cavity onto the thus functionalized surfaces ("click-on" chemistry). Alternatively, the azurin-molecular wire complex was reconstituted in solution and followed by the attachment to gold surfaces.

For the first approach, the attachment of two, structurally related molecular wires on gold surfaces was investigated, and this is the main subject of **Chapter 2.** Because of the difficulty of assembling them in a "standing-up" configuration, we have made use of molecular structural props in the form of alkanethiol self-assembling monolayers. The self-assembling monolayers consisting of mixed molecular phases, was investigated at single-molecule level with Scanning Tunneling Microscopy and with Atomic Force Microscopy and ellipsometry. In so doing, aside from the details of the attachment to the gold lattice, an

interesting behavior was also discovered, in the form of conductance "switching" for one of the molecular wires. Such phenomenon can be attributed to the lateral diffusion in the alkanethiol matrix, and the contrasting behavior of the two molecular wires is suggested to be linked to the effect of intermolecular interactions on the energetic barrier for the free lateral diffusion.

To better characterize not only the structural aspects of the surface assembly of the molecular wires, but also some of their functional traits, we have further studied their electron transfer properties, at single-molecule level, by means of Scanning Tunneling Microscopy and Conductive-Atomic Force Microscopy, as presented in **Chapter 3.** The increased conductivity of the molecular wires, compared to that of the alkanethiol monolayers used as reference, makes them good candidates for efficient electron coupling to the azurin mutant. The observation that the current-voltage spectra presents current peaks is suggestive of the involvement of the molecular orbitals in the electron transfer, and is in line with observations made for other oligo-phenylenevinylenes.

Direct coupling of the H117G azurin-molecular wire complex on the gold surface is described in **Chapter 4.** The structural aspects of this attachment is characterized by a combination of UV-Vis, ellipsometric and AFM measurements. The electron transfer properties of the assembled complexes have been further investigated with the Conductive-Atomic Force Microscopy. The introduction of a redox-inactive metal (Zn) in the protein cavity leads to both a reduced conductance (by an order of magnitude compared to the Cu-containing complexes) and to the absence of negative differential resistance events. Such phenomena are attributed to the tunneling via the protein's redox-level. Furthermore, the linear dependence of the electrical resistance with the applied forces (over a certain range) of Cu and Zn-containing complexes, reconstituted with (un)conjugated molecular wires, may reflect the importance of a continuous conjugated path for efficient electron transfer from the protein's redox moiety to a surface.

Chapter 5 makes use of both strategies for the adsorption of H117G azurin reconstituted with different molecular wires. The focus is here on the characterization of an ensemble of complexes by electrochemistry. Redox potentials similar to that of native azurin in solution, surface coverages and electron transfer rates were measured after the adsorption on two different surfaces, i.e. (functionalized) gold and carbon and comparisons with the adsorption of the wild-type azurin on similar surface are drawn.

Samenvatting

Eiwitten zijn de werkpaarden van de cel. Ze katalyseren biochemische reacties, hebben een sleutelrol in de communicatie met de omgeving, en sturen talrijke biologische processen. De hoge specificiteit en functionaliteit van eiwitten en enzymen zijn aantrekkelijke eigenschappen die mogelijk gebruikt kunnen worden voor de ontwikkeling van nieuwe technische toepassingen en apparaten. Dit is het uitgangspunt van toenemende activiteit op dit gebied met een sterk accent op toepassingen met een commerciële potentie. Een zeer succesvol voorbeeld daarvan is de glucose biosensor.

Belangrijke aspecten in het hier beschreven onderzoek zijn de adsorptie, activiteit en functionaliteit van eiwitten die geïmmobiliseerd zijn op verschillende oppervlakken. Op deze gebieden is nog belangrijke vooruitgang te boeken, en dienen er nog veel obstakels uit de weg geruimd te worden. Daarvoor is het noodzakelijk om meer kennis te vergaren over adsorptie, oppervlaktekatalyse, specifieke chemische binding aan oppervlakken, moleculaire self-assemblage, en om controle te hebben over de orientatie en configuratie van biomoleculen. Adsorptie van eiwitten is gevoelig voor veranderingen in de zuurgraad, temperatuur, ionsterkte, en de oppervlaktelading en -ruwheid. Specifieke koppeling van een eiwit aan een oppervlak vereist controle over de bindingsplaats aan het eiwit, en over de vlakheid en de chemie van het oppervlak. In dit proefschrift wordt dit gerealiseerd door gebruik te maken van een gemodificeerd eiwit (azurine H117G) met een holte aan de buitenkant die ontstaat als een histidine (residu 117) vervangen wordt door een glycine. Dit eiwit geeft externe moleculen toegang tot de redox-actieve cofactor, een koperatoom. Via deze holte kan een geschikt molecuul met een pyridine- of imidazool-groep zich binden aan het Cu-atoom, terwijl het andere uiteinde van het molecuul een binding kan aangaan met het oppervlak van het substraat (in dit geval via een thiolgroep aan een goudoppervlak). Dit koppelmolecuul kan dan functioneren als een moleculaire geleider voor electronoverdracht tussen het redoxcentrum van azurine en het (metaal)oppervlak. Het doel van het onderzoek in dit proefschrift was, om deze vorm van binding tussen azurine en een goudoppervlak te karakteriseren, en het effect daarvan op electronoverdracht te meten

Deze innovatieve techniek voor de verankering van eiwitten op een oppervlak kan op twee manieren worden uitgevoerd. Het koppelmolecuul kan eerst worden gebonden aan het goud-oppervlak, waarna het eiwit zich in een volgende stap kan binden aan het uiteinde van het koppelmolecuul (zgn. "click-on" chemie). De andere methode is om het eiwit eerst te

reconstitueren met het koppelmolecuul, waarna dit kan reageren met het goudoppervlak om het eiwit te verankeren.

De eerste methode wordt toegepast in **hoofdstuk 2**, waarin de eigenschappen van twee structureel vergelijkbare koppelmoleculen worden bestudeerd, met aan het ene uiteinde een pyridinegroep en aan het andere uiteinde een thiolgroep. Om deze koppelmoleculen rechtop te laten staan is het nodig om ze te nestelen in een monolaag van alkaanthiol moleculen. Deze monolaag vormt zich spontaan op een (111) goudoppervlak met een hoge mate van tweedimensionale ordening. De organisatie en verdeling van koppelmoleculen in deze monolaag werd onderzocht met behulp van "scanning tunneling microscopy" (STM), atomaire kracht microscopie (AFM) en ellipsometrie. Eén van de twee koppelmoleculen vertoonde een dynamisch gedrag, waarbij de geleiding als het ware aan- en uitschakelde in opeenvolgende afbeeldingen die werden gemeten met de STM. Dit gedrag heeft waarschijnlijk te maken met diffusie van het koppelmolecuul in de alkaanthiol-monolaag.

Om de electronische en andere functionele aspecten van de geïmmobiliseerde moleculaire geleiders in meer detail te bestuderen werden STM- en geleidende AFM-metingen gedaan aan individuele moleculen. De resultaten daarvan worden gepresenteerd in **hoofdstuk 3.** In vergelijking met alkaanthiol-moleculen hebben de koppelmoleculen een aanzienlijk hogere elektrische geleidbaarheid. De stroom gemeten als functie van de spanning vertoont een karakteristieke structuur die kan worden toegeschreven aan de bijdrage van moleculaire electronische toestanden aan de electronoverdracht, in overeenstemming met eerder waargenomen effecten in soortgelijke moleculen.

De directe binding van de H117G azurine mutant via de koppelmoleculen aan een goudoppervlak wordt beschreven in **hoofdstuk 4.** De structurele aspecten werden gekarakteriseerd met behulp van UV-Vis spectroscopie, ellipsometrie en AFM metingen. De geleidende eigenschappen werden bestudeerd met geleidende AFM technieken. De geleidbaarheid wordt aanzienlijk gereduceerd, met ongeveer een factor 10, als het koper-atoom in het redox centrum van azurine wordt vervangen door zink dat niet redox-actief is. Het redoxcentrum speelt dus een actieve rol in electron tunneling tussen de geleidende AFM-tip en de goudelectrode. De elektrische weerstand blijkt (binnen bepaalde grenzen) lineair te variëren met de kracht die de AFM tip uitoefent op de azurine/koppelmolecuul combinatie. Het geconjugeerd karakter van de koppelmoleculen is bepalend voor de efficiëntie van de electronoverdracht tussen azurine en het goudoppervlak.

In **hoofdstuk 5** worden beide strategieën voor moleculaire koppeling van de H117G azurine mutant met een goudelectrode gebruikt om de electrochemische eigenschappen van deze structuren te meten met behulp van cyclische voltammetrie. De redoxpotentiaal blijkt vergelijkbaar te zijn met die van azurine in oplossing. De ladingsoverdracht komt overeen met een oppervlaktedichtheid van een vrijwel volledige monolaag van azurine. De snelheid van electronoverdracht blijkt aanzienlijk hoger te zijn dan de snelheid die werd gemeten aan een aspecifiek gebonden azurine op een alkaanthiol-monolaag.

Sumar

Proteinele sunt componente de baza ale celulelor. Ele catalizeaza majoritatea reactiilor si au roluri deosebite structurale si in semnalizarea celulara. Ca atare, exista o cerinta in crestere pentru incorporarea ori perfectionarea trasaturilor lor evolutive in aparate electronice moderne. Un interes crescand in posibilitatile practice ale acestei sinergii este in desfasurare si a condus la un numar de aplicatii viabile economic, de pilda senzorii optimizati pentru detectia nivelului de glucoza in sange. Mai mult, un numar ridicat de studii asupra adsorptiei si activitatii unui numar de proteine sau ADN pe diferite suprafete are si un interes teoretic deosebit, mai ales legat de conjunctia intre cataliza la suprafete, polimerizare, auto-asamblare si originea primelor molecule ale celulelor. Cu toate aceste avansuri, numeroase obstacole inca impiedica implementarile practice, un rol deosebit avand aici lipsa controlului asupra chimismului atasarii pe suprafete. Acest fenomen, aplicat la proteine, depinde de schimbari in pH, temperatura, tarie ionica sau de rugozitatea sau sarcini electrice presente pe suprafete. In studiul nostru, am folosit proteine mutant (azurina H117G), cu o cavitate deschisa si acces liber la centrul redox; mai mult, atasarea la suprafata a fost conceputa in asa fel incat o molecula cu rol de legatura sa cupleze foarte specific doar la metalul din cavitatea redox, odata cu atasamentul covalent pe suprafete (atomic plate) de aur.

In aceasta ordine de idei, am folosit doua abordari pentru atasarea complexului azurina H117G – ligand molecular. O cale a constat in adsorbtia ligandului pe o suprafata de aur, urmata de atasarea proteinelor, continand cavitatea deschisa (chimism "click-on"). Alternativ, complexul azurina-ligand a fost reconstituit in solutie, urmat de atasarea pe suprafate.

Pentrul prima cale, atasarea a doi liganzi cu structuri moleculare foarte similare pe suprafete de aur a fost investigata la nivel de singura molecula cu Microscopul de effect tunnel, Microscopul de forta atomica si prin masuratori elipsometrice (**Capitol 2** al acestei teze). Datorita dificultatilor de a produce liganzi adsorbiti intr-o configuratie perpendicular fata de suprafata, am folosit filme auto-asamblante de alcantioli. Ca urmare, in afara de detaliile de adsorbtie ale fiecarei faze moleculare din solutie pe suprafata, un comportament interesant a devenit discernibil, in forma unor schimbari de conductanta electrica in timp. Acest fenomen a fost atribuit difuziei laterale ale liganzilor in matricea de alcantioli, iar comportarea diametral opusa a fiecarui ligand a fost legat de legaturile intermoleculare care pot impiedica sau nu difuzia libera. Importanta acestor observatii a fost pusa in legatura cu

contextul larg al altor observatii similare din literature, sugerandu-se de asemeni o noua interpretare pentru acest fenomen.

Pentru o caracterizare mai buna nu doar a aspectelor structurale ale asamblarii pe suprafete, ci si a unor caracteristici functionale, am studiat in continuare mecanismul de transfer de electroni prin acesti liganzi, cu ajutorul Microscopului de effect tunnel si al Microscopului de forta atomica cu capacitate de detectie a conductivitatii moleculare (**Capitol 3**). Conductanta crescanda a liganzilor, fata de conductanta alcantiolilor inseamna ca primii pot functiona ca eficienti candidatii pentru cuplarea electronica eficienta a azurinei pe suprafete. Observatia ca spectrele current-voltaj au trasaturi de rezisitivitate negative a sugerat implicarea orbitalelor moleculare in transferul de electroni, in acord cu alte masuratori facute asupra unor molecule de structura asemanatoare.

Cuplarea directa a complexului azurina H117G-liganzi pe suprafete de Au este descrisa in **Capitolul 4**. Insertia propriu-zisa a diferiti liganzi in cavitatea redox a fost caracterizata cu o serie de tehnici, precum absorbtia in spectrul vizibil, elipsometrie si Microscopia de forta atomica. Transferul de electroni prin aceste complexe, asamblate pe suprafete, a fost caracterizat cu Microscopia de forta atomica cu capacitate de detectie a conductivitatii moleculare. Introducerea unul metal inactiv redox (Zn) in cavitatea proteinei duce la o reducere in conductanta electrica (cu un ordin de magnitude comparative cu complexul proteinic care contine Cu) si la o absenta a trasaturilor de rezistenta electrica negative din spectrele de current-voltaj. Aceste fenomene au fost puse in legatura cu conductia prin effect tunnel prin nivelul redox proteinic. Mai mult, dependenta lineara a resistivitatii electrice cu forta aplicata asupra proteinelor continand Cu sau Zn si reconstituite cu liganzi (ne)conjugati, poate reflecta importanta unei continuitati de structura moleculara conjugate pentru transfer ridicat de electroni de la azurina la suprafete.

In **Capitolul 5** am folosit ambele strategii pentru adsorbtia azurinei H117G, reconstitutita cu diferiti liganzi moleculari si am caracterizat ansamblurile formate electrochimic. Potentialele redox similare cu cele ale azurinei native in solutie, acoperirea pe suprafete si ratele de transfer de electroni au fost masurate dupa atasamentul pe electrozi (de pilda carbon sau aur, functionalizat sau nu) si comparatii cu proprietati similare ale azurinei native asamblate in conditii similare au fost facute.

Acknowledgements

Curriculum Vitae

Razvan Stan was born on December 8th 1979 in Curtea de Arges, Romania. After graduating from the University of Babes-Bolyai (Cluj-Napoca, Romania) in 2002 with a degree in Biology, he continued with his Master's studies in Biophysics at the same university, with research on the application of bifurcation and catastrophe theory in the self-assembly of lipids in liposomes and black membranes. After graduating in 2003, he went for a Marie Curie Training Stage at the University of Florence (Italy), working on the expression and genetic engineering of matrix metalloproteinases. In 2004 he moved to the University of Leiden in the groups of prof. Thijs Aartsma and prof. Gerard Canters to continue with the doctoral studies. The results of his research are described in this thesis. After graduation, he will move to Indiana University/Purdue University to work on the evolution of the enzymatic specificity for substrates.